The Dissertation Committee for Frank Ryan Male certifies that this is the approved version of the following dissertation:

Application Of A One Dimensional Nonlinear Model To Flow In Hydrofractured Shale Gas Wells Using Scaling Solutions

Committee:

Michael P. Marder, Supervisor

Tad W. Patzek, Co-Supervisor

Harry Swinney

Larry Lake

Vernita Gordon

Application Of A One Dimensional Nonlinear Model To Flow In Hydrofractured Shale Gas Wells Using Scaling Solutions

by

Frank Ryan Male, B.S., B.A.

Dissertation
Presented to the Faculty of the Graduate School of
The University of Texas at Austin
in Partial Fulfillment
of the Requirements
for the degree of
Doctor of Philosophy

The University of Texas at Austin
May, 2015

Acknowledgments

This thesis focuses on the work done to characterize the performance of wells and draw conclusions about their productivity. First, Professors Tad Patzek and Michael Marder and I developed a minimal model to describe performance (Patzek et al., 2013, 2014). This model was applied to several major shale gas basins, as one small piece in an interdisciplinary effort to understand US shale gas production. Adaptation of the model to unique geology and production methods, and application of the model to young wells was done in the context of this large group, with Dr. Svetlana Ikonnikova and John Browning, along with the aforementioned, providing insights and direction for performing this task. Production data was provided from the IHS Cera database, DrillingInfo, the Texas Railroad Commission, the Pennsylvania Department of Environmental Protection, the West Virginia Department of Environmental Protection, the Louisiana Department of Natural Resources, and other sources. Figures were created using the open source IPython (Pérez and Granger, 2007) and Matplotlib libraries available in Anaconda Python.

There are many people who have helped me on this journey. You know who you are. For everyone else, though, I would like to give a partial list. My parents and grandparents have been loving, supporting, and understanding of my journey through graduate school. They've always had more faith in me than I do. Without them, there is no way I could have made it this far. My band-mates are my best friends, support group, and co-adventurers in the fields of life, graduate school, and music. I am forever in debt to them. Without Virginia, my girlfriend, I would not have navigated academia nearly as gracefully as I have. I cannot thank her enough for this, much less the edits, advice, and life lessons she's given me.

Application Of A One Dimensional Nonlinear Model To Flow In Hydrofractured Shale Gas Wells Using Scaling Solutions

Frank Ryan Male, Ph.D.
The University of Texas at Austin, 2015

Supervisors: Michael Marder and Tad Patzek

Estimations of shale gas reserves rely heavily on decline analysis of existing wells. In this work, I describe a new method of production analysis for shale gas reservoirs using a minimal model. This method relies on formulating a universal production curve for wells in each shale gas field such that production from a hydrofractured shale gas well in a particular field is only distinguished from other wells by two scaling parameters: the time to boundary-dominated flow and the total hydrocarbon in place. This technique bridges the gap between the simple empirical models often used for decline analysis and the complex analysis offered through full 3-dimensional reservoir simulations.

I provide production forecasts and estimated ultimate recoveries for wells in the Barnett, Fayetteville, Haynesville, and Marcellus shale gas plays, and propose an extension to the method to facilitate analysis of the Eagle Ford and Bakken shale oil plays. The simplicity and power of this method makes it ideal for performing decline analysis on large numbers of wells.

Contents

List of Figures

Nomenclature

SRV, Stimulated reservoir volume — the portion of the shale with gas accessible by a well.
EUR, Estimated ultimate recovery — the total gas a well is expected to produce.
OGIP, Original gas in place — the amount of gas in the reservoir before drilling. In the energy industry, this is often calculated on a per-mile basis. I will also use the term to describe the gas in the stimulated reservoir volume.
PVT, Pressure-Volume-Temperature — the real gas properties relating pressure, volume, and temperature of a natural gas sample.
Transient flow — the flow regime where natural gas does not flow from the entire SRV and the well acts as though it is in a semi-infinite reservoir.
Boundary dominated (influenced) flow — the flow regime where natural gas flows to the well from the entire SRV.
Type Curve — the fractional hydrocarbon production over time for a well.

Symbols

c = Isothermal compressibility, 1/psi [1/Pa]
d = hydrofracture spacing half-length, ft [m]
k = permeability, md
H = height of hydrofractures, ft [m]
L = half-length of hydrofractures, ft [m]
m = real gas pseudopressure,
$\mathcal{M}$ = mass of gas in place, lb [kg]
N = number of fractures
p = pressure, psia [kPa]
RF = recovery factor function
S = saturation
t = time, s [s]
u = superficial flow rate ft/s [m/s]
x = distance, ft [m]
$\mathbf{y}$ = gas composition
α = hydraulic diffusivity, ft^2 /s [m^2/s]
ϕ = porosity
ρ = density, lb/ft^3 [kg/m^3]
μ = viscosity, cp [MPa.s]
τ = time to interference, d [s]

Subscripts

g = gas
i = initial conditions
s = scaling for throttling
f = condition at the wellbore

Diacritics

$\sim$= scaled version of quantity

Chapter One: Introduction

"And now, for something completely different."

— John Cleese, *Monty Python's Flying Circus*

The topics of reservoir and decline analysis have engaged interest ever since the first commercial oil well. In 1859, Edwin Drake drilled the Drake Well in Pennsylvania. While that well was only 20 m deep, cost approximately $3,000, and produced about 10 barrels per day (Pees, 2004; Dickey et al., 1959), modern shale gas and oil wells are much larger endeavors. The average well in the Marcellus field in Pennsylvania is in excess of 3,000 m deep, with a lateral section extending one kilometer underground, costing $6 million and producing billions of cubic feet of gas over its lifetime.

How did we get from the Drake Well to the modern Marcellus field? There have been enormous advances in hydrocarbon recovery. Let's go even further back in time. Natural gas and oil have seeped from the ground since before humans even walked the earth. The Oracle of Delphi was possibly influenced by gas seeping from faults (de Boer et al., 2001) and natural gas has been collected as an energy source for millennia. In ancient China, natural gas extracted from wells was used to evaporate brine and produce salt (Jiexin and Palmer, 2009). Drilling rigs were first built circa 500 B.C. in ancient China using percussive cable drilling which could reach depths of hundreds of meters. These were succeeded by Leonardo da Vinci's designs of rotating drill bits (Kopey, 2007). The next major step was drilling oil wells in the late 1850s, the most famous of which is the Drake Well. Why was oil desirable? Well, it was marketed for several things: in order to produce light and heat, and for presumed medicinal qualities, which is why Edwin Drake was employed to drill for oil. When the Drake well proved productive, the first oil rush started, and by the end of 1860, there were 74 oil wells producing a total of 1,165 barrels per day (Dickey et al., 1959).

According to Curtis (2002), the first gas well was drilled in 1821 in Fredonia, New York. It was drilled in a Devonian shale formation — a shale from the same geologic period as the Marcellus shale. The natural gas provided by this well was used for lighting. Shale gas fields had been drilled across the eastern United States by the

1920s. Most gas production has come from more porous and permeable reservoirs, though. The geologic definition for permeability is the conductivity of fluid flow through a rock.

In the United States, limestones and sandstones were the most popular reservoir to produce from, with porosities several times larger than shales and permeabilities millions of times larger than shales. As recently as 2005, the total gas produced from shales in the United States has been minuscule. Instead, gas has been produced from conventional limestone and sandstone reservoirs, either by itself or coexisting with oil; this is because limestones are so much more permeable than shales, and therefore allow much easier flow of natural gas through the reservoir.

Outside of the United States, almost all gas and oil production is from limestone and sandstone reservoirs. The most famous reservoirs in the world, such as the Ghawar Field in Saudi Arabia (limestone), the Burgan Field in Kuwait (sandstone), Prudhoe Bay Field in Alaska (sandstone) and the Bolivar Coastal Field in Venezuela (sandstone), are high porosity, high permeability, limestone and standstone fields.

Although the definitions for conventional versus unconventional reservoirs are sometimes arbitrary, in general limestone, sandstone, and other permeable reservoirs found under land are considered conventional reservoirs, while anything more difficult to access than this is unconventional. Therefore, deep-water offshore reservoirs, "tight" sandstone of less permeability than limestone, methane recovered from coal deposits, and shale are all thought of as unconventional.

Over the next several decades, drilling technology improved tremendously, and many of those high permeability reservoirs have been emptied in the U.S. With the easily accessible gas reservoirs drained, natural gas prices crept up, production fell, and people started searching for new places to produce from. Out of this came the push to drill in shale gas formations.

In order for natural gas fields in shale to be economical it is not sufficient to simply drill to the gas-bearing shale. Because the reservoir has such a low diffusivity, not enough gas would be produced without doing something more. Hydraulic fracturing and horizontal drilling were both developed in order to increase the contact area between the reservoir and the well bore and to improve production. These technologies are not particularly new, and in fact fracturing was done as early as 1947 while the first horizontal well was drilled in the 1930s (King et al., 2012). However, adapting these technologies to exploit shale gas deposits economically took generations.

The first major, modern shale gas field, the Barnett shale, has been developed for 30 years, but it was 1997 before hydrofracture treatments allowed effective production of natural gas (Bowker, 2007), and 2004 before the advent of economic horizontal drilling. After the technology was proven in the Barnett shale, companies began exploiting several other natural gas fields. Production from shale reservoirs jumped from less than 1 trillion cubic feet (Tcf) of gas in 2005 to more than 10 Tcf in 2013. The combination of horizontal drilling and hydraulic fracturing caused the US shale boom. My research is motivated by the question, "How much gas will these shale plays provide?"

Shale gas fields are different in several ways from conventional fields. The wells drain from a much smaller volume, requiring many, many more wells to drain the field. They require the advanced technology I highlighted above. Also, production from shale wells decline far faster than from conventional wells. This means that a field's future is determined to a large degree by how quickly companies drill new wells. In conventional fields, this is less of a concern, and other methods are employed to maintain production from a field.

How does physics get involved in this discussion? There is a rich history of physicists applying their thinking to engineering problems. A brief examination of the Nobel prizes awarded in physics brings many examples to light, from the 1909 awarding of the Nobel prize to Guglielmo Marconi and Karl Ferdinand Braun for inventing the radio to the 2014 prize given to Isamu Akasaki, Hiroshi Amano, and Shuji Nakamura for inventing blue LEDs. This work is not nearly so ambitious, but it is just as firmly grounded in employing physics methods to inform other disciplines.

I have laid out this dissertation in six chapters and an appendix. Chapter 2 provides an overview of the body of work done in fluid mechanics, scaling analysis, and production decline analysis. Chapter 3 discusses the proposed model. The strategy used to characterize shale gas production is this: build a simple, one-dimensional model of flow, using realistic fluid properties, and apply a scaling to collapse real production onto a universal curve that describes the past and predicts the future. There are two primary flow regimes which arise from the model, and knowing the performance of a well in one flow regime guarantees no knowledge of when the well switches to the second flow regime. When the production decline switches has severe implications for the well's ultimate production. Therefore, Chapter 4 describes attempts to determine when these wells switch and forecast ultimate recovery. In

Chapter 5, I apply the model to four major shale gas fields. Chapter 6 finishes the thesis with a discussion of conclusions from the research and questions left to future work. In Appendix A, I discuss extensions to the model to include tight oil and condensate fields.

1.1 Bureau of Economic Geology Shale Resource and Reserve Study

The Alfred P. Sloan Foundation has funded a study by the Bureau of Economic Geology (BEG) to perform shale gas and oil resource and reserve estimates. The BEG is a research unit inside the Jackson School of Geosciences. They have two primary missions: conducting basic and applied research to increase understanding energy resources, and curating an enormous core and cutting library and a well log library. Their core collection is the largest in America and brings researchers from around the world. However, it is the first mission which is important in this context. Sloan funded this project in expectation of being responsible for the most detailed publicly accessible survey of shale gas resources in the US ever done.

This study is being done by an interdisciplinary team and is intended to work on several shale resource plays from the ground up (well, below the ground). The team includes geologists, engineers, and economists, and is led by co-principal investigators Scott Tinker, director of BEG, and Svetlana Ikonnikova, Research Associate at BEG. I have been part of this project since 2010, assisting on the engineering side. The study has followed a specific work-flow, detailed in Fig. 1.1.

There are other assessments of natural gas resources that are available, done by the US Energy Information Agency (EIA) and the US Geologic Survey. However, these assessments are either out of date, in the case of the Geologic Survey study, or lacking the granularity provided by the BEG study. The EIA does not have as much geologic information to draw their decisions from and uses a simpler production analysis method than provided in this thesis. They provide annual reports of shale gas resources and expected production for all energy resources in the US, which is a much broader scope than the BEG study.

Here is a brief and simplified description of the BEG process: In the Sloan funded study, we use extensive well logging information and occasionally information from

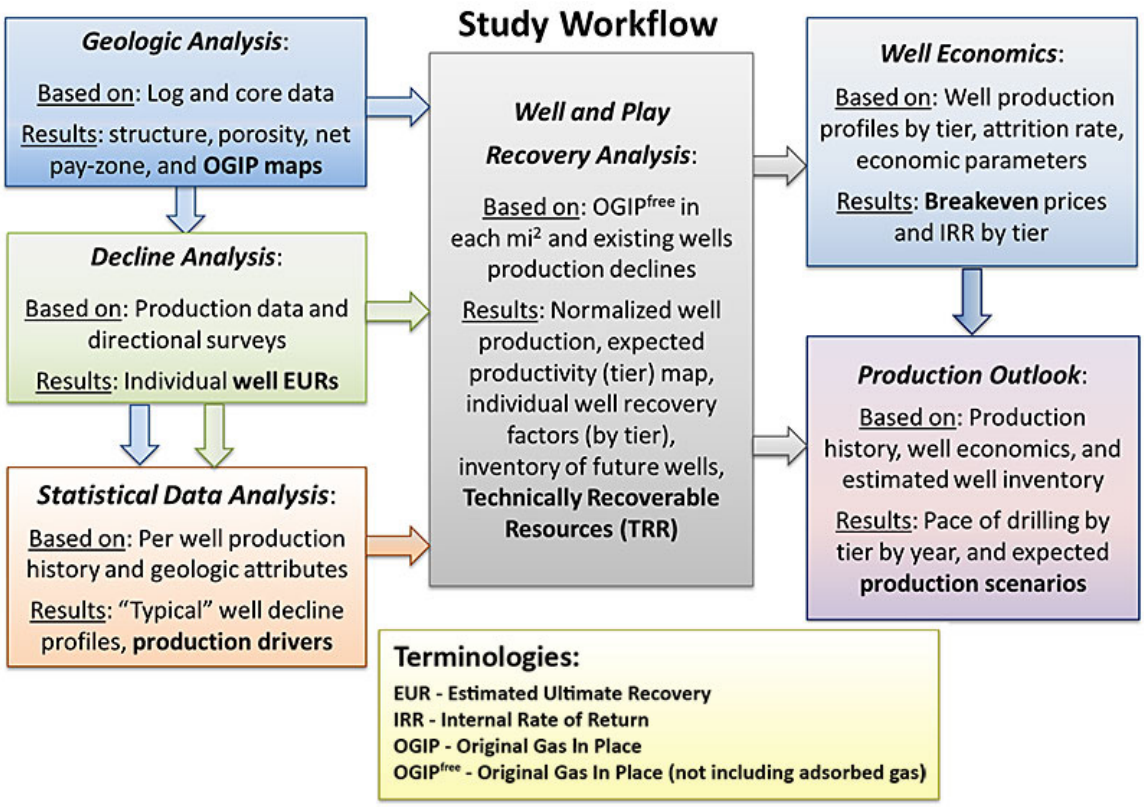

Figure 1.1: Flowchart for the BEG shale play study generated by the BEG. This has been applied to the Barnett, Haynesville, Fayetteville, and Marcellus shale gas plays and is being applied to the Eagle Ford and Bakken shale oil plays.

core samples to determine geologic parameters and map them onto a mile-by-mile square grid throughout the entire field boundary.

We use the production decline analysis included in this thesis to determine productivity for each square mile where wells have been drilled. This decline analysis builds on much of the recent literature of decline analysis, which is discussed in Section 2.3. The economic team assigns each of these square miles to a productivity tier, and those tiers are extrapolated to areas where there are no active wells that have been drilled, using geology and spatial relation to current wells.

At this point, each tier is given a potential well inventory, determined through an empirical analysis of how many wells can conceivably be fit into the acreage given. Tiers have their own individual average well production profile built from the historical and predicted production from all of the wells found in the tier. This profile has

a productivity tied to it.

Productivity multiplied by the selling price for natural gas gives the income generated by the average well in a tier. Supplementary income can come from selling longer chain hydrocarbons like ethane, propane, etc. There are several factors that come into determining the cost of a well, including the drilling and completion price, the gathering cost, maintenance, and others. All of the economics are taken into consideration to determine what the return on a well investment is, and this sets the pace at which drilling from the potential well inventory occurs.

In the model, good tiers have more wells drilled, up to the point at which the well inventory starts to shrink by some percentage (say 20% a year), and continue in this fashion until there are no more wells left. The study found that tiers that are not economic are still drilled, and gives them a lower limit of how many wells are drilled, but these tiers are never fully drilled.

Using this economic model, the BEG team has investigated each natural gas field and provided outlooks for the field's production for each year through at least 2035. They have performed sensitivity analysis on the economic variables, chief among them price, and given forecasts for several scenarios.

The group has published more than ten manuscripts of their findings. Browning et al. (2013b) and Browning et al. (2013c) give estimates of long-term production from the Barnett shale. Browning et al. (2014) provide estimates of Fayetteville shale reserves, and forthcoming articles detail the estimates of Haynesville and Marcellus shale reserves.

Numerous media outlets have reported these results as groundbreaking, and both sides of the fracking debate have used the findings to support their arguments. The media reported on the study because the Barnett, Haynesville, Fayetteville, and Marcellus fields comprise a significant portion of the total natural gas production in the U.S. Widespread drilling in shale gas fields is fairly new, and it is sufficiently different than the aforementioned sandstone and limestone fields that it is difficult to predict what the future holds. How these fields play out also has several implications for the energy industry and the environment. Forbes, The Wall Street Journal, National Public Radio, Bloomberg, and others have written about the project and its findings. For an up-to-date view of the project, publications, people, and media coverage, please look at the website `http://www.beg.utexas.edu/shale`, which is maintained by the team and is the source for much of the information presented above.

Chapter Two: Overview of previous research

"A common fallacy in much of the adverse criticism to which science is subjected today is that it claims certainty, infallibility and complete emotional objectivity. It would be more nearly true to say that it is based upon wonder, adventure and hope."

—Sir Cyril Norman Hinshelwood, Presidential Address to Classical Association, 1959

This work relies on two complementary bodies of previous research, the physics of fluids, with the tools of scaling analysis and universality, and the extensive work done by engineers on reservoir analysis. These fields are somewhat blurred, with reservoir engineering leaning heavily on the fluid mechanics tradition. This chapter is not intended to be an exhaustive overview of all fluid mechanics research nor all reservoir engineering work, but it will serve as an introduction to the methods that inform our use of scaling arguments to elucidate answers to the reservoir engineering problem of decline analysis.

2.1 Fluid mechanics

Fluid mechanics is an ancient discipline, with contributions from such luminaries as Archimedes, Isaac Newton, Blaise Pascal, and Daniel Bernoulli. Fluid dynamics in particular owes a serious debt to Newton, Bernoulli, and Pitot; the latter is responsible for the ubiquitous pitot tube used for measuring local velocity of fluids. Newton dedicated part of his *Principia* to fluid mechanics, where he discussed friction and viscosity.

Benedetto Castelli and Evangelista Torricelli, two of Galileo's students, are credited with large contributions to the discipline of hydrodynamics. Torricelli explained why a jet of water taken from a reservoir can rise to the same height as the reservoir itself. His explanation took into account his theory that air has weight, and he used this thinking to explain how a barometer works. He is considered to be the inventor of the barometer, but Galileo's work with Giovanni Battista Baliani (a well known Genoan scientist) on vacuums actually led to Gasparo Berti (an Italian astronomer)

building a barometer to test whether vacuums can exist. This work was reinterpreted by Torricelli as a test of pressure, and he changed the medium to mercury in order to make a more compact barometer in 1643.

News of this work reached France, where Pascal was studying hydrostatics. Pascal expanded Torricelli's work and used the theories to create two machines that are in very widespread use today: the hydraulic press and the syringe. Now let us skip a few centuries to 1815 and Jean Léonard Marie Poiseuille's work.

Poiseuille was a bright student at Ecole Polytechnique with an astounding list of teachers. He learned from Cauchy, Ampère, and Petit. His doctoral work on fluid mechanics required him to develop a U-tube mercury manometer capable of measuring arterial pressures for horses and dogs. He then published a series of articles in such fields as engineering, medicine, biology, and physics. However, it is for his work in blood flow that he is mentioned here. Since frogs are not particularly good experimental containers, he performed a series of studies on the flow of flow of water through tubes. An interesting note is that Cauchy actually opposed this research rather forcefully, apparently because the scientific work on hydraulics at the time involved much larger pipes and higher flow velocities than one might expect in a frog. By varying the pressure drop, length of the tubes, diameter, and fluid temperature, he was able to derive what is now known as Poiseuille's law (Sutera and Skalak, 1993).

The equation for Poiseuille's law exists in its modern form thanks to Hagenbach (1860), and for a pipe of length L and radius r reads

$$Q = \frac{\pi r^4}{8\mu}\frac{\Delta P}{L}, \tag{2.1}$$

where the ΔP is the change in pressure, μ is viscosity, and Q is the volumetric flow rate.

Essentially all of fluid mechanics is describable by the Navier-Stokes equations, including Poiseuille's law. Navier-Stokes comes from the fairly simple, but very powerful, assumptions that fluids conserve mass, momentum, and energy. Stokes started with the Euler equations and included viscosity effects in 1823, deriving the Navier-Stokes equations (Navier, 1823). Cauchy, Poisson, Saint Venant, and Stokes made several expanded Stokes' work (Gad-el Hak, 1998). Cauchy is responsible for the momentum equation that is a starting point for fluid flow equations,

$$\rho\left(\frac{\partial \mathbf{u}}{\partial t} + \mathbf{u}\cdot\nabla\mathbf{u}\right) = \nabla\cdot\sigma + \rho\mathbf{g}, \tag{2.2}$$

where σ is the stress tensor. Expanding out the stress tensor leads to Navier-Stokes.

For a compressible Newtonian fluid, the momentum equation is

$$\rho\left(\frac{\partial \mathbf{u}}{\partial t}+\mathbf{u}\cdot\nabla\mathbf{u}\right)=-\nabla p+\mu\nabla^2\mathbf{u}+\left(\zeta+\tfrac{1}{3}\,\mu\right)\nabla(\nabla\cdot\mathbf{u})+\rho\mathbf{g}, \tag{2.3}$$

where $\mathbf{g}$ is the gravity vector, μ is the viscosity, and ζ is the bulk viscosity, which is often neglected. For nearly incompressible flow this equation can be simplified by setting $\nabla\cdot\mathbf{u}=0$.

The next step forward for fluid mechanics was getting Navier-Stokes to fit and describe experiments. Ludwig Prandtl helped this endeavor with his work on boundary layers (Prandtl, 1904). He found that the friction between an object and the fluid it is moving through is confined to a small boundary layer (Anderson Jr, 2005). The idea of a boundary layer is that there is a no-slip boundary condition, so that the velocity of a fluid tangent to an object is zero, and there is some distance into the fluid where the velocity is affected. Inside this distance there are large velocity gradients and therefore a force applied on the object, and outside of this distance the gradient disappears. The length of this boundary layer for a semi-infinite plane is calculated via the Blasius equation,

$$\begin{cases} f'''+\frac{1}{2}ff''=0 \\ f|_{\eta=0}=0 \\ f'|_{\eta=0}=0 \\ \lim_{\eta\to\infty}f'\to 1 \end{cases} \tag{2.4}$$

where $\eta=y\sqrt{U/\nu x}$ is a scaled length and the velocity tangential to the surface is $u=Uf'(\eta)$. U is the velocity of the fluid away from the boundary, and ν is the kinematic viscosity of the fluid. This is a non-linear ODE, which is rather entertaining to solve numerically. A solution to the ODE with the correct value for $f''(\eta=0)\approx 0.332$ is given in Fig. 2.1.

The boundary layer concept allowed laminar flow situations to be properly investigated (Gad-el Hak, 1998).

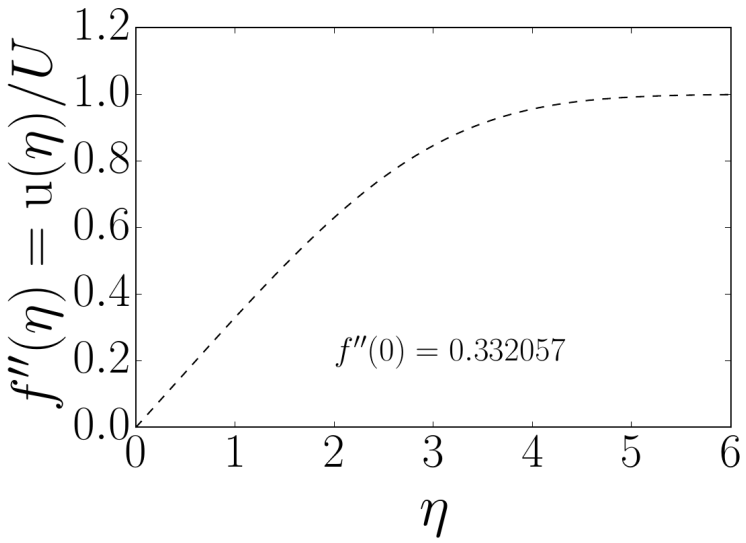

Figure 2.1: Numerical solution to the Blasius boundary layer problem (2.4). u/U is the flow velocity relative to the bulk flow velocity. The dimensionless length is $\eta = y\sqrt{U/\nu x}$. I solved this boundary value problem with a shooting method. The shooting method systematically varies the initial condition $f''(0)$ until the final condition $f'(\infty) = 1$ is satisfied. In this example $f'(10)$ is taken to be a reasonable approximation of $f'(\infty)$.

2.2 Scaling Arguments

George Stokes is also responsible for that most famous scaling quantity, the Reynolds number, having noticed this similarity in his equations. Reynolds performed experiments studying the drag problem (an inviscid fluid would be expected to apply no drag force on a sphere) and developed the similarity law, which was later popularized by Lord Rayleigh and Prandtl. Prandtl's boundary layer idea served to solve the drag problem, and he supplied the idea of a critical Reynolds number where flow in the boundary layer went from laminar to turbulent (Rott, 1990). The question of what exact conditions lead to the onset of turbulence is still under active investigation (Lemoult and Hof, 2014).

The idea of dimensionless quantities is a well-motivated one. Being able to perform calculations of a system once, then apply it to a large set of circumstances makes computational fluid dynamics (CFD) much more useful. The theory behind build-

ing dimensionless groups rests upon the Buckingham pi theorem, first developed by Bertrand (1878) to use in electrodynamics problems, then brought to fluid dynamics by Rayleigh (1892), and finally generalized independently by several scientists, including its namesake, Buckingham (1914). The idea is very powerful, but lends itself to easy abuse (Munroe, 2010). Therefore, one must take care to choose sensible dimensionless parameters.

Dimensional analysis owes a debt to James Clerk Maxwell (Roche, 1998, p 202), whose idea was that much information could be gleaned from the dimensions of calculations. In fact, according to Roche, Bohr might have been inspired to develop his atomic model because he noticed that Planck's constant has the units of an angular momentum.

Power-law relationships are close kin to dimensional analysis and focus on the concept of scale invariance. The idea is that a fundamental law does not change if its scale does. For instance, Newton's laws are accurate at any classical scale (please ignore quantum and relativistic corrections). These relationships also show up in many empirical situations where the underlying law is impossible to determine and might not even exist.

This appears to be slightly counter-intuitive. For instance, it is clearly evident that certain effects take on greater importance in some scales. If you take someone and drop them four feet, then it is an amusing practical joke, because people are accustomed to falling small distances and the cohesive forces inside their bodies are able to tolerate that fall. If you drop them 40 feet, then you get arrested for murder, because the accelerations they feel upon hitting the ground overwhelm their body's ability to tolerate. However, in this situation the laws of physics have not changed, given different scales. What has instead happened is the magnitudes of the forces inherent in these laws have changed as the scale has changed. This is the fundamental concept in most scaling factors: there are two competing properties, and the scaling factor tells which dominates. For instance, the Reynolds number compares inertial and viscosity-driven effects on a fluid.

Scaling theories are found throughout physics, and are frequently associated with phase transitions. One of the most popular vehicles physicists have used to investigate phase transitions is the Ising model (Ising, 1925). The Ising model is popular because it is very simple, and in two dimensions it exhibits a phase transition. A quick explanation of the two-dimensional Ising model is such: Imagine a 2-D lattice, where

each site is assigned a positive or negative spin. Then take a Hamiltonian with an external magnetic field interacting with each site and sites interacting with their nearest neighbors, either desiring to have neighbors with the same (ferromagnetic) or opposite (anti-ferromagnetic) spin.

The energy of the system with no external magnetic field is

$$H = -\sum_{\langle ij \rangle} J\sigma_i\sigma_j \tag{2.5}$$

where $\langle ij \rangle$ are nearest neighbors, J is the coupling constant, and σ denotes spin and can take the values 1 and -1.

Peierls (1936) investigated the phase transition in the 2-D Ising model and found "that for sufficiently low temperatures the Ising model in two dimensions shows ferromagnetism." The test for ferromagnetic behavior is a lower bound on the number of boundaries between spin 1 and spin -1 sites. The number of potential paths one can take of length L on a square lattice is

$$N(L) = 4^L. \tag{2.6}$$

Setting a limit on the area enclosed by closed boundaries and how many sites can be cut off by open boundaries shows that for low enough temperatures, the Ising model allows ferromagnetism. The spin "clumps" that appear in the Ising model at sufficiently low temperatures are now named Peierls droplets. This phase transition is seen in many very complicated systems, but arises in this simple system.

Onsager (1944) was able to develop a full solution to the two-dimensional Ising model. This solution shows a sharp transition between ordered spin clumps and disorder at a critical temperature T_c, determined by the equation $\tanh[J/k_BT_c] = \sqrt{2} - 1$.

Parallel to description of spontaneous magnetization in the Ising model was work on the liquid-vapor transition. Widom and Rice (1955) took critical isotherms and isobars for xenon, carbon dioxide, and hydrogen, and found a universal exponent for these systems. They create the dimensionless quantity $\gamma\rho_c^4 P_c^{-1}$ to describe the differential pressure dependence upon pressure and density near the critical point. This essentially introduces the idea of scaling and universality to critical phenomena. Later, Widom (1965) added nonclassical behavior of compressibility for fluids to improve the theory of surface tension near their critical point.

Kadanoff (1966) made the assumption that near the critical point of a system, where there are many fluctuations, the long-scale fluctuations are the only ones that are important. These fluctuations should dominate the short-scale fluctuations and because they behave in some universal way, one can treat a block of spin sites as a single unit and use a single effective spin inside this block. The blocks then can be described by a relatively simple set of differential equations. These equations give rise to scaling laws.

Wilson (1971) developed a renormalization group theory to describe behavior of magnetic systems near the critical point. He starts with the quantum field theory version of renormalization group theory developed by Gell-Mann and Low, and applies it to Kadanoff's theory of scaling. He calls Kadanoff's theory, "absurd [but] the basis for generalizations which are not absurd," and from the renormalization group differential equations finds scaling laws.

Not at all coincidentally, the Ising model gives rise to the same critical exponents as the boiling transition for fluids. As Wikipedia explains it, "The key observation is that at a phase transition or critical point, fluctuations occur at all length scales, and thus one should look for a scale-invariant statistical field theory to describe the phenomena."[1] There have subsequently been many analyses of scaling theory for the Ising model. Fisher (1974) compared critical phenomena that appear in magnetization to those in fluids. He explains the renormalization group approach thus: transform the Hamiltonian to a new, renormalized Hamiltonian via a renormalization group operator $\mathbf{R}$ via

$$\mathcal{H} \Rightarrow \mathcal{H}' = \mathbf{R}[\mathcal{H}].$$

$\mathbf{R}$ is designed to reduce the number of degrees of freedom in the Hamiltonian. Make certain that $\mathbf{R}$ preserves the partition function of the Hamiltonian. Rescale the correlation functions, momenta, and spin fluctuation magnitude inside the Hamiltonian. In practice, this is a difficult process. However, Fisher works through the process using a linear operator operating on the Hamiltonian near a fixed point

$$\mathcal{H}' = \mathbf{R}[\mathcal{H}] = \mathbf{R}[\mathcal{H}^* + hQ] = \mathcal{H}^* + h\mathbf{L}Q + O(h^2),$$

where $\mathbf{L}$ is the linear operator. Using this he is able to gather critical point exponents from the linearized renormalization group. He discusses that this works over large

[1] Quoted from http://en.wikipedia.org/wiki/Scale_invariance

classes of Hamiltonians, which explains why the critical exponents are the same for fluids and ferromagnets. As he puts it, "the character of the scaling functions do not depend upon the 'details' of the Hamiltonian."

Wu et al. (1976) developed a scaling theory to explain correlation functions between spin sites in the Ising model. First, there is the assumption that there is a universal function for correlation, $F(t)$, where t is the distance between points divided by the correlation length. Then they let temperature approach critical temperature and developed scaling exponents for the correlation function based $(1 - T_c/T)^{\alpha}$. This leads to a better understanding of what happens during a phase transition.

The ideas of the Ising model have also been used to examine social phenomena. Touboul (2014) has taken a statistical model very similar to the one-dimensional Ising model and extended it to include a time delay before information transmits between adjacent sites. He uses this model to explain hipster fashion. Specifically, the time delay between information arrives at the "hipster" sites causes them to misjudge the dominant fashion, which leads to a phase transition in the system where hipsters' fashions align. So hipsters are trying to be anti-ferromagnetic but failing.

Scaling theory of localization: a road map

The scaling theory of localization, developed by Abrahams et al. (1979), is of particular interest in this work. Abrahams et al. started with scaling theories of localization that were developed by Edwards and Thoules (1971).

The problem is on why electron localization might occur inside a semiconductor, an idea posited by Anderson (1958). Anderson discovered that given a random lattice, there are situations where defects at some of these sites causes a transition from electrons having extended states to localized states. This was something he discovered while working for Bell Labs on semiconductors. Semiconductors can sit on the edge of conductive (which would mean their electrons obtain extended states) and insulating through "doping" them with defects. Disorder causes a metal-insulator transition. This is the basic principle exploited for semiconductor computing. Anderson spent decades working on this problem, won the Nobel Prize in Physics for the work (and other work on magnetism), and then, *after* getting the Nobel Prize, published a solution utilizing completely different means with Abrahams.

The solution to this problem is to assume that there is a scaling law relating con-

ductance in a system to its length scale. Marder (2010, p 547) provides an explanation of Abrahams' solution this way:

1. *Assume that there is a universal function relating R to l, $R(l) = R(L/L_0)$.* This first step is the hardest. Abrahams had to take a leap of faith that he could describe conductivity by imagining a series of quantum resisters randomly hooked together.

2. *Find the quantization of resistance, $R_H \cong h/e^2$.* In order to come up with a dimensionless quantity for resistance, he wanted to use a fundamental quantity. Resistors smaller than R_H behave differently than those larger when hooked in a series, but that is not obvious from the first look.

3. *Perform analysis by considering a lattice of resistors with resistances much larger and smaller that R_H.* Now that he claims there is a function, he can make informed guesses about its form. For weak resistors at long lengths, you would expect to be able to recover the macroscopic theory of resistance, $R_d \propto L^{2-d}$. For strong resistors, it should increase exponentially, like $R \propto \exp L$.

4. *Use the ansatz that the change in the logarithm of resistance with respect to the logarithm of length $\beta_d(R)$ is smooth and monotonically increasing.* Here is the money line. The form of

$$\beta_d(R) = L\frac{\partial \ln R_d(L/L_0)}{\partial L}$$

   is guessed at. It is chosen because it agrees with step 3. Also, choosing β_d rather than R is curious. This is because in three dimensions, R does not monotonically increase; it actually has that weird behavior from step 3.

5. *From this and knowledge of the macroscopic scaling of resistance, show that in three dimensions, $\beta_d(R)$ must have certain small and large R behavior.* Plugging β_d into the results from the macroscopic theory, he finds that for small R, $\beta_d \sim 2 - d$ and for large R, it goes as the logarithm of R. This means that in three dimensions, it crosses through zero, which means that there are two branches for R.

6. *Find the universal curve that follows this behavior.* At this point, he starts drawing things. Marder (2010, p551) provides plots of the scaling function for

a three dimensional cubic lattice with some disorder, showing where disorder gets large enough to create extended states. Ahlskog et al. (1997) has measured conductivity on doped poly (phenylene vinylene) and varied the amount of doping to cause the polymer to change from an insulator to a conductor. Marder shows that the resistivity curves can be analyzed in the same way that Abrahams et al did.

This process can be distilled down into its most fundamental elements to provide a framework for solving any number of problems. In its generalized form, the procedure is thus:

1. Find two dimensionless variables of interest in a system, X and Y.
2. Assume that there is a universal function $Y(X)$.
3. Use what knowledge you have of the asymptotics and shape of $Y(X)$ to find a universal relationship between your quantities. (Guess if necessary.)
4. Profit.

When I was first presented with this strategy, I was skeptical. It seems too general to be useful. At the same time, how do you decide what Y and X are? Indeed, in developing the scaling theory that my supervisors and I used to analyze gas production, Professor Marder indicated some difficulty in deciding which dimensionless groups to use. Nevertheless, a theory of this type is effective in describing natural gas production from hydrofractured wells, though, and that is the topic of this thesis.

Scaling theories have also been of interest in the fluid and fracture mechanics fields. Barenblatt (1996) is responsible for one of the most comprehensive looks at scaling relationships. He comments that scaling laws are more important than they might at first seem, providing information about their self-similarity. In fact, without his help, we might have never published our paper on gas production.

2.3 Fluid Dynamics in Reservoirs

The most important fluid dynamics results for this work lay in work on fluid flow in reservoirs. Henri Darcy is responsible for determining the equations describing

flow through porous media (Darcy, 1856). His experiments were on flow of water through sand columns, but the results have been generalized to fluids in porous media. His experiments also did not investigate high velocity fluids — he was retired and fairly sick at the time he did his groundbreaking experiments. Dupuit (1863) and Forchheimer (1901) extended the law to include faster flow.

Darcy's law in its current form states that flow through porous media depends upon pressure p, permeability of the media to the fluid k, and viscosity of the fluid μ by the relation

$$\mathbf{u} = -\frac{k}{\mu}\nabla p. \tag{2.7}$$

This work had been picked up in the scientific community, but it was not understood by those in petroleum engineering until far later. It was Hubbert (1940), a prominent geoscientist, who wrote it in the differential form of (2.7) and used it to describe the flow of water in underground reservoirs.

The Forchheimer correction to this includes an inertial permeability k_1, which changes the equation to

$$\frac{\mu}{k}\mathbf{u} + \frac{\rho}{k_1}|\mathbf{u}|\mathbf{u} = -\nabla p. \tag{2.8}$$

The correction is required because of the formation of eddies in the pores. Chauveteau and Thirriot (1967) showed that eddies grow in the pores when the Reynolds number grows past 1, and Chaudhary et al. (2011) showed that these turbulent eddies can cause a large reduction in the apparent permeability by decreasing the advective pore volume.

Irmay (1958) derived Darcy's law and the Forchheimer law from the Navier-Stokes equation. The Kozeny-Carman equation, proposed by Kozeny (1927), then modified by Carman (1937, 1956), reveals the same result as Darcy's Law, but was derived by applying Poiseuille's equation for laminar flow to the problem of fluid flowing in a series of tubes through a packed bed of spheres.

There is another important extension to Darcy's law. The pore size in shale varies greatly, and the size of the throats between these pores can be as small as 5 nm (Nelson, 2009). Samples from organic rich Devonian shales average a pore-throat diameter of 22 nm in that study. Methane molecules are approximately 0.38 nm in size, so continuum models can break down. The Knudsen number, the ratio of the mean free path for a particle and the size of the pore $\mathrm{Kn} = \lambda/L$, is used to describe whether continuum mechanics can be used, and at this scale it approaches

1, indicating Knudsen flow. The Klinkenberg (if you're a petroleum engineer), or Knudsen (if you're not), effect is applied to account for this.

Klinkenberg introduced a correction that allows gas to slip along the pore throat wall in order for researchers to still be able to use close approximations of the continuum equations. There have been many efforts to quantify the breakdown of the no-slip boundary condition and estimate how that changes flow. Klinkenberg's definition of permeability is

$$k = Cu\mu\frac{p_1}{a}G\left(p_1^2 - p_2^2\right)^2, \tag{2.9}$$

where C is a constant required to convert units, G is a geometric factor, a is the radius of the pore throat, and p_1 and p_2 are pressures on either side of the pore throat (Klinkenberg et al., 1941).

One might wonder whether using a Klinkenberg correction is sufficient at such small scales, or whether it is better to replace continuum fluid mechanics models entirely with statistical models and molecular dynamics simulations. Roy et al. (2003) ran numerical models tested against experimental data to determine the effect of Knudsen flow on gas flux. They found that the Knudsen diffusivity varied less than 5% from the value given by the analytic solution for a nanopore with diameter 200 nm. Itaya et al. (1984) studied Knudsen flow with alumina pores of sizes as small as 10 nm and found that these are still within the Knudsen regime and do not require abandonment of continuum flow mechanics.

Javadpour (2009) analyzed how Knudsen diffusion affects gas production in detail. He determined that for pore sizes below 10 nanometers, Knudsen diffusion contributes more than 30% of gas flux. However, this effect is only readily apparent at the nanometer scale and pressures well below reservoir pressure (below 1MPa), and therefore likely only contributes significant flow near the end of the well life.

Islam and Patzek (2014) show that the Knudsen scale is not always appropriate for reservoir conditions, using PVT schemes to perform their investigation. Knudsen flow was designed for rarified gases, rather than gases at high temperature and pressure within tight confines. Though they find the effects of slip at 1 nm pore sizes and low pressure, slip effects are much smaller at reservoir pressures and typical pore sizes.

Determining how the production from wells falls over time is the field of decline analysis. Decline analysis traces its history back to Coleman et al. (1930), who developed a theory of decline in reservoir pressure as gas and oil are produced from a well,

assuming ideal gases and perfect solutions. Schilthuis et al. (1936) expanded Coleman's work to allow for real fluids. This leads to a material balance equation which is an important starting point for reservoir engineering. Schilthuis also developed the concept of a fluid reservoir as a thermodynamic engine, where the trapped gas and oil expand from their confined state to standard temperature and pressure on the surface. Therefore, one can consider the reservoir as a system with thermodynamic energy that is expended as the hydrocarbon is extracted.

Dake (1983, p 74) presents the material (volume) balance as

$$\begin{aligned}\text{Underground withdrawal} &= \text{Expansion of oil and gas}\\ &+ \text{Expansion of originally dissolved gas}\\ &+ \text{Reduction in hydrocarbon pore volume due to water}\\ &\quad \text{expansion and decrease in pore volume,}\end{aligned}$$

where underground withdrawal is the observed surface production of oil and gas. Oddly, Dake's calculation includes the influx and outflux of water into the reservoir as part of the underground withdraw term, but net water influx could be added to the right hand side. In the modern parlance of reservoir engineers, this would be called a tank model equation. As a physicist, I would call it a material balance approach.

Jones (1942) provided the prototype for empirical decline analysis, proposing that production could be predicted by fitting a line to the logarithm of decline rate versus log time.

The grand-daddy of decline curves was provided by a series of review articles written by Arps (1945, 1956). He included three curves based on solutions to the differential equation

$$\frac{1}{q}\frac{dq}{dt} = -dq^b \tag{2.10}$$

where q is the production rate, t is time, b is an empirical fitting constant related to how quickly production declines, and d is an empirical fitting constant related to the initial production. This has hyperbolic, exponential, and harmonic decline solutions, based on the value of b. These solutions are

$$q(t) = \begin{cases} q_i e^{-D_i t} & b = 0, \text{ exponential} \\ q_i(1 - bD_i t)^{-1/b} & 0 < b < 1, \text{ hyperbolic} \\ q_i/(1 - D_i t) & b = 1, \text{ harmonic} \end{cases} \tag{2.11}$$

where D_i is the initial decline rate. The decline curves are ubiquitous in decline analysis and still used in their unaltered form today. Their simplicity allows anyone, from field engineers to energy investors with access to public production data, to make an approximate estimate of how much a well will produce at a given time. These curves are also used by energy companies to report reserves estimates to the Securities and Exchange Commission.

Arps' solutions are not physical when $b > 1$, where they predict infinite ultimate production. However, attempts to fit these curves to hydrofractured shale wells often lead to b values far greater than one.

Fetkovich et al. (1980) explained both the unusual accuracy of the Arps equation in describing flowback from oil reservoirs and why it breaks down in certain reservoirs. Fetkovich derived the Arps decline curves by solving the flow equations for radial flow from a reservoir to a vertical well. He also introduced a dimensionless rate and time as scaling factors for his equations. In setting up the problem, Fetkovich assumes that there is a boundary to how far the well could draw production from, and after some time, which I will call τ, that boundary causes production to switch from transient to boundary dominated flow. After $t > \tau$, the production rate declines rapidly, following exponential decline.

Boundary dominated flow is a concept that will be referenced frequently in this work. This is the portion of the flow period where the pressure transient has traveled from the wellbore to the boundary. No flow is allowed across the boundary, which means that the flow to the wellbore is no longer transient and coming from a semi-infinite reservoir. Flow is instead from a well defined volume, and as that volume is drained, production slows.

For more on boundary dominated flow, read Walsh and Lake (2003, Chapter 9).

The Arps model is accurate only after wells have begun boundary dominated flow. Because the permeability in shale gas reservoirs is orders of magnitude less than in conventional reservoirs, these wells typically spend years in transient flow before experiencing the boundaries, whereas they spend only days or months in transient flow for conventional reservoirs.

There have been several researchers who have developed models useful for accounting for the unique flow regimes and geometry in shale gas wells. The most popular models are Stretched Exponential Production Decline (SEPD), developed by Valko and Lee (2010) (which can be derived directly from Jones (1942)), the power-law ex-

ponential decline developed by Ilk et al. (2008), and the Duong model of rate-decline linear flow (Duong, 2010, 2011).

The SEPD model is exactly what it sounds like. Time is scaled by a characteristic time, τ, leaving decline as

$$q(t) = q_i \exp\left[-(t/\tau)^n\right] \tag{2.12}$$

with n serving as the decline exponent.

The power-law exponential model is

$$q(t) = q_i \exp\left(-D_\infty t - D_i t^n\right) \tag{2.13}$$

where D_∞ is the decline rate at infinite time and n once again sets the decline exponent. Ilk et al. (2008) built this to describe unconventional (shale) wells in particular, without sacrificing usability from Arps' approach.

Rate-decline linear flow predicts

$$q(t) = q_i t^{-n} \exp\left[\frac{a}{1-n}\left(t^{1-n} - 1\right)\right] \tag{2.14}$$

where n is the slope of q/G_p (rate over cumulative production) vs time in log-log coordinates and a is the intercept. Duong's model is focused on describing wells that are in transient linear flow. To describe the full life of a well, it must switch to Arps' exponential decline after a certain point. Joshi and Lee (2013) modified Duong's model to correct this deficiency.

Other empirical and semi-empirical models have been proposed, such as the logistic growth model proposed by Clark et al. (2011). Johnston (2006) built a parallel flow model to describe production where there is a sum of exponential decays contributing to flow.

Ogunyomi et al. (2014) ties together empirical curve fitting — with the parallel flow model and logistic growth model — and numerical simulation in an integrated workflow for fitting and predicting production from shale wells. They use the empirical models to identify flow regimes, then search for relationships between production and the reservoir and well completion properties.

Probabalistic curve fitting

Jochen et al. (1996) and Cheng et al. (2005) developed probabilistic forecasting techniques for gas wells. Gong et al. (2013) applied Bayesian probabilistic decline curve

analysis to the Eagle ford oil and gas field.

Jochen et al. (1996) applied a bootstrap method using Monte Carlo analysis in two fields being water flooded, with the Arps decline curve. They use the bootstrap method because it does not require them to know the probability distribution of the parameters going into the decline curve. There is a trade-off, however, because they must assume that their model does predict reservoir performance, and, more importantly, that the data is independently distributed, with identical distributions between the bootstrap data and the general population. The bootstrap requires building several synthetic data sets from the original data, removing some original data, then fitting the decline curve to these synthetic data sets. This works well for determining the distributions of the original data, but requires that random measurement error be the reason for deviations from the decline curve, when these fluctuations are usually the result of operators adjusting, *e.g.* the bottomhole pressure or choke of the well. The greatest benefit of this method is the ability to easily quantify uncertainty.

Gong et al. (2013) sought to use a different Bayesian method that does not require bootstrapping. He was concerned about the original data being modified as part as the bootstrap process, and the lack of commercial software that utilizes these methods. Gong uses Markov Chain Monte Carlo with the Metropolis algorithm to address these concerns, while retaining the ability to quantify production uncertainty. The Metropolis algorithm uses a series of proposal (meaning test) distributions to start the method, then selects the best candidate at each iteration until the method converges on the best posterior distribution. This posterior distribution can provide P_{90}, P_{10} and P_{50} values. For those unfamiliar with this language, the P_x value has an $x\%$ chance of being exceeded. Gong uses the Arps model, Duong model, Power-law model, and stretched exponential model to provide several production forecasts in the Eagle Ford.

These Bayesian methods have not been developed for full transient flow models, due to the difficulty in simplifying physics-based models to the point where they can be used. The model I describe in this paper is sufficiently simple that it is a good candidate for Bayesian methods, and a possible problem for future work is developing a Markov Chain Monte Carlo method with the scaling model. This would bring clearly quantified uncertainty to estimates of forecasted reserves, something not often seen in industry estimates.

Transient Flow Models in Reservoirs

Transient flow models that are explicitly based on physics have also been developed. Fetkovich et al. (1980), mentioned above, tied a physics-based model using material balance and rate equations into the empirical model popularized by Arps. He was not the first, having drawn on the experience of several papers that demonstrated that exponential decline is a solution to the physical equations at large time (Moore et al., 1933; Hurst, 1934; Hurst et al., 1943; Van Everdingen and Hurst, 1949). One might claim that this is an almost obvious result, but there is a temptation to start including flow from further and further away from the wellbore, with worse conductivity, which would change the result if it were generally true (there does appear to be a limit).

Fetkovich's results have been fashioned into type curves by reservoir engineers. The idea of a type curve is that a well will produce some percentage of its total production by some time, and given the cumulative production for a well at time t, you can read off what it will have for total production. This will, naturally, be in the form of a curve. Carter (1985) demonstrated that type curves derived from flow results like Fetkovich could be used to describe well production in a range of different reservoir shapes, independent of the length of the hydrofracture wings which serve as adsorbing boundaries for the reservoir fluid. The type curves themselves were generated with a finite difference simulator working in radial coordinates.

Most of the early work in applying transient flow analysis focused on the early life of the well, when operators try to gather as much information about the hydrofracture extent and reservoir as possible by performing well tests. These tests are done by relating the early well production to the reservoir and wellbore pressures. The pressure at the bottom of the wellbore can be altered either by using pumps to artificially lower it, or by restricting how much gas can be produced via varying the choke on the wellhead.

Prats et al. (1961) analyzed the problem of flow of a slightly compressible fluid into a well with vertical fractures. Their model is that of a cylinder where the fluid can flow (no flow enters nor exits the cylinder). The wellbore is placed in the center of that cylinder and depletes the reservoir. For this setup they determine the pressure distribution around the fracture and well production at different times.

Russell et al. (1964) solved the problem of compressible fluid flow into a vertically fractured system from the reservoir. They determine the effect of a transition in flow

regimes from linear flow at early times to radial flow as the pressure transient drives further into the rock.

Gringarten et al. (1974) looked specifically at what happens at the very beginning of a well's life. Their geometry is a vertically fractured well sitting in an infinite reservoir. There are different results depending on whether the fracture wings are of infinite conductivity or allow a uniform flux along the fracture. They look at how the fracture length affects the effective well radius for these two cases and find that Russell and Truitt better matched the infinite conductivity fracture model than Prats, which I presume is a result of the former group including fluid compressibility.

Wattenbarger and Ramey (1969) investigated the effects of real gas and turbulence in well testing results. Real gas was substituted for ideal gas and simply means gas with compressibility and viscosity that vary with pressure and temperature. They find that accounting for real gas was important in interpreting the drawdown curve and early flowback.

Well testing results are not always reliable. Due to flowback of fracturing fluid, turbulent gas flow, quickly varying bottom hole pressure (the pressure at the wellbore where it is contacting the reservoir), and other factors, well testing data can be noisy and even erratic. This makes it difficult to analyze production and pressure data in the first days and months of the well, and it is worthwhile to revisit well production data as these effects lessen in intensity. There has been exhaustive research into how wells perform in this phase of their life, when they produce the majority of their ultimate resource.

There has also been analysis of wells used to "flood" a reservoir with water, increasing pressure and pushing the oil to production wells. Patzek (1992) used the material balance equation and Darcy's law to investigate the performance of water injection wells. He found that injection rates for hydrofractured wells followed the inverse of the square root of time.

Palacio and Blasingame (1993) developed a type curve analysis that was more rigorous than previous methods. They take Fetkovich et al. (1980) and Carter (1985) and modify these curves, using a new algorithm to allow liquid decline curves to be used to predict gas decline and calculate the gas in place from a matched type curve.

This equivalence between liquid and gas decline curves is only possible if one uses a pseudopressure transform for gas, such as the one done by Al-Hussainy et al. (1966). The essential idea of this pseudopressure is that one can replace the combi-

nation of pressure, viscosity, and gas expansion factor with pseudopressure by taking an integral, which greatly simplifies the flow equations for real gas. The diffusion equation for this pseudopressure is identical to the equation for diffusion of pressure for a slightly compressible fluid (such as water or oil).

The basic concept applied by Al-Hussainy et al. has also been developed to study heat transfer by several researchers, among them Joyce (1975), Lally et al. (1990), and Bonani and Ghione (1995), which I will present as an analog. Fourier's law for heat transfer is generally written as

$$q = -\kappa \nabla T, \tag{2.15}$$

saying that heat flow is equal to conductivity times the negative gradient of temperature. Conservation of heat states that

$$\nabla q = \alpha \frac{\partial T}{\partial t} \tag{2.16}$$

in a system where no external heat is added. Because the conductivity, κ, is dependent upon temperature, this differential equation is nonlinear unless one applies a Kirchoff transformation to remove the dependence of κ on temperature. This integral transformation takes the form

$$\theta = T_s + \frac{1}{\kappa_s} \int_{T_s}^{T} \kappa(T') dT', \tag{2.17}$$

where θ is now the pseudo-temperature calculated relative to a reference temperature T_s. Performing a similar transformation on time through the integral

$$\kappa_s \tau = \int_0^t \kappa(\theta) dt \tag{2.18}$$

generates a completely linear PDE,

$$\alpha_s \nabla^2 \theta = \frac{\partial \theta}{\partial \tau}, \tag{2.19}$$

where α_s is the diffusivity at the reference temperature and τ is the pseudo-time. Al-Hussainy et al. used this procedure to linearize pressure diffusion equations.

Consider a model where hydrofracture treatment has been used to generate a stimulated area with higher permeability to flow. Most solutions for hydrofractured wells expect that at long time, gas starts flowing from the unstimulated reservoir

into the stimulated region. This would make three relevant regimes: flow from the fractures into the well, flow from the stimulated reservoir into the fractures, and flow from the unstimulated reservoir into the stimulated reservoir. The last of these could be like the radial flow seen in high permeability reservoirs, or linear.

Wattenbarger et al. (1998) generated solutions to linear flow into fractured wells, where there is no switch into a radial flow geometry. They formulate the problem this way because there are observations that wells in low-permeability gas reservoirs reach drainage boundaries before the well can enter radial flow. Essentially, these wells have hydrofractures that reached the limits of the no-flow boundary. Two regimes exist in this model: initial transient flow in one dimension, and boundary-dominated flow. When the boundary-dominated flow begins, they can calculate the original gas in place (OGIP), but this is not enough information to find permeability, porosity, nor fracture height. The geometry is precisely the same as in the model presented in this dissertation, and is shown in Fig. 2.2. However, Wattenbarger et al. derived their solutions for a slightly compressible fluid.

Lewis and Hughes (2008) extended Wattenbarger's work to include compressible gas and included the effects of desorption of gas from the rock matrix into the pore space. They modeled production based on a dual porosity model, called such because the porosity (and therefore rock flow properties) are different for the matrix and the fracture network. It is necessary to model production in such a way because flow through the matrix is several orders of magnitude slower than flow through the fracture network.

Al Ahmadi et al. (2010) investigated the models that fit linear flow and describe certain relationships between hydraulic fractures and rock in the matrix. They present ways these models can be used to provide useful information about the fracture network. Particularly, they derive an area of the fracture-matrix interface to use as a proxy for hydrofracture treatment effectiveness.

Kelkar (2008) reviews all stages of gas recovery, from the motivation for producing natural gas to how wells are drilled and completed, to how gas flows in the reservoir, to what happens when gas is brought to the surface. In his discussion of decline analysis, he reviewed the work from Carter, Van Everdingen, Fetkovich, and others, but focused on transient flow without boundary effects.

Lee and Sidle (2010) offered a review of the most common methods used for estimating gas reserves. The major methods they review are volumetric and material

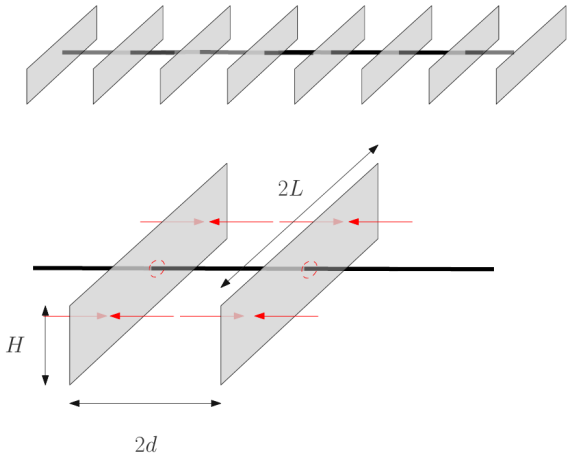

Figure 2.2: Schematic of a shale well with a series of large, planar hydrofractures (gray). Hydrofractures have bi-wings of total length $2L$, height H, and spacing $2d$. The well drains fluid in between the hydrofractures, which have a higher permeability than the virgin reservoir because of the violent nature of the hydrofracture process. The fluid flows horizontally and normal to the hydrofractures. Once inside the hydrofracture plane, fluid flows approximately radially to the wellbore (black). This happens on a much faster timescale than flow to the fractures. Taken from Patzek et al. (2014).

balance models, empirical decline curves, and type curve building and fitting. Among their conclusions is a call for researchers to put a high priority on understanding the physics behind production. This would improve the type curves used and shrink the uncertainty in reserves estimates.

Silin (2011); Silin and Kneafsey (2012) performed a full decline analysis model including compressible gas flow. They start with an examination of the shale pore structure and develop an analytic solution for pseudo-pressure diffusion, Then they apply Darcy's law to arrive at a decline curve. This work is very closely related to mine, so let me provide an overview of their calculations. Another investigation of decline analysis was done by Nobakht et al. (2011).

The starting point for building a linear flow model is the material balance equation. In a natural gas reservoir, there are three processes that can change the material balance: flow via Darcy's law or Forchheimer's law, expansion or contraction due to local pressure changes, and gas desorbing from the rock matrix. For a given flow $\mathbf{u}$, porosity ϕ and density ρ, this equation becomes

$$\frac{\partial \phi \rho}{\partial t} + \rho_0 \frac{\partial \rho_R S_R f(p)}{\partial t} + \nabla \cdot \rho \mathbf{u} = 0 \tag{2.20}$$

with $f(p)$ being the pressure-dependent adsorption/desorption. Silin and Kneafsey then use Darcy's law to set $\mathbf{u}$, rearrange terms, and assume that matrix density ρ_R is constant across pressures. They define a pressure-dependent compressibility $c_\phi(p) = \partial\phi/\partial p$. This is necessary because they assume a constant total stress; when gas is depleted, that stress must deform the rock. Gas desorption is described by $c_f(p) = \partial f/\partial p$. This leads to the equation

$$\left[c_\phi \rho + \phi F'(p) + \rho_0 \rho_R S_R c_g(p)\right] \frac{\partial p}{\partial t} = \nabla \cdot \left(\frac{k\rho}{\mu(p)} \nabla p\right) \tag{2.21}$$

where the right side is flow, and the left side is porosity contraction and desorption. F here denotes the Z-factor for compressibility of pressure; the authors assume $F(p) = c_g p$. Taking this linear-compressibility assumption, using a linear adsorption isotherm, and neglecting compression of the rock, they arrive at the final continuity equation

$$2\left(c_g \phi + \rho_0 \rho_R S_R c_f\right) \frac{\partial p}{\partial t} = \nabla \cdot \left(\frac{k}{\mu} \nabla p^2\right) \tag{2.22}$$

Free gas comes from $c_g\phi$, and adsorbed gas from $\rho_0 \rho_R S_R c_f$. They then go into great detail solving this differential equation for an initial value problem with the fracture

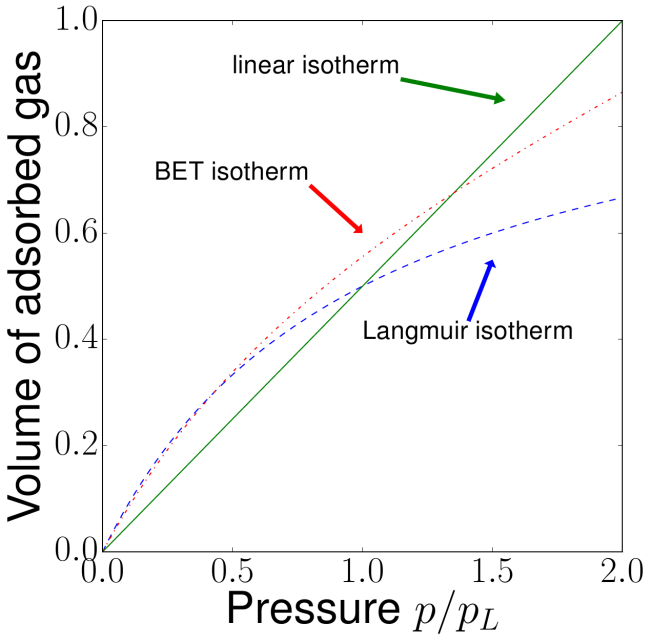

Figure 2.3: Comparison between the fraction of the total volume of gas stored in the matrix predicted by the Langmuir, BET, and linear isotherms. The linear isotherm overestimates the gas in the matrix above the Langmuir pressure, p_L. The BET isotherm follows the Langmuir isotherm at low pressure, but deviates at high pressure.

face serving as an adsorbing boundary and the midpoint between fractures serving as a no-flow boundary. The resulting decline curve is a double-decline-rate model. There are two flow regimes, the initial transient linear flow characterized by production rate q following $q \propto 1/\sqrt{t}$, and boundary-dominated flow described by $q \propto e^{-\alpha t}$ with α depending on physical parameters.

Adsorption

Bumb et al. (1988) addressed the contribution from adsorbed gas for Devonian shales. They find that gas desorbes from the matrix following a Langmuir isotherm. To reiterate, Silin and Kneafsey instead choose a linear adsorption isotherm in order to simplify their solution to the point where it can be derived analytically. The isotherms are compared in Fig. 2.3, along with an alternate isotherm that comes from the Brunauer–Emmett–Teller theory.

Langmuir (1918) developed the Langmuir isotherm from studies of the adsorption of gases onto planar surfaces. His work shows that adsorption onto a surface can be modeled by assuming that there are a series of identical sites that gas can adsorb onto, and there are no interactions between those sites. For this model, each site can hold either zero or one molecules, so there is no multilayer adsorption. Brunauer et al. (1938) allow multiple molecules as a generalization of Langmuir's theory, to explain results that they saw of adsorption of several gas species onto charcoal.

Comparing the Langmuir isotherm to adsorption values reported in industry is a good exercise. Offering rough, order of magnitude estimates, the porosity of a rock system can be described by the equation

$$\phi = n_{pores}\frac{4}{3}\pi r^3, \tag{2.23}$$

where n_{pores} is the number density of pores and r is the characteristic pore radius. The area for a pore is $4\pi r^2$, so the area of pore space in a volume of rock is

$$A = 3\phi V_{rock}/r. \tag{2.24}$$

The maximum number of methane molecules adsorbed onto the pores is $n_{gas} = A/l^2$, for a lattice spacing l. Lattice spacings for methane are approximately 0.418 nm (Press, 1972). Combining equations, I reach an expression for the number of methane molecules, n_{gas}

$$n_{gas} = 3\phi\frac{V_{rock}}{rl^2}. \tag{2.25}$$

The Langmuir isotherms reported in industry are given in cubic feet of natural gas at standard temperature and pressure per ton of rock. To convert the available space for methane molecules to a volume, I apply the ideal gas law,

$$PV_{gas} = n_{gas}k_BT. \tag{2.26}$$

At standard temperature and pressure (20°C and 101.3 kPa) the Z-factor is $Z = 0.998$ for methane, and the ideal gas law is appropriate. Plugging (2.25) into (2.26) and solving for the volume of potential adsorbed gas at standard temperature and pressure yields

$$V_{gas} = 3\phi V_{rock}\frac{k_BT}{Prl^2}. \tag{2.27}$$

The shale found in natural gas reservoirs has a density of approximately two metric tons per cubic meter McCulloh (1967). A typical porosity for shale gas fields is

$\phi = 0.1$. The characteristic size of shale pores is more difficult to pin down, with Kuila and Prasad (2013) claiming that most pores are below 50 nm, while Loucks et al. (2009) claims that the median pore size is 100 nm. With a pore size of 100 nm, the adsorbed gas is 5.7 cubic meters of gas per cubic meter of rock, which translates to 101 scf/ton.

Heller and Zoback (2014) measure methane adsorption isotherms from several of the fields studied in this thesis. They find very good fits to the Langmuir isotherm model for cores from the Barnett, Marcellus, and Eagle Ford fields. The highest Langmuir volume they measure is for a core from the Barnett field, with $v_{L,gas} = 75$ scf/ton.

Both initially free and initially adsorbed gas contribute to the total gas produced. To answer the question "How important is adsorbed gas?" I need a direct comparison between the two. In the Barnett, the median well experiences a gas pressure of around 3,500 psi and has a porosity of 6%, which leads to a volume slightly less than 200 scf/ton of free gas. This makes free gas two and a half times more abundant than adsorbed gas in the Barnett at typical values.

The precise equation for ratio of free to adsorbed gas is

$$\frac{n_{adsorbed}}{n_{free}} = 3 \left. \frac{Z_g k_B T}{r l^2} \right|_{\text{initial reservoir conditions}} . \tag{2.28}$$

There is another check, because Ross and Bustin (2009) have reported surface area estimates for some shales. They see effective surface areas of ~ 10 m^2/g. Comparing that to (2.25) for 100 nm diameter pores leads to an area of 7.5 m^2/g, which is the correct order of magnitude.

In the Marcellus, with a higher average pressure (4,000 psi) and gas filled porosity (0.1), the free gas volume is approximately 400 scf/ton. Yu et al. (2014b) analyze gas adsorption in the Marcellus shale. They give adsorbed gas storage capacities from 100-200 scf/ton. This is one fifth to one third of the total gas in place. Furthermore, they find that the BET isotherm better describes desorbtion than the Langmuir isotherm.

The BET isotherm differs from the Langmuir isotherm because it allows sites to be occupied by multiple layers. This was proposed by Brunauer et al. (1938) and offers the isotherm

$$v = \frac{v_L C p}{(p_s - p)[1 + (C-1)p/p_s]} \tag{2.29}$$

where v_L is now the maximum adsorbed gas volume for a monolayer (identical to the Langmuir volume), p_s is the gas pressure at saturation, and C is a constant that relates the heat of adsorption for different monolayers of gas.

Langmuir isotherms show desorption occurring at the end of life for wells, where pressure is fairly low (below the Langmuir pressure). BET isotherms, on the other hand, allow desorption at higher pressures and therefore earlier in the lifetime of the well. The fits to production shown later in this work do not require using the BET isotherm, but it could easily be incorporated if the effect of gas adsorbed onto multilayers is necessary to describe production or gas in place estimates.

Reservoir Simulations

As computational power has increased, it has become far easier to perform full reservoir simulations. Lee and Sidle (2010) and Kelkar (2008) have both provided extensive reviews of the current methods of numeric simulation. Lee notes that the limitations of these models include lack of understanding about the basic physics affecting flow. The prevalence of Knudsen flow, accuracy of effective medium theory in describing shale conductivity, and influence of Forchheimer flow are all under debate. Even the geometry of hydrofractures is uncertain.

Other limitations of full-scale reservoir simulation include difficulty in measuring reservoir properties with the granularity necessary for accurate model inputs, and the computational and time expenditures necessary for running these models. However, they can be used to provide reasonable bounds on reservoir properties using history matching to existing wells, and might be able to provide resource in place estimates.

There are several software packages used by companies to perform simulations. The most popular are the closed source software packages CMG, offered by the Computer Modelling Group, and ECLIPSE, maintained by Schlumberger. These suites both offer a black oil simulator, a compositional simulator, and a thermal simulator. Black oil simulators can handle flow for oil, gas (both dissolved and free), and water in the reservoir. Compositional simulators consider natural gas of different species and allow gas to condense into liquid below its dew point. Thermal models are used to model heavy oils that require steam to be injected into the formation in order to flow. Compositional simulators are the most common choice for shale gas reservoirs.

Among the variables that one can modify for simulators are initial reservoir pres-

sure, bottom-hole pressure, reservoir temperature, gas viscosity, thickness of the reservoir, matrix porosity, gas saturation inside the porosity, rock compressibility, fracture height, fracture locations, fracture conductivity, matrix permeability, and wellbore length. Several solvers can take first guesses at these properties and vary them to match known production from a well.

Reservoir simulations have been used to investigate several problems in shale gas. Yu et al. (2014a) studied how the geometry of hydraulic fractures can change production from shale gas wells, using CMG. The pressure distribution after 10 years for several cases is provided in Fig. 2.4. Yu et al. found that, given this geometry, longer half-lengths for outer fractures increased production more than longer half-lengths for inner fractures.

Due to the large number of wells I had to investigate over the course of this research (approximately 47,000 gas wells), it was not practical to use reservoir simulations to forecast well production. In some cases, in order to probe the likely physics of flow in the reservoir or spot-check results of my analysis, simulations were run by Wei Yu, Amin Ettehad, and Amin Gherabati. Wei gave estimates for time to interference in the Fayetteville, Amin Ettehad compared production estimates in the Marcellus, and Amin Gherabati investigated the effects of multiphase flow in the Eagle Ford. These were all compositional simulations, using one of the two above-mentioned simulators.

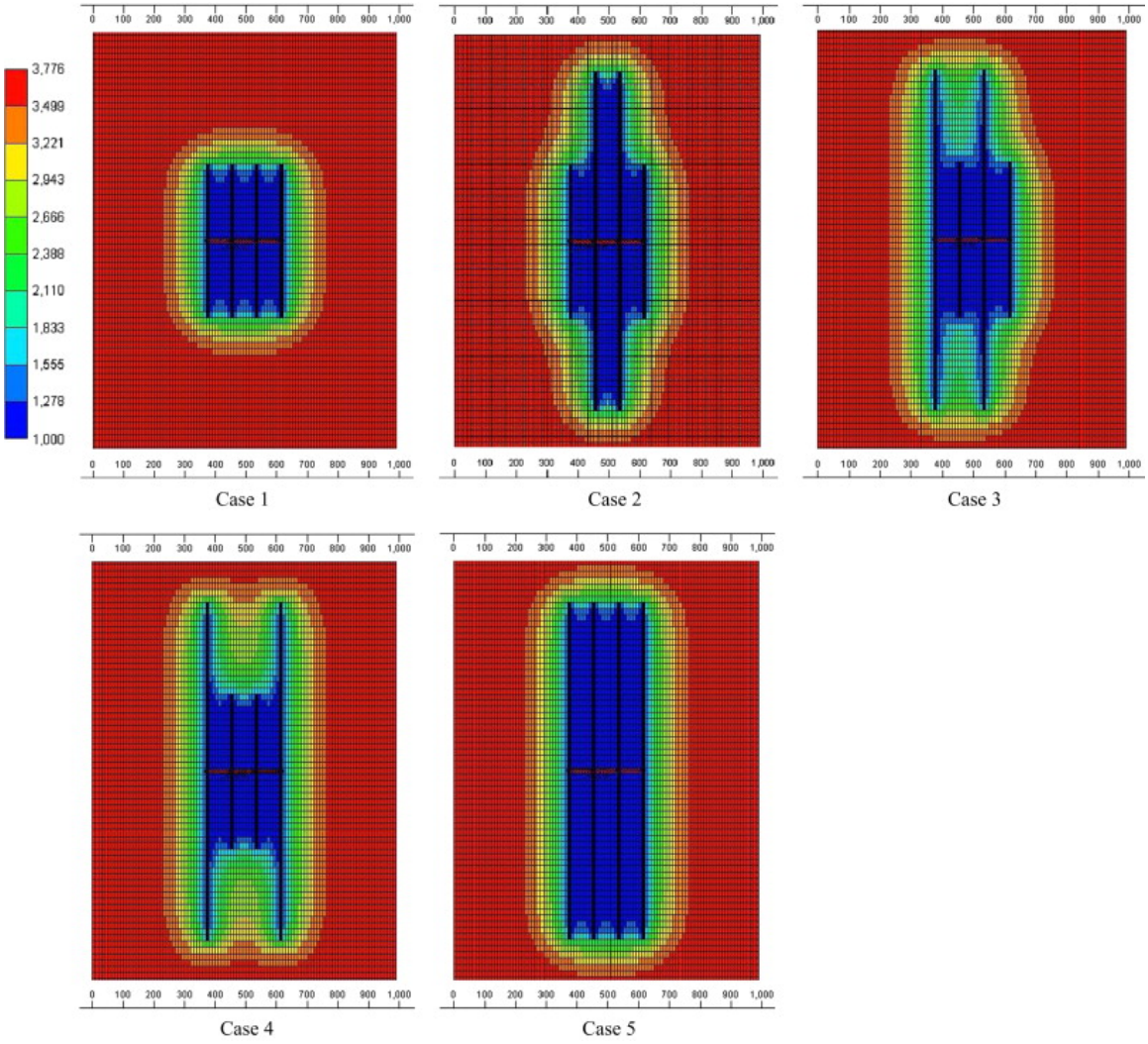

Figure 2.4: The pressure distribution around a well and hydrofractures after 10 years of production. The wellbore is red and hydrofractures black. Pressure is given in psi, and distances are in feet. The length of various hydrofracture wings was varied between cases. The fracture spacing is approximately 200 ft, and fracture half-length varies between 250 ft and 550 ft. This figure is reproduced from Yu et al. (2014a, Fig. 12)

Chapter Three: Scaling Solution of a one-dimensional nonlinear model

"Fashion models and financial models are similar. They bear a similar relationship to everyday world. Like supermodels, financial models are idealized representations of the real world; they are not real; they don't quite work the way that the real world works. There is celebrity in both worlds. In the end, there is the same inevitable disappointment"

—Satyajit Das, *Traders, Guns & Money*

The model used in this work for analyzing gas production is far simpler than most currently used models.[1] This is due to a set of simplifying assumptions and relaxing the requirement that the final result be an analytic expression. The simplifying assumptions are necessary to prevent the results from being a full, three dimensional reservoir model, such as in Sec 2.3. These assumptions also make it easier to determine how changes in the parameters affect production.

The first assumption is that flow can be described with a one-dimensional model. For this to be true, the pressure in the rock between hydrofracture planes must be dependent only upon the distance to the nearest hydrofracture. If this is satisfied, then the gradient of pressure, which determines the direction of flow, will have only one vector component.

Also, there must be no contribution from the area outside of the hydrofracture planes. This assumption is justified because the permeability of the rock outside of the area between hydrofractures is vanishingly small. Laboratory measurements of the permeability of rock give values on the order of nanodarcys Vermylen (2011). For comparison, the rock inside the hydrofracture planes has an effective permeability of microdarcys. I will call the volume of rock in between the hydrofracture planes the stimulated reservoir volume (SRV), after Mayerhofer et al. (2008).

[1]This model has been derived in Patzek et al. (2013, 2014). Patzek chose the flow geometry and derived the flow equations. Marder determined the best scaling parameters. All authors were involved in designing research, performing research, and analyzing data. I extended the model to include gas desorption and allow for arbitrary gas mixtures in Male et al. (2014).

Briefly, the idea of an SRV is that during the hydrofracture process a large volume of rock is rendered more permeable to flow. There are two competing mental models for how this happens, and they both create the same flow situation. Fig. 2.2 is the basis for one mental model. In this picture, there are large, planar hydrofractures created by the water and held open by sand. The area in between the hydrofractures is made more permeable during the hydrofracture process. This could be because the process breaks bonds and connects pores in the rock matrix. The volume of enhanced permeability is drained during the lifetime of the well, with the pressure front traveling tens of meters over years.

In the second mental model, the water creates a highly ramified fracture structure which fills the SRV. This fracture structure drains the very low permeability rock that it contacts, and the pressure front only travels meters away from the fractures over years. These two mental models are virtually indistinguishable using current methods. I will use the first mental model to motivate decisions in the derivation in the interest of simplicity, but the second model is equally valid, and leads to the same equations describing flow.

In addition to flow being one-dimensional, the hydrofracture planes must have near-infinite conductivity. This is a reasonable assumption if the permeability inside the hydrofracture plane is much larger than the permeability of the stimulated region.

The starting point is the mass balance equation for gas in a porous rock.

$$-\frac{\partial}{\partial x}\left(\rho_g u_g\right) = \frac{\partial}{\partial t}\left[\phi S_g \rho_g + (1-\phi)\rho_a\right], \tag{3.1}$$

where ρ_g is the density of the free gas, u_g is the gas velocity, S_g is the gas saturation, ϕ is porosity, and ρ_a is the density of adsorbed gas (given in kilograms of gas per cubic meter of rock matrix). The free gas density for a real gas is described by

$$\rho_g = \frac{M_g p}{Z_g R T}, \tag{3.2}$$

where M_g is the molecular mass, R is the universal gas constant, 8,314.462 J/mol·K, and Z_g is the compressibility factor, and T is the temperature. The compressibility factor is the ratio of the molar volume of a gas to the molar volume of an ideal gas at the same conditions. It is equal to one for ideal gas.

Applying Darcy's law (2.7) to the mass balance equation to replace the gas velocity and using the chain rule to make p the independent variable, we obtain a nonlinear

partial differential equation,

$$\frac{\partial}{\partial x}\left(\frac{k\rho_g}{\mu_g}\frac{\partial p}{\partial x}\right) = \phi S_g \frac{\partial \rho_g}{\partial p}\frac{\partial p}{\partial t} + (1-\phi)\frac{\partial \rho_a}{\partial \rho_g}\frac{\partial \rho_g}{\partial p}\frac{\partial p}{\partial t}, \tag{3.3}$$

which requires the assumption that the porosity does not change over time. Dong et al. (2010) investigated the dependence of porosity on pressure, and it is very weakly dependent, decreasing by 10–20% when the confining pressure of the shale is increased from 3 to 120 MPa. For comparison, in shale gas reservoirs, the pore pressure starts at 20 to 40 MPa and drops to 2 MPa over the lifetime of the well.

To simplify this PDE, we introduce the isothermal compressibility of gas and the isothermal differential equilibrium partitioning coefficient of gas. Compressibility is

$$c_g = \frac{1}{\rho_g}\left(\frac{\partial \rho_g}{\partial p}\right)_T = \frac{1}{\rho} - \frac{1}{Z_g}\frac{\partial Z_g}{\partial p}, \tag{3.4}$$

and the differential equilibrium partitioning coefficient is

$$K_a(p,T) = \left.\frac{\partial \rho_a}{\partial \rho_g}\right|_T. \tag{3.5}$$

Adding these to the right side of (3.3), we arrive at the general nonlinear PDE

$$\frac{\partial}{\partial x}\left(\frac{k\rho_g}{\mu_g}\frac{\partial p}{\partial x}\right) = \left[\phi S_g + (1-\phi)K_a\right] c_g \rho_g \frac{\partial p}{\partial t}. \tag{3.6}$$

At this point we use the Kirchhoff transformation first applied to gas flow by Al-Hussainy et al. (1966), replacing pressure with real gas pseudopressure via the integral

$$m(p) = 2\int_{p^*}^{p} \frac{p'}{\mu_g Z} dp' \tag{3.7}$$

where p^* is the reference pressure. This is invertible to provide a $p(m)$. To simplify the later numerical calculations, set p^* to the pressure at the fracture face. Using this in the general PDE and canceling out density, the equation becomes

$$\frac{k}{\mu_g}\frac{\partial^2 m(p)}{\partial x^2} = \left[\phi S_g + (1-\phi)K_a\right] c_g \frac{\partial m(p)}{\partial t},$$

which we further simplify by introducing the diffusivity, defined as

$$\alpha(p) = \frac{k}{\left[\phi S_g + (1-\phi)K_a\right]\mu_g c_g}, \tag{3.8}$$

to arrive at

$$\frac{\partial m(p)}{\partial t} = \alpha(p)\frac{\partial^2 m(p)}{\partial x^2}. \tag{3.9}$$

In order to solve this numerically, set an initial pseudopressure, m_i, and boundary conditions for $x = 0$, $x = d$. The initial pseudopressure is

$$m[p(x, t = 0)] = m(p_i), \tag{3.10}$$

and the pseudopressure at the fracture face is

$$m[p(x = 0, t)] = m(p_f). \tag{3.11}$$

To indicate that the box is of finite size, set the gradient of the pseudopressure midway between hydrofractures to zero

$$\left.\frac{\partial m}{\partial x}\right|_{x=d} = 0, \tag{3.12}$$

which makes this a no-flow boundary, because flow is proportional to the gradient of pressure. In order to describe all gas wells of a given gas equation of state and initial and fracture pressure, we redefine this set of equations in a scaled form.

Choosing the scaling terms is a most laborious process. Justifying these scaling terms *post hoc* is far easier, so I will address how the scaling terms are justified. The three most important considerations for a well are:

1. How much hydrocarbon is down there?
2. How much hydrocarbon can you get?
3. How quickly can you get it?

The answers come in the form of a volume of gas, a volume of gas, and a rate (or, better, a time), respectively. Because the first two questions have answers in the same units, only one should be picked.

Because the answers to the first two considerations are in the same units as cumulative production, it is clear that the production curve should be scaled by one of these answers. Then, it is a matter of preference whether to scale production by the ultimate production or the gas in place. Gas in place estimates are readily available (if not necessarily reliable) and can be used to calculate recovery factors, so gas inside the SRV, which will be called $\mathcal{M}$, can be used to scale production.

Now that it has been decided that production is scaled, it doesn't make particular sense to also scale by rate. This appears to be some sort of scaling of the scaling, which obfuscates analysis. Instead, and in keeping with the spirit of Fetkovich et al. (1980), making time dimensionless is logical. Looking at the work of Silin (2011), the best time to scale by is the time to boundary dominated flow.

Now, to formalize this thinking. The first scaling is

$$\tau = d^2/\alpha_i, \tag{3.13}$$

the characteristic time to interfracture interference, also known as the time to boundary-dominated flow. This time is dependent upon the gas diffusivity at the initial reservoir pressure and the distance between hydrofractures d. The second scaling is

$$\mathcal{M} = (N+1)4LHd\left[\phi S_g \rho_g(p_i) + (1-\phi)\rho_a(p_i)\right], \tag{3.14}$$

the original mass of gas in place, where N is the number of hydrofracture stages and the densities of free and adsorbed gas are taken at the initial reservoir pressure.

Dimensionless time, distance, and pseudopressure are defined as

$$\begin{aligned} \tilde{t} &= t/\tau, \\ \tilde{x} &= x/d, \\ \tilde{m} &= \frac{1}{2}\left(c_g p \mu_g Z/p^2\right)_i m(x,t). \end{aligned} \tag{3.15}$$

The new transport equation and boundary conditions then read

$$\begin{aligned} \frac{\partial \tilde{m}}{\partial \tilde{t}} &= \frac{\alpha}{\alpha_i}\frac{\partial^2 \tilde{m}}{\partial \tilde{x}^2} \\ \tilde{m}(\tilde{x}, \tilde{t}=0) &= \tilde{m}_i \\ \tilde{m}(\tilde{x}=0, \tilde{t}) &= 0 \\ \left.\frac{\partial \tilde{m}}{\partial \tilde{x}}\right|_{\tilde{x}=1} &= 0. \end{aligned} \tag{3.16}$$

The scaled pseudopressure evolution over time given these equations is given in Fig. 3.1. I solved this system of equations by writing a Python program that performed timestep integration of the PDE with a fully implicit solver that uses the variable coefficient ODE solver VODE library provided by SciPy. My program computes the scaled pseudopressure Laplacian with a second order finite differences solver I implemented in Fortran 95.

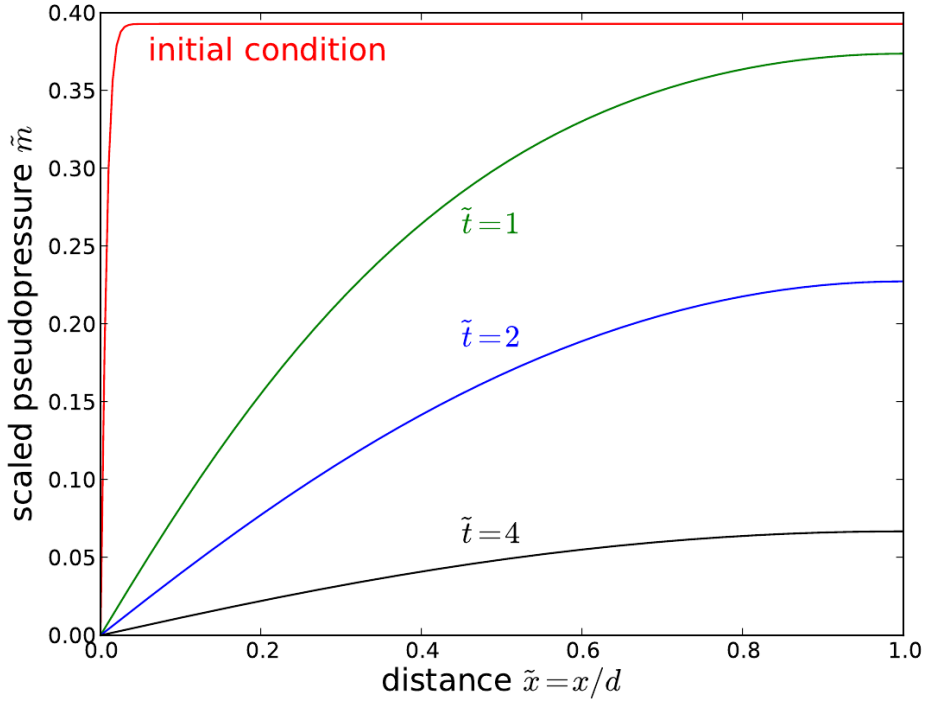

Figure 3.1: Scaled pseudopressure profiles over time, a numeric solution to (3.16). The fracture face is at $\tilde{x} = 0$, and the midpoint between fractures is at $\tilde{x} = 1$. This example is for a Marcellus well in the rich gas region with an initial reservoir pressure of 5000 psi and a fracture pressure of 500 psi. The rich gas region is called such because it has larger ethane and propane proportions than regular, "dry" gas composed almost entirely of methane. This region covers much of southwestern Pennsylvania and West Virginia. Desorbed gas contributes to the mass balance of this well, which has a Langmuir pressure of $p_L = 710$ psi and a Langmuir volume of $v_L = 119$ standard cubic feet of natural gas per imperial ton of rock (scf/ton).

In order to convert between scaled pseudopressure and unscaled regular pressure, I use a Matlab (Mathworks) program written by Akand Islam (Male et al., 2014). This is a PVT package which uses the Peng-Robinson equation of state (EOS) on a natural gas mixture to determine the PVT properties (Redlich and Kwong, 1949). The PVT package is designed such that given a composition of several species of gas $\mathbf{y}$, including hydrocarbon chains up to hexane, oxygen, nitrogen, helium, and carbon dioxide, it finds the density ρ and compressibility factor Z for a set of pressures, temperatures, and volumes. Viscosity μ is calculated by Lee's formulae (Lee et al.,

1966). Isothermal compressibility c_g is calculated from the formula given by Matter and Brar (1975).

Now, given a solution to that system of equations, I can get instantaneous production at a fracture face by finding the slope of the scaled pseudopressure at $x = 0$,

$$q = 2HL\rho(p_f)\frac{k}{\mu(p_f)}\left.\frac{\partial p}{\partial x}\right|_{x=0} = HLk\frac{M_g}{RT}\left.\frac{\partial m}{\partial x}\right|_{x=0}. \tag{3.17}$$

Gas flows into the fracture from both the $-x$ and $+x$ direction, so production should be doubled. Then consider a full complement of N hydrofractures inside the stimulated reservoir volume. This can be simplified even further by converting to dimensionless distance and using the scaling terms τ and $\mathcal{M}$ from (3.13) and (3.14). The gas mass flow rate, then, for all hydrofractures from the stimulated reservoir volume, is

$$q = \frac{\mathcal{M}}{\tau}\left.\frac{\partial m}{\partial \tilde{x}}\right|_{\tilde{x}=0}. \tag{3.18}$$

Production rates for real gas wells can be erratic, and I am interested in how much gas is ultimately recovered from each well, so I integrate this over dimensionless time and introduce the recovery factor, RF. Cumulative production is given by Q. This leads to the result

$$\frac{Q}{\mathcal{M}} = \mathrm{RF}(\tilde{t}), \qquad \text{where} \qquad \mathrm{RF}(\tilde{t}) \equiv \int_0^{\tilde{t}} \left.\frac{\partial \tilde{m}}{\partial \tilde{x}}\right|_0 (\tilde{t}')\, d\tilde{t}' \tag{3.19}$$

Recovery factor is a function of the time $\tilde{t}$, initial and fracture pressures, p_i and p_f, the gas composition $\mathbf{y}$, and the temperature T. The recovery factor and recovery rate are sketched out for one particular case in Fig. 3.2. This case is similar to those for other fields and wells, which will be shown in subsequent chapters. Each well is matched to the recovery factor curve for its reservoir properties in order to estimate its $\mathcal{M}$, τ, and estimated ultimate recovery (EUR).

Coming back to the questions posed above, the three most important questions (and answers) for a well are:

1. How much hydrocarbon is down there?
   The total gas inside the SRV is $\mathcal{M}$

2. How much hydrocarbon can you get?
   The fraction of gas that can be produced is $\mathrm{RF}(\infty)$ (at least in theory)

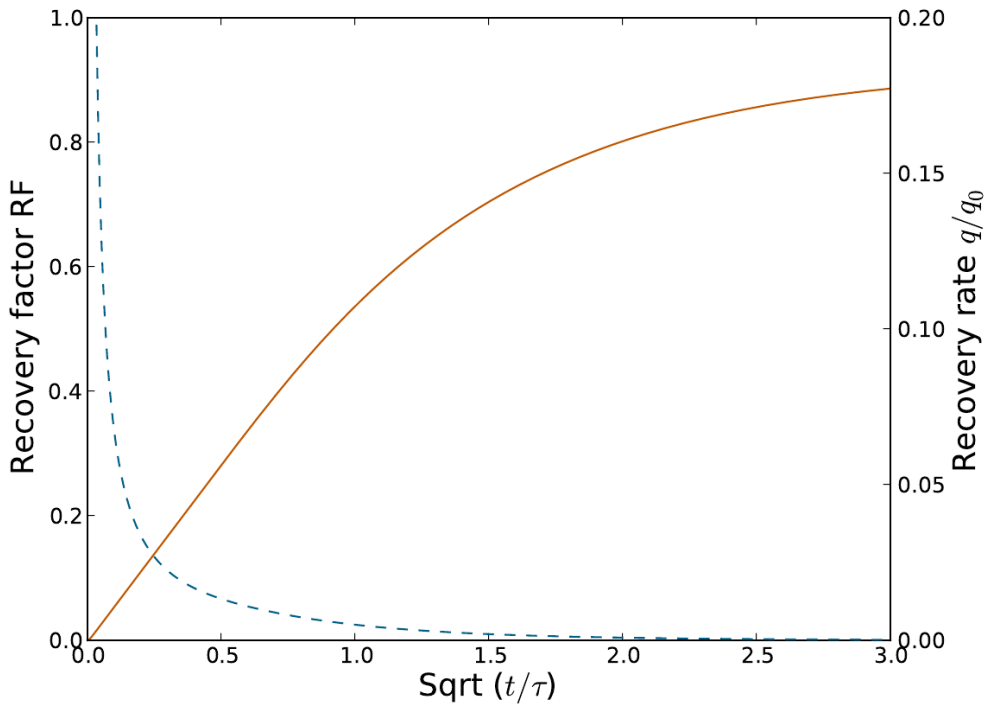

Figure 3.2: Recovery factor and recovery rate versus square root of scaled time are shown here. The rate quickly falls as $1/\sqrt{\tilde{t}}$ while the recovery factor increases as $\sqrt{\tilde{t}}$ until the boundary effects start to emerge at approximately $t/\tau = .64$. This particular curve is for a Marcellus well in the rich gas region with an initial reservoir pressure of 5000 psi and a fracture pressure of 500 psi. This production results from the pressure drawdown shown in Fig. 3.1

3. How quickly can you get it?

   The entire SRV is connected to the wellbore and depleting once $t \geq \tau$

3.1 Curve fitting procedure

Here is the fitting procedure: First, I make a series of RF curves for a field, with the average field-wide gas composition $\mathbf{y}$, fracture pressure p_f, and temperature T. Each of these curves has a unique initial reservoir pressure p_i, which I vary from the lowest to highest pressures in 100 to 400 psi increments. These curves are calculated from solving (3.16), in the manner noted above.

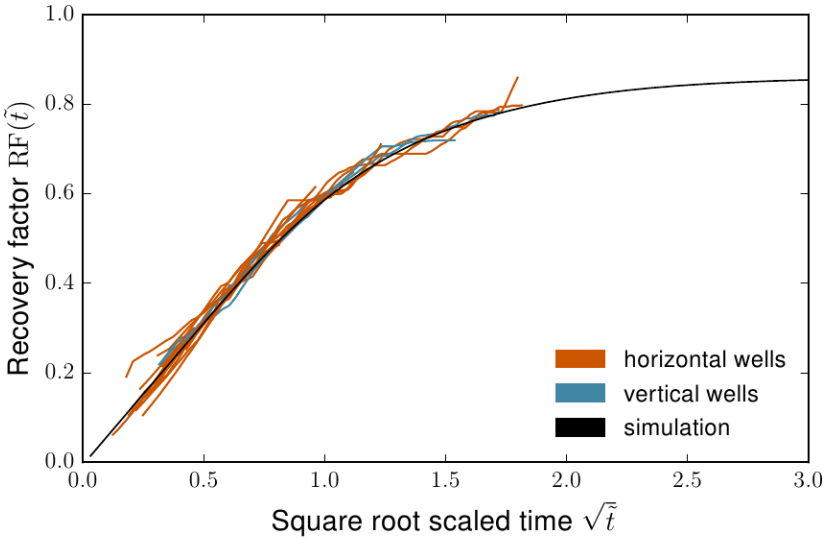

Figure 3.3: Test of curve fit for small number of Barnett wells. This figure was generated to show the accuracy of the recovery factor curve for a small set of wells. There are 12 horizontal and two vertical wells from the Barnett field that have been fit to the RF curve.

The curve for an individual well is interpolated from this series of curves to its given reservoir pressure. I run a series of parallel simulations with different initial reservoir pressures from zero time to $\tilde{t} = 25$, then feed this into the interpolator. The interpolator is offered by SciPy, and uses Qhull to implement linear barycentric interpolation.

Next, cumulative production for a well is calculated from the monthly production rate data. Then I choose a time offset for the entire field, t_0. The time offset $t_0 = 1$ month yields the best fits with production for the fields in this analysis. I perform a sequential least square fit utilizing the equation

$$\sum_i \left(Q_{well,i} - \mathcal{M}\mathrm{RF}[(t_i - t_0)/\tau]\right)^2 \tag{3.20}$$

which fits for $\mathcal{M}$ and τ. I use SciPy's minimization software that wraps the Fortran FITPACK library to perform this fit in Python.

Some wells, though, have not begun to show interference, and therefore I cannot know their time to interference or gas in place without further information. In the next chapter I discuss several methods I have developed to try estimating these values

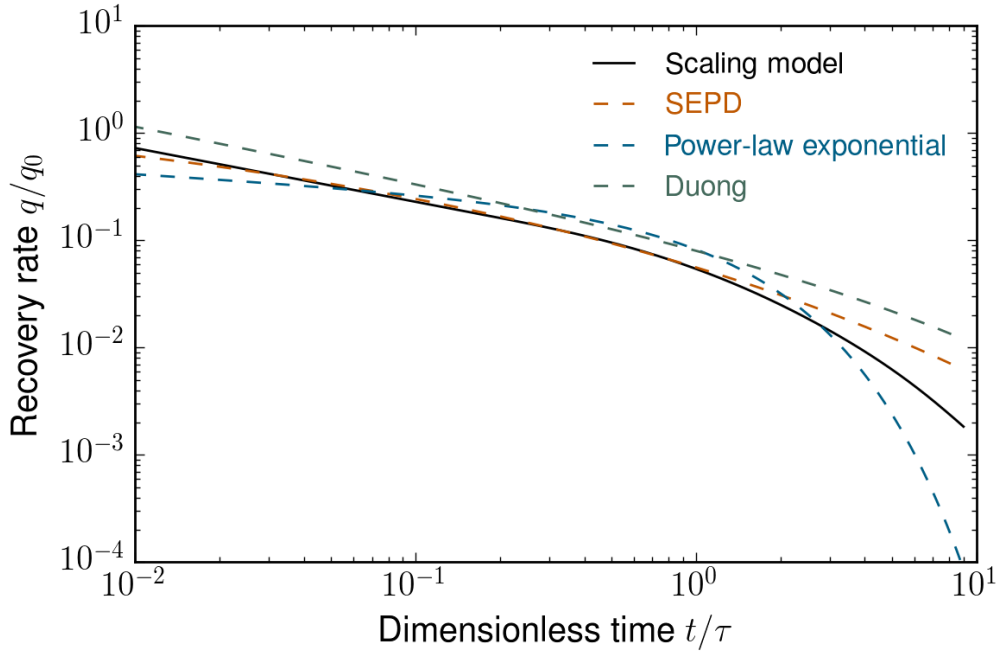

Figure 3.4: Comparison of scaling solution to empirical curves used in industry. These curves are those mentioned in Chapter 2. They are the Duong decline (2.14), power-law exponential model (2.13), and stretched exponential production decline model (2.12).

and their associated uncertainties.

The relationship between $\mathcal{M}$ and τ in the transient flow period is

$$\mathcal{M} = K/\kappa\sqrt{\tau}, \tag{3.21}$$

where K is the slope of production and is given in units of gas mass divided by the square root of time and κ is the dimensionless initial slope of the RF curve, given by

$$\mathrm{RF}(\tilde{t}, p_i, p_f, \mathbf{y}, T) = \kappa(p_i, p_f, \mathbf{y}, T).$$

Both K and κ, can be determined for wells in transient flow. Therefore, in transient flow one knows that $\mathcal{M}(\tau)$ lies on a line.

3.2 Comparison to empirical curves

The scaling model holds several advantages over the empirical models frequently used to fit and forecast production of shale gas wells. First, it has fewer fitting parameters.

Its scaling terms, $\mathcal{M}$ and τ, are the only parameters that are varied to ensure a fit to well production. For the SEPD model, there are three fitting parameters: q_i,τ, and n. Duong's model contains the three fitting parameters q_i, a, and n. It also needs to be spliced together with an Arps curve — which requires two more fitting parameters — in order to describe production in boundary dominated flow.

Figure 3.4 offers a graphical comparison of the models. It also highlights the second advantage of the scaling model. During boundary dominated flow, there is one well-defined and physical curve that production can follow. The SEPD, power law, and Duong models have extremely variable tail-end performances that can appear due to minute differences in the early production of a well. This is because these models include exponents of the form e^{t^n}, which can be very unstable when fitting noisy data.

Furthermore, the scaling solution takes production fits and converts them into knowledge about the reservoir. Time to interference and gas in place have real physical meaning. This is not a design consideration for empirical curves. One might think that because the SEPD model has a characteristic time, τ, that it relates in some way to an observable timescale for the well. However, it seems far divorced from the time to boundary dominated flow. In the comparison curve, the τ for the SEPD model is approximately 0.003.

This is not to say that empirical models have no value. They require no knowledge of geology, well geometry, nor fluid parameters. They also are very fast to implement, test, and tweak. Duong (2010) is able to use the model to fit wet and dry gas wells with equal accuracy. They simply are not the best choice when you do have coarse geology and fluid information to feed a model.

With this all in mind and a model in hand, I can now turn to predicting production for wells in transient flow.

Chapter Four: Determining production for wells in transient linear flow

"The paradigm of physics — with its interplay of data, theory and prediction — is the most powerful in science."

—Geoffrey West

Gas wells are in one of two classes, according to the model developed in Chapter 3. There are wells that are in boundary influenced or dominated flow and wells that are still in transient flow.

For wells that have reached $\tilde{t} \approx 0.64$, I can estimate τ and $\mathcal{M}$ to within 20% uncertainty. Wells that are at $\tilde{t} < 0.64$, though, have not experienced the boundaries of their SRV, and curve fitting does not result in a τ. In order to forecast production from these wells, I need to leverage some other information.

The process used for estimating time to boundary dominated flow has evolved over time, and therefore I will explain the different methods in order of when they were used. First, I made estimates of the upper and lower bounds on time to interference from the production data and theoretical gas in place. Next, I made assumptions about the fracture spacing and permeability inside the SRV. I utilized full-scale reservoir simulations to estimate time to interference from these estimates. After determining that this could be simplified, I started using the model's predictions for time to interference for a given well geometry and geology. Finally, I used a regression relating initial production to gas in place, $\mathcal{M}$. This is the current methodology.

The process's evolution took place over several fields, but I will draw all examples from the Barnett shale play, because it has the longest production history. For an overview of the Barnett shale play and a summary of the results from that play, I entreat you to read the next chapter.

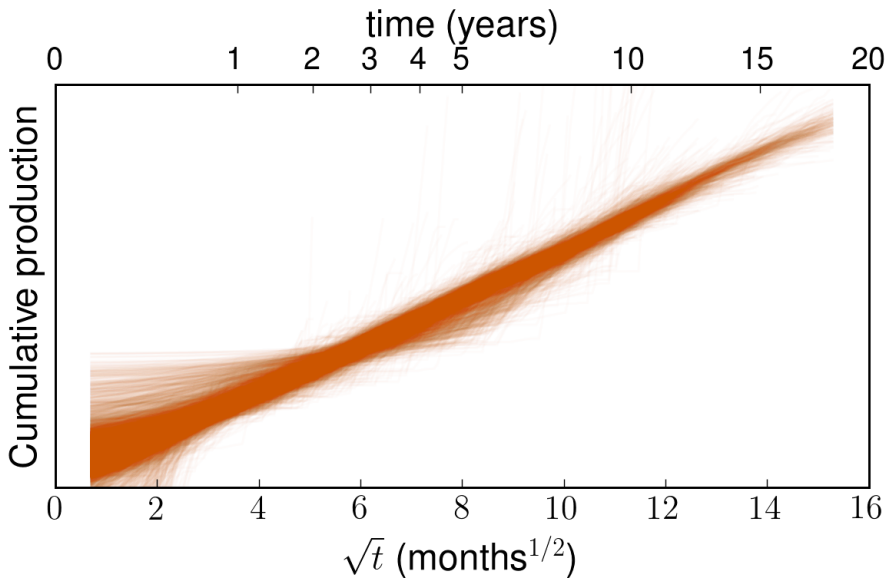

Figure 4.1: Production from Barnett wells in transient flow. The x-axis is in square root time so that cumulative production falls on a straight line. Each well's cumulative production is scaled so that they all lie on the same curve. This is done by normalizing production by the slope of cumulative production. A well producing at 10 MMcf per square root month and a well producing at 1 MMcf per square root month, with no deviations from transient flow, will look identical in this plot. There are 12,560 wells' productions plotted.

4.1 Bounds on time to interference and gas in place

I took monthly production data for wells in the Barnett, then removed wells that have less than 12 months of production or have been recompleted. Recompletion is a process that many operators use to increase the SRV in a well, either by conversion from a vertical well to a horizontal well or hydrofracture treatment. I identified wells as having been recompleted by assessing whether their cumulative production versus square root time is better fit by two straight lines than one using a Chow test (Chow, 1960).

In the data set, the Barnett shale gas field has 3,721 wells in boundary dominated flow. Another 9,346 wells are in transient flow. It is that 9,346 well data set that I investigate in this section. In Chapter 5, I investigate the other fields.

Production from the wells in transient flow is given in Fig. 4.1. The geologic parameters and well geometry must be known in order to determine the bounds on the τ and $\mathcal{M}$. The lower bound on τ is fairly straightforward: if interference is identifiable just after the well reaches $t/\tau = .64$, then the lower bound is that boundary influenced flow begins immediately, and $\tau = 1.56t$.

The probability of every well immediately shifting from transient to boundary dominated flow is very low, so this can only exist as an extreme lower bound on the time to interference. Because $\mathcal{M} \propto \sqrt{\tau}$, this would also serve as a lower bound on the gas in place. One might think that this is a strict lower limit, but in rare cases, when I have added production history to a well that appears to be in transient flow, it turns out to have been in boundary influenced flow before that previous lower limit. This is a result of the noisy nature of well production histories.

The upper bound is derived from finding the upper bound on the SRV. Hydrofracture treatments are designed by companies to achieve a specific SRV, usually with the stipulation that this should not interfere with production from neighboring wells. Ikonnikova et al. (2014) performed a spacing study to determine how closely wells in the Barnett could be spaced before affecting their neighbors' production. They find that the area a well drains from varies with its total production, as one might expect. A typical spacing for wells in the most productive area of the field was 200 m between parallel, horizontal wellbores. This corresponds to an SRV which reaches 100 m on each side of the wellbore, for a total SRV width of 200 m.

They also find that the best correspondence between a map of the gas in place inside the Barnett formation and well productivity happens when only gas within the first 300 feet (91 m) from the bottom of the Barnett was counted. This could be explained by considering that fractures either do not extend more than 300 feet (91 m) from the wellbore, or that fractures that do extend that far are not well-connected and do not contribute to flow.

Therefore, I choose the SRV to be the length of the well times 200 m times the thickness of the formation, limited to 91 m. How much gas is in the SRV is dependent upon the reservoir pressure, gas composition, gas-filled porosity, and adsorbed gas. Fu et al. (2015) extracted pressure, thickness, and gas-filled porosity from maps they created from industry well logging data. I use this geologic data.

I compare the upper limit on $\mathcal{M}$ from this geometric and geological argument to the observed gas in place in Fig. 4.2. Not only does this visualization show that this

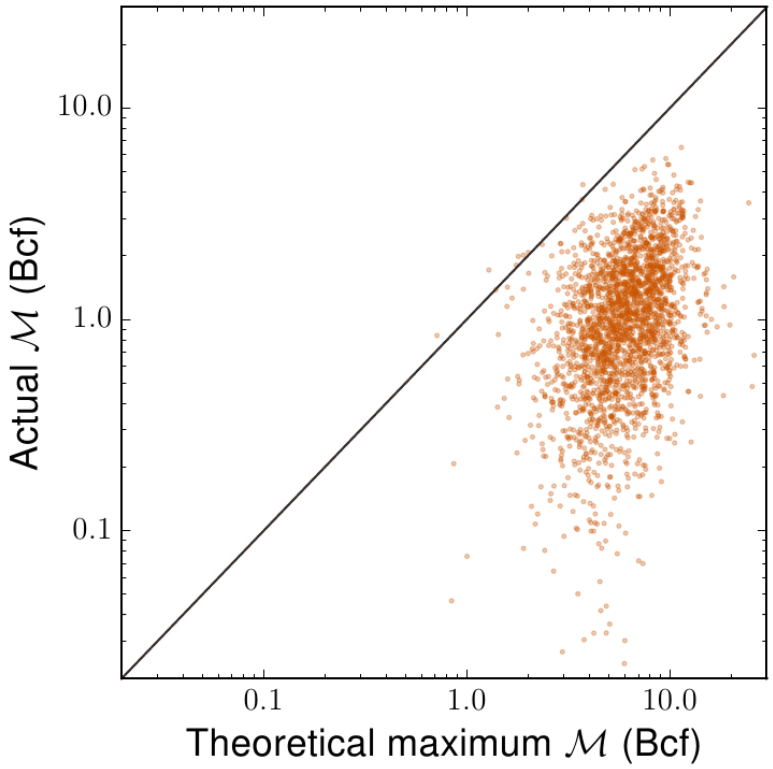

Figure 4.2: Gas in place, $\mathcal{M}$, for 2,439 horizontal, boundary dominated flow wells in the Barnett is compared to the upper limit on gas in place from the well geometry and geology. The SRV is limited to 300 feet in the vertical direction, 300 feet from the wellbore in the perpendicular direction, and the length of the well. The gas inside the SRV is calculated from porosity and reservoir pressure data, and with the assumption that there is no contribution from adsorbed gas to the SRV. The median well produces from an SRV 17% of the upper limit.

is a reasonable upper limit on the gas in place, it calls to attention the fact that the average well produces from a volume approximately 5 times smaller than it could theoretically produce from, and the bottom 10 % produce from a volume less than 6.3% of that intended by the operators.

This makes the upper limit on $\mathcal{M}$ very optimistic in most cases. Therefore, it cannot be used as a prediction for the real $\mathcal{M}$ on a well nor to forecast production. In order to produce defensible forecasts, I must make further assumptions.

4.2 Estimating permeability and fracture spacing

The starting point in estimating time to interference is the equation $\tau = d^2/\alpha$. Given the fracture half-spacing d, and the hydraulic diffusivity α, calculating the time to interference is trivial. But first I need to address concerns about whether effects that were ignored in our production model contribute to the time to boundary dominated flow.

In order to answer concerns about such effects as flow from outside the SRV, finite permeability hydrofractures, and well-to-well interference, I turned to reservoir simulations. Wei Yu ran a suite of 25 simulation runs with these effects included, while varying porosity, reservoir pressure, permeability, and fracture spacing. He then ran a regression to determine how well the parameters could control time to interference. The results of this regression are in Fig. 4.3.

I used the regression that Wei Yu arrived at in order to determine time to interference in the Fayetteville field (Male et al., in preparationb). The regression found time to interference (in months) to be calculable from

$$\begin{aligned}\frac{12}{\tau^2} &= .22022 - 2.18146\phi + 4.43053 \times 10^{-4} p_i \\ &+ 121.0414k - 7.04465 \times 10^{-4} d \\ &- 3.31978 \times 10^{-3} \phi p_i - 653.84863 \phi k \\ &+ 0.012650 \phi d + 8.95441 \times 10^{-3} p_i k \\ &- 2.60166 \times 10^{-7} p_i d - 0.082744 k d.\end{aligned} \tag{4.1}$$

This regression works well for typical reservoir values found in the Fayetteville, but exhibits unusual behavior at extremes of any of these values. For instance, when I accidentally introduced a fracture half-spacing d several orders of magnitude too high, the time to interference fell sharply, in contradiction to what would expect. In addition, the regression is neither transparent nor intuitive.

Because of these problems. I switched to a simpler and more transparent way of determining time to interference, the equation for τ (3.13). On a positive note, the simulations and subsequent analysis show that, at least from a simulator's standpoint, the relation between τ, d, k, and ϕ holds true.

From Fu et al. (2015)'s data, I have ϕ. I gathered the gas composition from Hill et al. (2007) and the gas viscosities and densities from Gonzalez et al. (1970). Next is a matter of deciding on a reasonable hydrofracture distance and rock permeability.

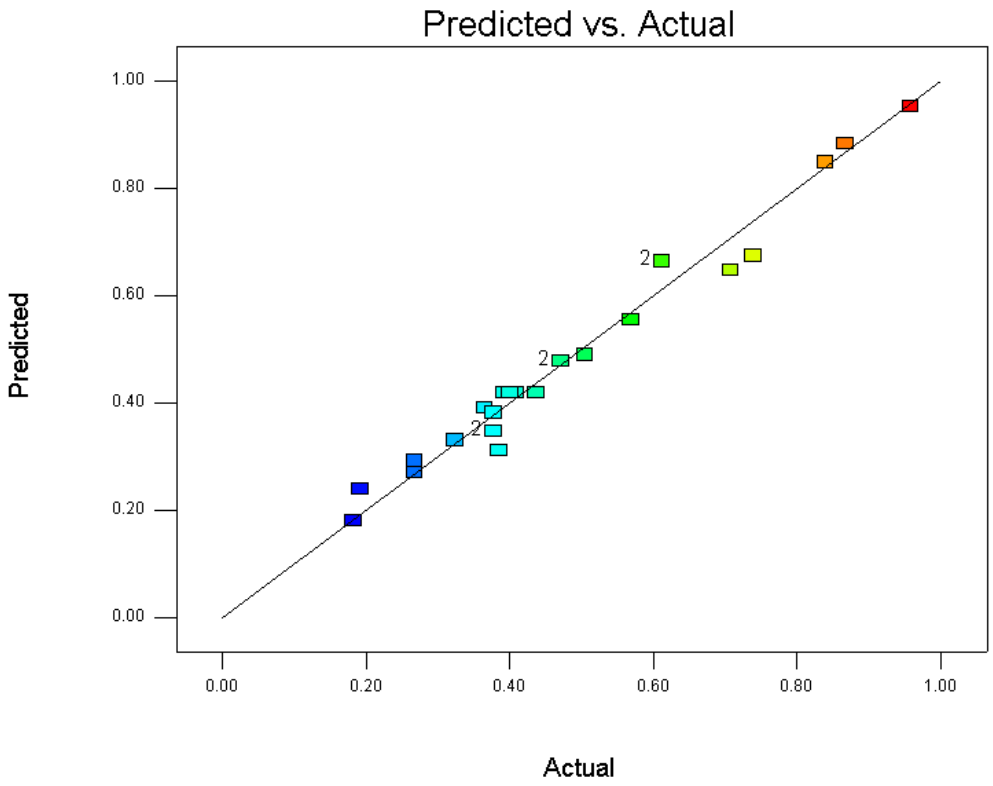

Figure 4.3: The regression analysis Wei Yu ran on his reservoir simulations. Each axis is $1/\sqrt{\tau}$; the x-axis is the result from the reservoir simulations, and the y-axis is the result from the regression. Color indicates the time to interference. This regression analysis shows that varying porosity, pressure, permeability, and fracture spacing almost completely explain all variations in the time to boundary dominated flow.

If I take a constant $2d$ that is 1/9 of the well length (so chosen because the typical number of hydrofracture stages for a Barnett horizontal well is 9), then I can get permeabilities for boundary dominated flow wells. The result of this exercise is the histogram provided in Fig. 4.4. It is clear from this exercise that either permeability, fracture spacing, or both vary greatly over the field. However, even taking the uncertainty as the half width at half maximum, this variation provides far tighter bounds than those given by the arguments from Section 4.1. The lower bound and the bound provided by the permeability histogram do overlap for a large number of wells, further decreasing the uncertainty in τ.

It is worth noting how a change in permeability would affect the gas in place for

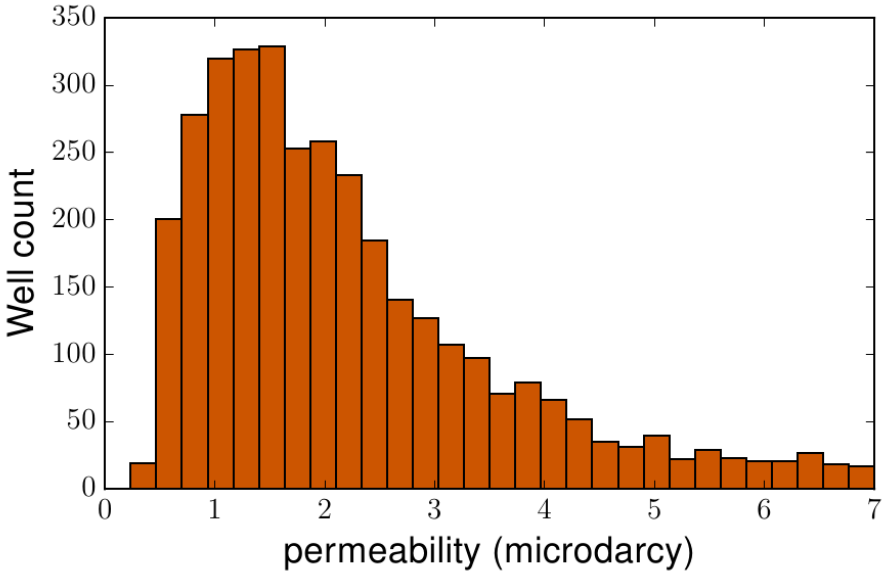

Figure 4.4: Permeabilities for 2,439 horizontal wells in the Barnett. These are inferred by applying (3.13) and (3.8) and estimating fracture spacing at 1/10 the well's lateral length. The distribution appears to be log-normal with an average permeability of 2.0 μdarcy, and the standard deviation about the mean is 3.3 μdarcy.

a well, in this model. $\tau \propto 1/k$, so $\mathcal{M} \propto k^{-1/2}$. This means that a four-fold increase in permeability for a well with a set initial production slope K would cause its gas in place to drop by a factor of two.

Setting the permeability to 1 microdarcy and the fracture spacing to 1/10 of the well length for horizontal wells in the Barnett, I get a reasonable estimate of the τ for each well. I can then fit an $\mathcal{M}$ to match the production history and forecast to 25 years of production. This is the method I used to predict the production from wells in transient flow when analyzing the Haynesville shale (Male et al., 2014).

The uncertainty on the production is still very high using this method. An additional concern is the ambiguity in what permeability means. In shale gas reservoirs, there are competing mental models with different definitions for permeability. There is the idea of permeability as a property of the rock, but there is also the idea of a stimulated permeability which is, in reality, the permeability of the system between fracture stages, both the rock and the micro-fractures through it. Depending on your mental model, your reaction to a permeability of 1 microdarcy will be very different:

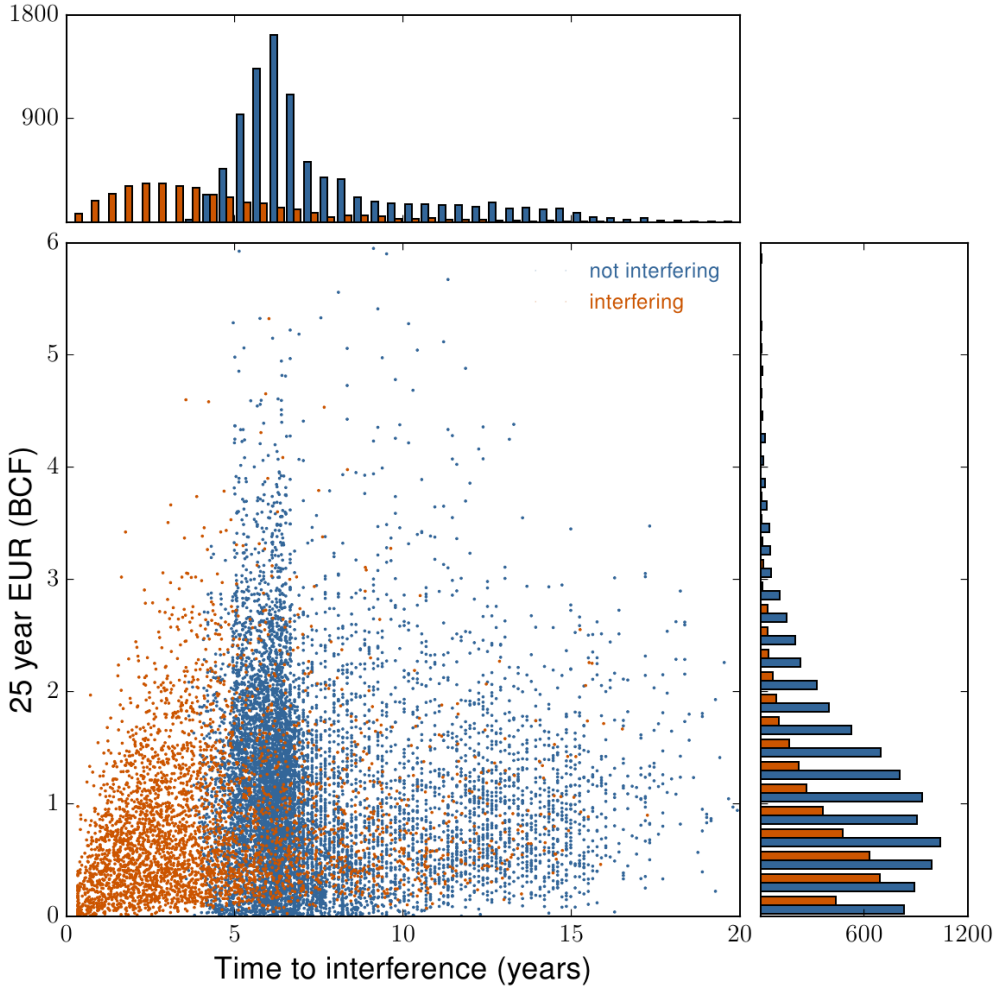

Figure 4.5: Time to boundary dominated flow and estimated ultimate production (EUR) for Barnett wells using a set permeability. I set a field-wide permeability of 1 microdarcy and a fracture spacing of 1/10 the well length to set the τ, then fit production to arrive at 25 year estimated ultimate recovery. Blue dots represent wells in transient flow and orange dots represent wells in boundary dominated flow. The right histogram shows the distribution of EUR's and shares the y-axis with the scatter plot. The upper histogram depicts the distribution of τ's and shares the x-axis with the scatter plot.

this is reasonable for the rock/micro-fracture system, but the matrix permeability is thought to be around 1 nanodarcy.

Furthermore, we cannot reliably measure the permeability. In the production data, the effects of permeability and fracture spacing on τ are indistinguishable. It is impossible to perform laboratory experiments on the rock in the reservoir, and the two proxies that we have for that: laboratory experiments done on core and well testing, both have limitations. They also give results that differ by several orders of magnitude.

With that in mind, I bring you to the current method for determining production from wells in transient flow.

4.3 Estimating total production from initial production

The method that Dr. Marder and I settled on requires an entire rethink of the process. In the course of analyzing production from the Marcellus shale, I looked at every piece of geologic information available to try to find something that correlated well with the time to interference or with the gas in place. Nothing rose above the noise (R^2 values below .2) until Dr. Marder suggested using the slope of the cumulative production versus square root time as an input. This method is effective for all fields I investigate.

For Barnett wells that are in boundary dominated flow, the correlation coefficient between the initial slope ($\tilde{t} < .6$) scaled by the initial slope for the corresponding RF curve and the gas in place for wells in boundary dominated flow is .855. A plot of the regression is given in Fig. 4.6. As you can see from the plot, almost every well falls within a factor of two of the trend line. This is far better accuracy than the previous methods I used.

In fact it is an odd result that the uncertainty of $\mathcal{M}$, given the initial slope is a constant percentage for any initial slope in the Barnett. I do not know why that is.

The regression provides relationship between $\mathcal{M}$ and K/κ, which I write in the form of (3.21),

$$\mathcal{M} \approx \left(\frac{K}{\kappa}\right)^m \sqrt{\tau_0}, \tag{4.2}$$

where m is the slope of $\mathcal{M}$ plotted against K/κ in log coordinates and $\sqrt{\tau_0}$ is the

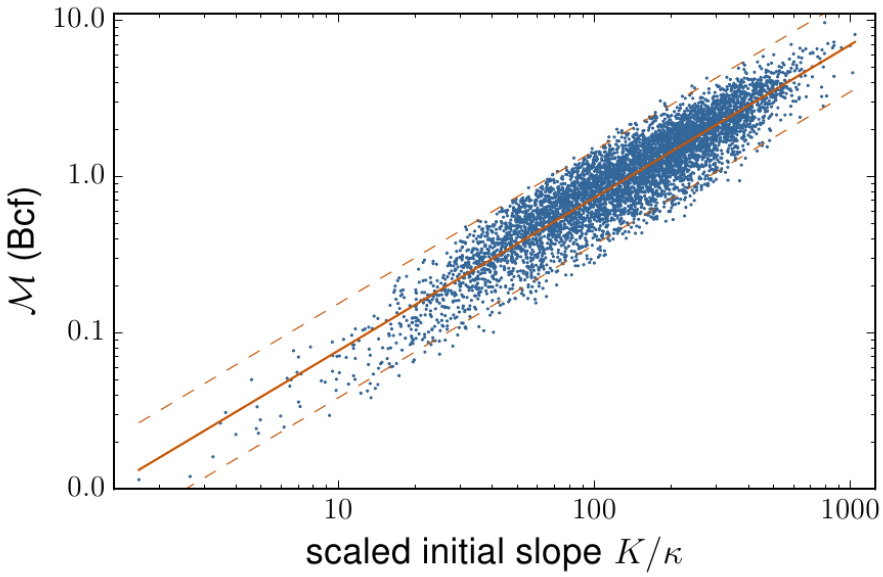

Figure 4.6: Initial production determines gas in place in the Barnett. The x-axis is the slope of cumulative production per square root time in the units MMcf/month$^{1/2}$ divided by cumulative production per square root time for the model I develop in Chapter 3. The y-axis is the gas in place. A trend line is given in orange, while individual wells are the blue dots. R^2 is 0.86. The dashed orange lines indicate values half and twice the trend line.

y-intercept. From this regression I have an estimate for the gas in place. Taking this equation and plugging it back into (3.21) to determine the time to interference yields

$$\tau \approx \left(\frac{K}{\kappa}\right)^{(m-1)/2} \tau_0. \tag{4.3}$$

When $m = 1$, then it simply is τ_0.

There are many advantages of estimating total production from initial production. It avoids the limitations of the earlier approaches, being extremely transparent and something that anyone with access to public well production data can do. There is no need to know the geology that the well has accessed; that information seems to be captured within the well's initial production. It is compatible with both mental models: the mental model of closely spaced 1-2 m hydrofractures draining blocks of low permeability and the model of large planar hydrofractures spaced tens to hundreds of meters apart and draining rock of higher permeability. Most importantly, it provides tighter bounds on ultimate production than the previous methods.

This does not mean it is perfect. The uncertainty is smaller, but companies depend on knowing how much wells will produce to far greater accuracy. The average horizontal well in the Marcellus costs around 6 million dollars, and the difference between that well producing, *e.g.* 4 million dollars worth of gas and 8 million dollars worth is huge. Some of this is helped by the sheer number of wells that these companies drill. The largest operators drill hundreds to thousands of wells, and the mean well performance at that point becomes more important than each individual well's performance. For smaller operators, though, each well is a risky endeavor.

Also, the universality of this relationship is difficult to establish. Presumably, the time to boundary dominated flow can be affected by how close hydrofractures are, changes in the matrix and effective permeability, or even voodoo witchcraft. The slope of $\mathcal{M}$ versus initial production is different for different fields, so it is not the same for each field. I don't know precisely why that is the case. I could make the argument that the geology is different for these wells, the pressure is different, the rock might respond to hydrofracturing differently, etc.; but I cannot say which effect is most important yet.

In summary, the current method is very good and a great improvement, but it is not perfect. There are several directions I can take to try to improve estimates of total production. I will discuss these in the conclusions chapter.

Chapter Five: Applications to Major Shale Gas Fields

"Their patch was a molecule with fangs under the words *exite! chemicus sum!* Which was Latin for, Back off, man! I'm a scientist!"

—Larry Correia, *Monster Hunter Vendetta*

A model can be a beautiful thing, but it is only useful if it either provides insight into a process or predictive capability. Never bring this up to a political scientist. In this chapter, I will show how the model given in the last two chapters provides insight into production from real shale gas wells in active fields, and use the model to make predictions. In other words, I will lay out the insights this model has given and make predictions of future production for wells in four major shale gas fields, the Barnett, Fayetteville, Haynesville, and Marcellus. The order is chosen not because it is alphabetical, but because it is chronological. The most intensively studied fields were the Barnett, which the model given in Chapter 3 was developed on, and the Marcellus, which has several interesting quirks, with the Fayetteville and Haynesville somewhat more straightforward.

5.1 Analysis of the Barnett

The first field analyzed was the Barnett field[1] in the Fort Worth Basin of Texas. This is the first major shale gas field, and the only one that had significant production before the introduction of horizontal drilling. Because this field is the oldest shale gas field and has the longest production history, it is an ideal starting point.

In 2006, the Energy Information Administration reported that the Barnett was the second largest-producing gas field in the US (EIA, 2006). Martineau (2007) offers a history of the Barnett shale. It owes its success to Mitchell Energy, who discovered

[1]My group has published several articles on the Barnett (Patzek et al., 2013, 2014). Patzek, Marder, and I worked together in developing the model and performing analysis. Although they are not among the authors, John Browning and Svetlana Ikonnikova provided invaluable insights during the analysis.

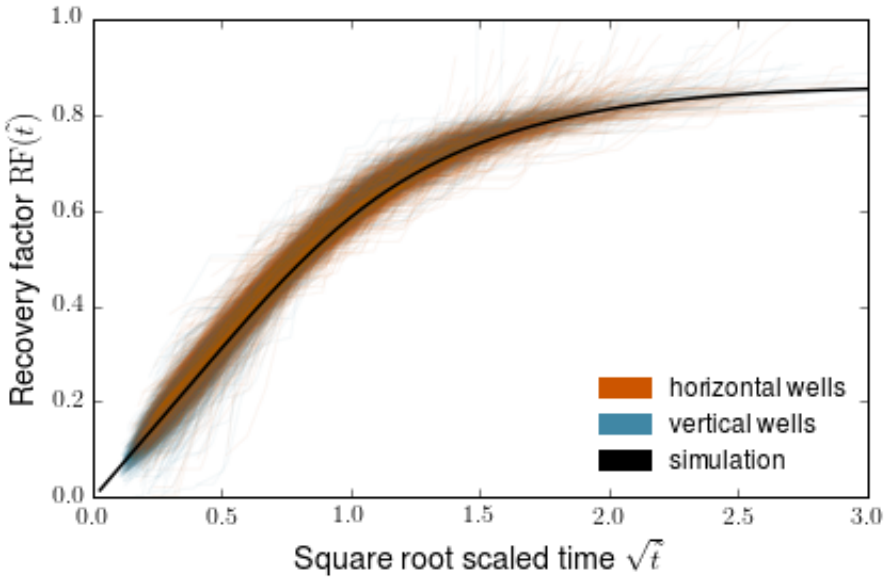

Figure 5.1: Scaled production versus square root of scaled time for wells in the Barnett. This includes production from 6,153 wells; 4,360 are wells where horizontal drilling has been used, shown in burnt orange, and the remainder are wells that have been drilled vertically through the shale formation, then hydrofractured, shown in blue. Horizontal and vertical wells follow production curves that are indistinguishable after accounting for time to interference and gas in place. Vertical wells are thought to have a radically different flow geometry than horizontal wells, but this shows that they might have very similar flow geometries.

the field in 1981. George Mitchell, the founder of Mitchell Energy, put decades of research into developing the technology to economically extract gas from the field. When Mitchell switched from gel fracturing to water fracturing, he started the shale gas revolution. These were the first modern, economic shale gas wells. Horizontal wells started showing up after Devon Energy purchased Mitchell Energy, and the number of producing wells kept climbing through 2006, with estimates that the field would produce 26 Tcf.

It took a sharp drop in natural gas prices for the Barnett's production to slow down. In spite of the slowdown, Browning et al. (2013a) estimates reserves at 45 Tcf. This is approximately enough gas to serve US needs for two years. Such a large field gathers economic and political interest, and it has been featured in a great number of news and opinion stories.

The Barnett field, like most in the study, has monthly production data for individual wells. This data is publicly available from the Texas Railroad Commission, and operators are required to report well-by-well production numbers to the state. Companies gather production data thus: frequently, several wells are drilled at one site. These wells have individual wellheads that collect the gas, then send it to a central location, such as a processing plant. That plant collects information on how much gas comes through the pipe from each site. To disaggregate production data from each site, companies perform flow tests on each well for a few hours each month. The results from those flow tests are then used to back-allocate the total amount to individual wells. Flow rates in thousand cubic feet of gas at the wellhead per day are then reported to the Texas Railroad Commission. I take these and convert them to monthly production by multiplying by 30.4 days/month.

As mentioned in 2.3, in the first several months of production, there are many things happening in the well. The water used in hydrofracture is still present underground: some of it is produced along with the water, and some is imbibed into the rock matrix. The gas near the wellbore quickly changes pressure, and essentially every parameter in the flow equations are dependent upon pressure, so they are varying rapidly at this time. The large pressure gradient near the fracture also means that there can be turbulent gas flow, forcing modelers to use non-Darcy flow equations. In the first few hours, the gas present in the largest well-connected hydrofractures flow radially into the wellbore.

The best way to address these problems is to ignore the first several months of production. The complexity is far beyond my scope to handle with publicly available production data, and the most interesting in the linear flow regime, which offers the opportunity to more accurately predict ultimate recovery than the very early flow regime.

The Barnett is the only field in this study which had a significant number of vertical wells. Vertical wells are subject to only one hydrofracture stage and all hydrofractures must emanate from one vertical line in the reservoir. This is significantly different from the method used for horizontal wells, with many hydrofracture pumping stages spaced along a horizontal line in the reservoir. I expected this to result in different flow patterns for vertical wells, but that does not appear to be the case. Both vertical and horizontal wells' cumulative production fit on the same universal curve, and they both experience boundary dominated flow in the same way. Many

of these wells are deep into boundary dominated flow. This lends credence to the idea that hydrofracture treatments creates a ramified structure, and there are not simply large, planar hydrofractures that evenly drain the reservoir from each side, then experience interference from adjacent hydrofractures.

Each Barnett well has a pressure assigned to in from the well's depth and a pressure gradient of 0.7 psi/ft.

If $\tau < 1.56t$ for a well, this well is in boundary influenced flow; if $\tau < t$, the well is in boundary dominated flow. Production curves for these wells are shown in Fig. 5.1. For other wells, I use the method given in Chapter 4 to estimate τ. Production curves for these wells are given in Fig. 4.1.

Taking the initial production ($\tilde{t} < .6$) and comparing that to $\mathcal{M}$ for the wells with interference yields the equation $\mathcal{M} \approx 8.05(K/\kappa)^{0.979}$ (MMcf) with an uncertainty in the exponent of 0.0065 and an $R^2 = 0.86$. A plot of the fit is in Fig. 4.6.

This provides sufficient information to make forecasts for each well. The most important number for each well is its 25 year estimated ultimate recovery (EUR). Twenty-five years is a shale well's economic lifetime, when companies can allow wells to flow without expecting to spend overmuch on maintenance and would be willing to fix mechanical problems for a dysfunctional well. Wells with production that dip below .3 MMcf/month produce a negative cash flow and are usually turned off, so these two constraints were used to stop production for wells. I forecast monthly production for a well until it reaches 25 years or .3 MMcf/month production rate.

The mean well in the Barnett, including both vertical and horizontal wells, is expected to interfere at 8.03 years and produce 1.2 ± 0.9 Bcf in 25 years. There is considerable scatter, as shown in Fig. 5.2. Some of the best horizontal wells are expected to produce in excess of 5 Bcf, while many vertical and even horizontal wells are expected to produce practically no gas. An illuminating explanation for this phenomenon can be provided by watching a time lapse of production in the Barnett over the last 10 years, several of which are available online. At high gas prices, operators felt comfortable drilling far away from the best areas in the Barnett, and this led to low quality wells. As gas prices fell, they stopped drilling as much in poor areas.

Another explanation is the revolutionary nature of the Barnett. When this field started, no one knew the best practices for extracting gas, and over time they introduced new technology — such as horizontal drilling — and new completion strategies,

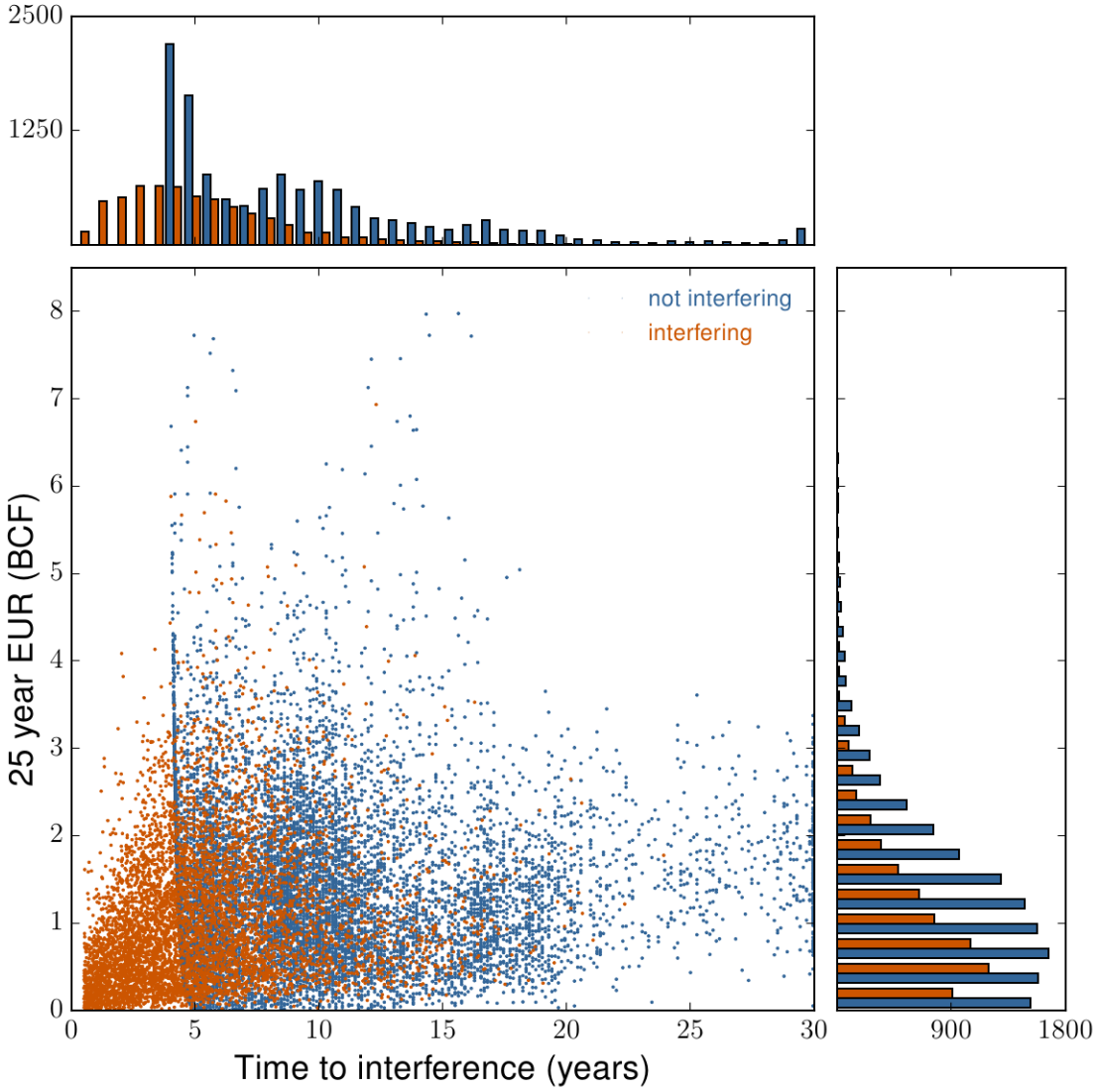

Figure 5.2: EUR and time to interference for all Barnett wells. Forecasted ultimate productions and τs are shown for 18,713 wells in the Barnett, with both horizontal and vertical wells shown. Blue dots stand for wells where τ has not been determined, and orange dots are for wells where τ is known. There is a histogram of τ given above the scatter plot, and a histogram of EUR shown to the right.

allowing them to produce more natural gas than they could previously obtain.

5.2 Analysis of the Fayetteville

The Fayetteville[2] is a Mississippian mudrock that lies under Arkansas and was deposited during approximately 350 million years ago. This field was developed after the Barnett, and therefore wells are almost exclusively horizontal wells with multiple stages of hydrofracture treatment along the length of the well. In the Fayetteville, pressure is low enough and adsorbed gas content is high enough that adsorption needs to be accounted for.

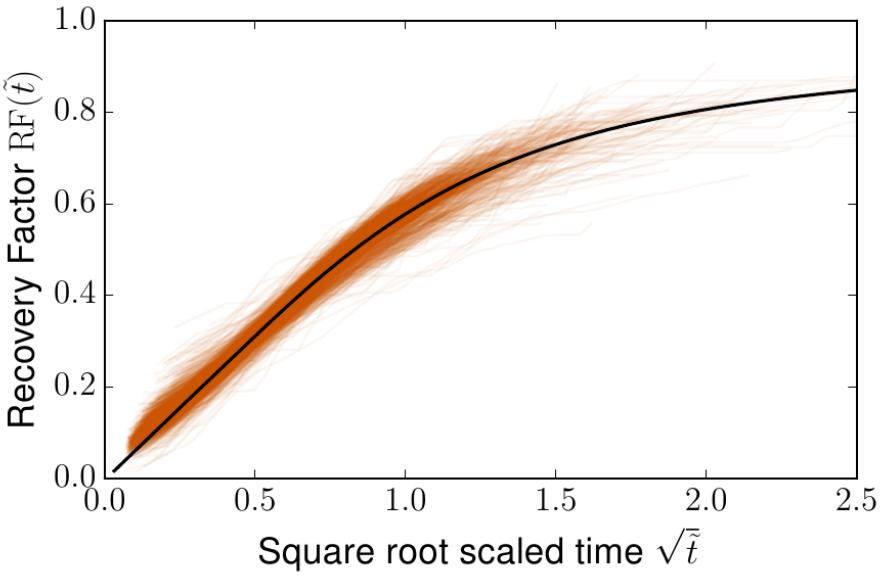

Figure 5.3: Production for Fayetteville wells in boundary influenced and boundary dominated flow. There are 1,253 individual wells with τ determined. These wells have initial reservoir pressures that vary greatly, which results in different scaling curves that they are being fitted to. An example curve for the average initial reservoir pressure, 1,500 psi, is given.

A unique aspect of the Fayetteville is that has been nearly all drilled by Southwestern Energy, with a small portion drilled by Chesapeake Energy and others. South-

[2]My analysis of the Fayetteville is being prepared for publication (Male et al., in preparationb). I performed the extension of the model and the analysis. Yu performed reservoir simulations. Marder, Patzek, Ikonnikova, and Browning assisted in the analysis.

western Energy used their large, continuous leases as testing grounds for how closely horizontal wells can be spaced and other completion techniques. This was an ideal situation for the company, but it presented a problem with analyzing production. In one instance, a processing plant was offline for long enough that it caused the operator to slow production from a large number of wells. Other shocks to the system that would be random error in other fields are systematic in this field.

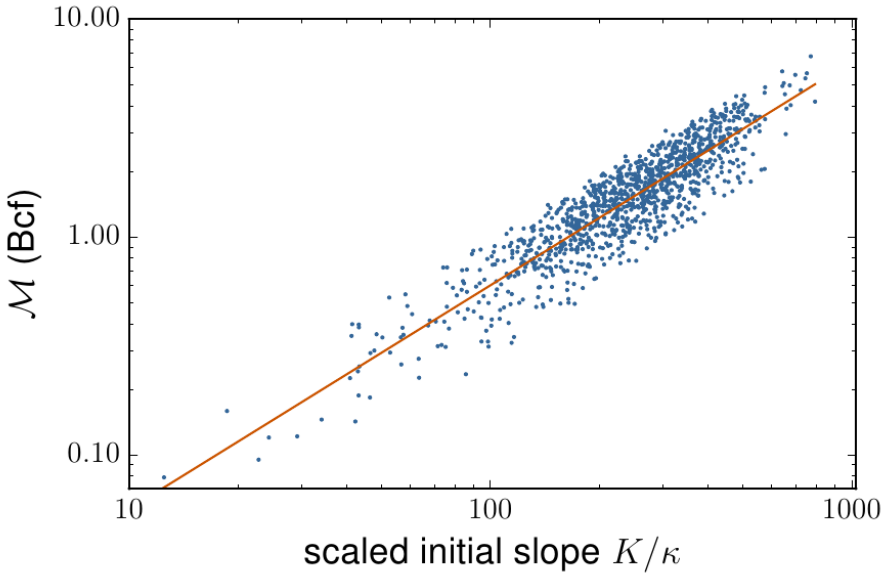

Figure 5.4: Initial slope predicts gas in place for interfering Fayetteville wells. There are 1,253 wells shown, and initial slope K/κ in MMcf/month$^{1/2}$ predicts gas inside the stimulated reservoir volume with surprisingly good certainty. The R^2 of this distribution is 0.84.

In spite of this and the general difficulty inherent in fitting monthly production data to a type curve, I can identify 850 wells that have experienced interfracture interference. Production from these wells is plotted in Fig. 5.3. In order to predict how wells that are not yet at boundary influenced flow, I look at the relation between the initial production and $\mathcal{M}$. That is plotted in Fig. 5.4, where $R^2 = 0.84$ for the relation $\mathcal{M} \approx 5.31(K/\kappa)^{1.03}$ (MMcf) with an uncertainty of 0.013 in the exponent. This leads to an expected time to interference of about four years for the average well.

The median $\mathcal{M}$ for a Fayetteville well, according to this analysis, is 1.89 Bcf, and the median τ is 4.8 years. The median well is predicted to produce 1.3 Bcf in 25 years,

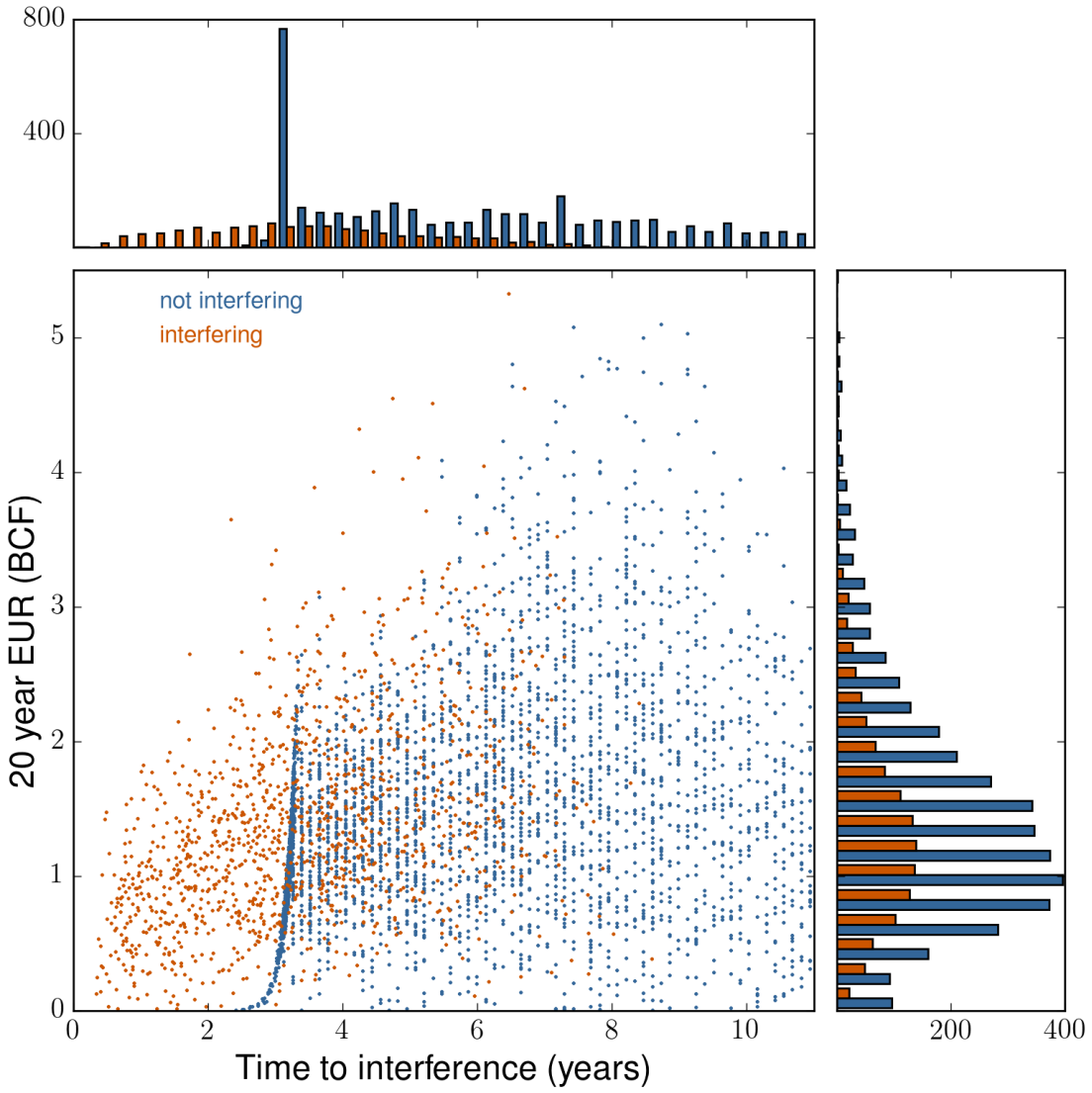

Figure 5.5: Production forecasts and time to boundary dominated flow for all Fayetteville wells. There are 4,989 wells shown. The upper histogram gives the distribution in time to interference, while the right histogram gives the estimated ultimate recovery. Blue dots denote wells in transient flow and orange dots denote wells in boundary dominated flow.

with the lowest 20% producing less than 0.8 Bcf and the highest 20% producing more than 2.0 Bcf. If you examine the forecasts given in Fig. 5.5, you see that there is considerably less scatter in the Fayetteville than in the Barnett. The EUR for most wells lies between .5 and 2 Bcf. This is likely due to consistent completion practices across the field (since it is leased by essentially only one operator), and not consistent geology amongst wells. In fact, the geology is fairly heterogeneous about the field, with pressure varying by more than a factor of two and the field criss-crossed by several large faults.

5.3 Analysis of the Haynesville

The Haynesville[3] is a Jurassic mudrock that lies under the Texas-Louisiana state line. It is deeper and hotter than the two previous fields studied. This has two main effects: wells cost much more to drill and hydrofracture, and gas in the reservoir is at a much higher pressure. With drilling costs so high, this field was not economic until the advent of horizontal drilling, and there are no vertical wells. The higher pressure means that gas initially is produced at a far higher rate than seen in the Barnett and Fayetteville. In order for operators to produce only as much gas as they can safely pipe to processing plants, they use chokes in the piping to limit production. Choking causes the pressure at the fracture faces to drop at a much slower rate. Rather the pressure dropping to a constant value in the first day of production, it can take years. It is difficult to obtain the bottom hole pressures for shale wells from public data, but I have one example from the Haynesville provided by IHS. Pressure over time for this well is shown in Fig. 5.6.

The original model, given in Chapter 3 does not account for a varying fracture pressure. It is not difficult to change this, though. In order to include varying fracture pressure, I changed the boundary condition at the fracture face and used this new

[3]My analysis of the Haynesville can be found in conference proceedings (Male et al., 2014) and peer-reviewed literature (Male et al., 2015). I performed the extension of the model and analysis. Marder, Patzek, Ikonnikova, and Browning assisted in the analysis. Islam developed the PVT package.

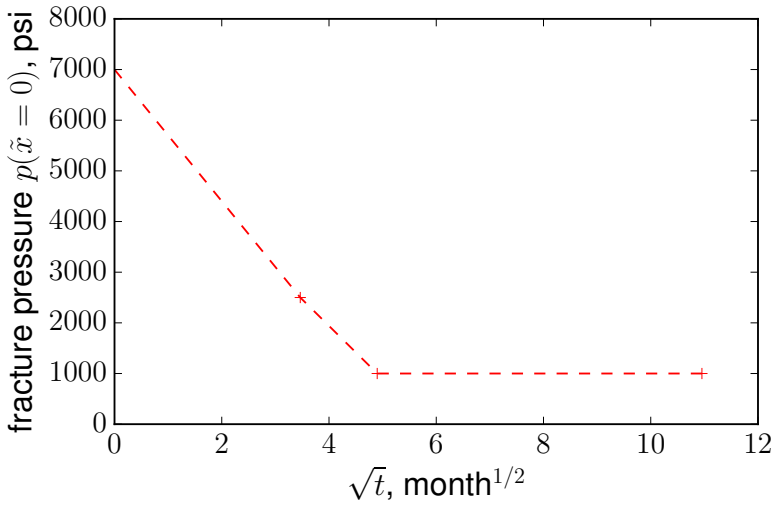

Figure 5.6: Bottom hole Pressure for a typical Haynesville well.

set of equations,

$$\begin{aligned} -\frac{\partial \tilde{m}}{\partial \tilde{t}} &= \frac{\alpha}{\alpha_i}\frac{\partial^2 \tilde{m}}{\partial \tilde{x}^2}, \\ \tilde{m}(\tilde{x}, \tilde{t}=0) &= \tilde{m}_i(\tilde{x}), \\ \tilde{m}(\tilde{x}=0, \tilde{t}) &= f(\tilde{t}/t_s), \\ \partial \tilde{m}/\partial \tilde{x}|_{\tilde{x}=1} &= 0, \end{aligned} \tag{5.1}$$

where t_s is a scaling time to convert back from $\tilde{t}$ into real time (so its units are inverse time) and $f(t)$ is the function of pressure at the fracture face in real time. The third equation is shown in red to highlight the difference from the system of equations given in Chapter 3. Selecting t_s is a subjective process. How quickly the pressure equilibrates is dependent upon several factors. The initial pressure of the reservoir, pipeline capacity to the processing plant, gas price, economic need of the operator, and other things can influence the choke schedule for a well. Fortunately, for the wells I analyzed, production consistently fit best for $t_s = 0.3$ inverse months.

The depth of the reservoir and high pressures cause the fracture face pressure to remain high, around 1,000 psi at steady state. Adsorption is negligible at this pressure, and it is not included in the model. The reservoir is mature and does not hold appreciable hydrocarbon condensate; it also has very little water in the matrix, with a gas saturation of around $S_g = 0.8$. Therefore, there is no need to consider

two-phase flow with water and gas.

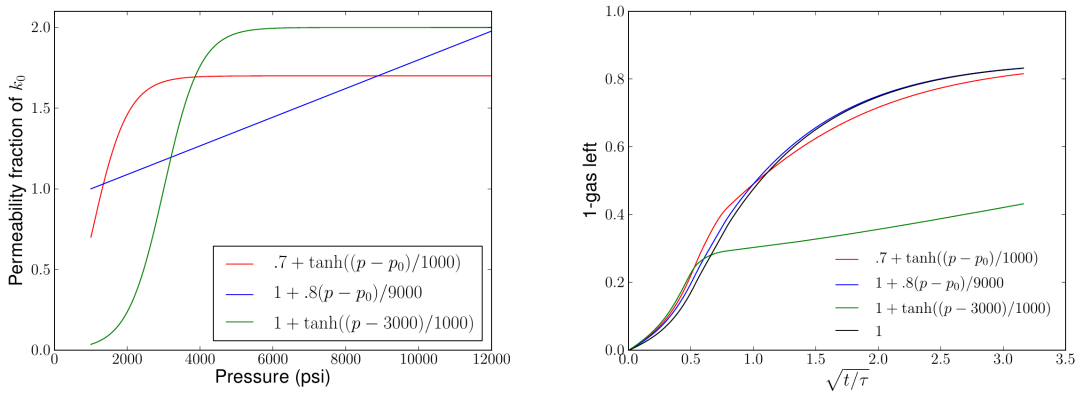

Figure 5.7: Effect of changing permeability on production. The right graph show permeability functions I selected to test. The left graph shows the effect of these permeability curves on production. Production is not greatly affected by changes of permeability up to a factor of two. Larger changes greatly change production and delay time to interference.

High pressure and the fact that the Haynesville is over-pressured (it has an abnormally high pressure compared to the formation above it) have given researchers the fear that as gas is withdrawn, fractures might close, lowering the permeability of the reservoir and negatively impacting production. In response to these questions, I have performed a sensitivity analysis of the production curve upon permeability, where I allow the permeability to drop as pressure drops.

Heller et al. (2014) used cores from the Barnett, Eagle Ford, and Marcellus shales to investigate the effect of pressure on permeability. In five of the six cores, they report a permeability that drops by a factor of two as the effective stress (confining pressure minus pore pressure) increases from 1,000 psi to 4,000 psi. In the other sample, it varies by an order of magnitude. To the first approximation this effect appears to be either linear or quadratic in pressure.

In order to select a function of permeability that is approximately linear over the given pressure ranges, I use a hyperbolic tangent. Permeability varies by a factor of

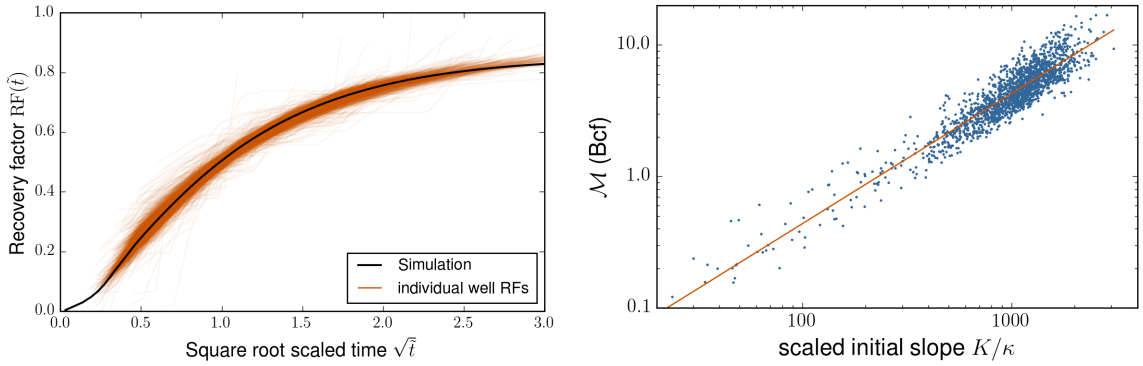

Figure 5.8: Production and gas in place for interfering Haynesville wells. On the left side is cumulative production scaled by $\mathcal{M}$ versus square root scaled time for 2,920 Haynesville wells that have entered at least boundary influenced flow. The line shows the scaling curve for an initial reservoir pressure of 10,100 psi. On the right is gas in the SRV versus the initial production for each of these wells. The line of best fit is given, and the $R^2 = 0.88$ for the regression.

two in one example, up to an order of magnitude, following the functions

$$k(p)/k_{init} = .7 + \tanh[(p - p_i)/1000]$$
$$k(p)/k_{init} = .7 + 1 + .8(p - p_i)/9000$$
$$k(p)/k_{init} = .7 + \tanh[(p - 3000)/1000].$$

The results from adopting these permeabilities are given in Fig. 5.7. Changing permeability by a factor of two does not affect production enough for it to easily be picked out of the noise inherent in well production data. Changing permeability by a factor of ten, on the other hand, makes an obvious change to the production curve.

In the production curves for fitting Haynesville wells, I choose to not include a dynamic permeability that changes with p. The analysis indicates that permeability has a weak effect on the cumulative production curve for the changes reported by Heller et al..

Smye et al. (in preparationa) used well log analysis to provide pay zone thickness, clay-corrected porosity, depth, and pressure gradients to feed into my analysis. The median initial reservoir pressure is around 10,000 psi and varies, so I calculated recovery factor curves for pressures from 7,000 psi to 14,000 psi to capture the pressure for each well.

The now standard fitting method for production identifies 2,365 of the 2,920 wells have entered boundary influenced or dominated flow. Production for these wells and the comparison between $\mathcal{M}$ and initial production are given in Fig. 5.8. This is the only field in the study where more than half of the wells are interfering, and this is likely because pressures are much higher in the Haynesville than in the other fields, leading to lower viscosity and faster depletion.

Calculating the gas inside the SRV from initial production yields the function $\mathcal{M} = 4.62(K/\kappa)^{0.99}$ MMcf with an uncertainty in the slope of 0.009 and an $R^2 = 0.88$. This translates to a time to interference of close to a year, so nearly all wells that have not been identified as in boundary dominated flow are expected to be. The forecasts for 25 year EUR and time to interference for all wells in the Haynesville are given in Fig. 5.9.

The median Haynesville well is expected to produce 4.2 Bcf over its first 25 years, with boundary dominated flow beginning at 1.4 years. The top 20% are expected to produce more than 5.7 Bcf and the bottom 20% are expected to produce less than 2.3 Bcf.

Haynesville wells are most interesting in that they interfere far earlier than wells in other fields. This certainly makes my job easier, because there are more wells to use in the regression between $\mathcal{M}$ and K/κ. It also offers a firm validation of the RF$(\tilde{t})$ curve, with many wells well into boundary dominated flow, occasionally as far as $\tilde{t} = 9$. If trilinear flow, that is, flow from outside the SRV into the fractures, was important enough to warrant including in this model, that would show by this point. In reality, though, the wells follow the curve just as tightly far into boundary dominated flow. This field therefore served as the first validation of my model for extreme late times.

5.4 Analysis of the Marcellus

The Marcellus field[4] is the largest gas-producing shale in the world. It stretches from New York, across Pennsylvania, to West Virginia and Ohio. Because New York currently does not allow hydrofracture and Ohio has very few active wells,

[4]I am preparing a manuscript detailing my analysis of the Marcellus (Male et al., in preparationa). Marder and I developed the methodology for predicting time to boundary dominated flow. Patzek, Browning, and Ikonnikova assisted in the analysis.

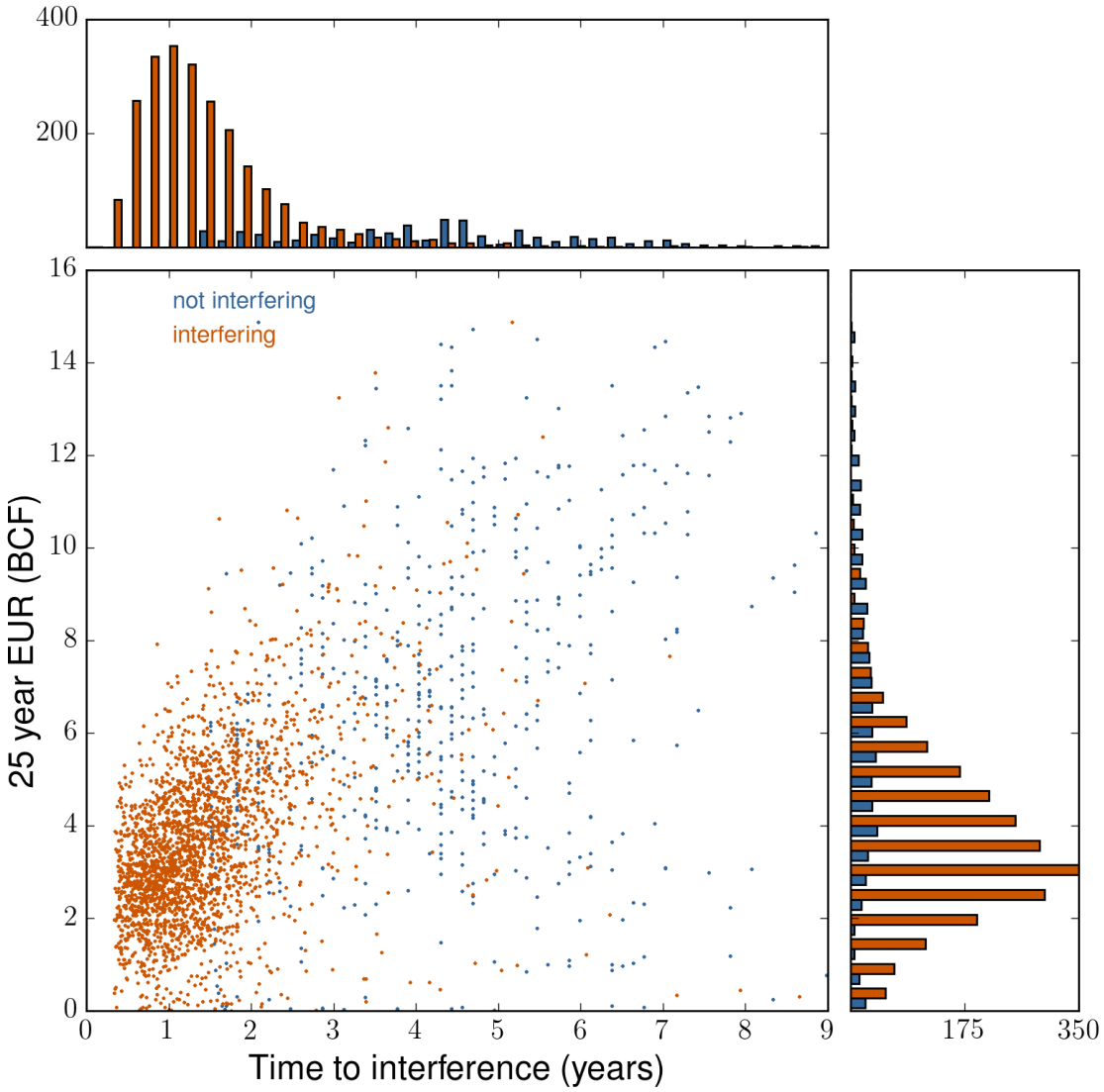

Figure 5.9: Ultimate production forecasts and time to interference for all Haynesville wells. Each of the 2,920 wells with 12 months of production history in the Haynesville is given an EUR and expected time to boundary dominated flow, τ in this plot. The upper histogram gives an idea of the distribution of τ, and the right histogram gives the distribution for EUR. Orange denotes interfering wells and blue denotes wells where interference has not been observed.

I only studied wells in Pennsylvania and West Virginia. As of January 2014, the Pennsylvania wells have produced approximately 6,126 Bcf of natural gas and the West Virginia wells approximately 603 Bcf.

There are a few problems unique to the Marcellus. First, because it stretches over a much larger distance than the other fields, it is essentially two fields: the dry gas portion in Northeast Pennsylvania which has moderate porosity and high thickness, and the wet gas portion in Southeast Pennsylvania and West Virginia with high porosity and lower thickness. Although permeability measurements are not particularly reliable, there are private claims in industry that the southwestern portion has a matrix permeability several times higher than the northeastern portion.

Some wells in the southwest are less thermally mature, which means that they have appreciable fractions of ethane and longer-chained carbon gases and liquids. This changes the flow properties in the reservoir and creates a different scaling curve than dry gas wells. In order to select the flow properties, I obtained several PVT reports from Range Energy that listed gas composition in the reservoir. Akand Islam's PVT package is able to take these compositions and produce PVT properties and viscosity for the gas accessed by these wells. I split the field into two gas regions following a line chosen between dry and wet gas regions by Smye et al. (in preparationb), and apply the appropriate production curve to each well.

The best performing gas wells have been drilled in Susquehanna and Bradford Counties in Northeastern Pennsylvania. My analysis indicates that they will produce more than 20 Bcf over their lifetimes, which makes them incredibly productive. If these wells were allowed to produce with a wellbore pressure of 500 psi, they would produce more gas than can be collected. In order to limit the rate at which they produce, the wells are put on choke for the first one to three years of production. This choking is much more dramatic than in the Haynesville, because the wells are making twice as much gas.

It is difficult to know how the choked Marcellus wells decline, because publicly available production data is only given in 6 month increments. This means that a well that has been producing, *e.g.* from July 2013 to January 2015, would only have 3 production data points. In the other fields, with a monthly production requirement, there would be 18 production data points. This severely hampers any analyst's ability to predict production from young wells and from choked wells. It even makes it more difficult to ascertain which young wells are choked.

The criterion for determining whether a well is choked is that the second year's production has dropped by less than 25% from the first year's production, or that the the third or fourth year has dropped less than 20% from the previous year's production. Using this criteria, There are 304 wells that follow this criterion and have been choked for at least 3 years, and there is a set of 869 wells that have been choked for at least two years. This is out of 6,448 wells that have at least 12 months of production, so it represents a large fraction of the field.

There is no easy way to predict production from the choked wells. I have chosen to fit wells with more than 3 years of production from the last month that they were choked. That point is 22 months for wells with two years of choking, 34 months for wells with three years of choking, and 56 months for wells with four years of choking. For wells that are less than 3 years old, I assume that they will produce at the same rate as in their last month until they are 3 years old, and then decline normally. I chose this approach following discussions with industry, especially Range Resources, and from performing hind-casting with incomplete data sets to see what choked wells in the past have done. I see that wells are normally kept on choke for three years, then allowed to decline normally.

Production predictions for each well are handed off to the economists in the Sloan team, and they use the predictions to value each well. Their model prefers monthly production data, so they have designed a scheme to convert 6 month data into monthly production. In order to convert 6 month production into monthly production, they assume that wells decline following the square root of time. We validated this approach by examining West Virginia wells, where we had monthly data, converting this to 6 month data, back converting to monthly, and comparing results. We also gave our estimated monthly production to the industry, and they verified the accuracy of our method.

Another dilemma introduced by the 6-month data points is how to characterize wells with productions that fluctuate. With monthly data, it is relatively easy to see patterns created by "off" months where the well had to have work done on it or the infrastructure limited how much gas could be collected. With six month data sets, it is much more difficult to decide what the "normal" production and decline for a well is.

Wells that behave erratically are identified by having a difference between the production for the first month of forecast in production and the last month of real

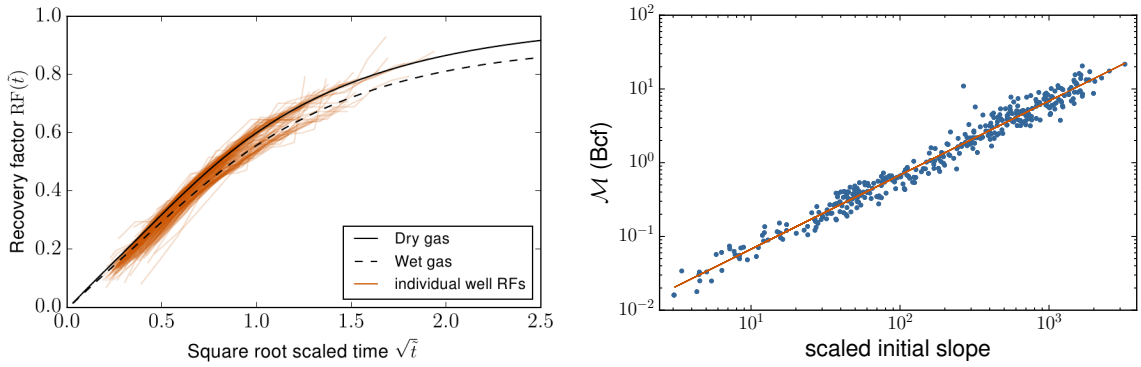

Figure 5.10: Production and gas in place for Marcellus wells in boundary influenced flow. On the left side see RF($\tilde{t}$) plotted for 175 horizontal Marcellus wells which have entered boundary influenced or dominated flow. There are two distinct clusters of curves because recovery factor asymptotes at different values for different pressures, and the pressure distribution in the Marcellus is approximately bi-modal. The black line shows the scaling curve for an initial reservoir pressure of 5,000 psi. On the right is $\mathcal{M}$ compared to initial slope. A line of best fit through this distribution is given.

production more than 8 MMcf/month. Also, production rate between the last month of the second to last reporting period and the first month of the last reporting period must have moved less than 8 MMcf/month. For wells where the last two reporting periods did not match at all, I fit to the entire well's production. These are not altered because it is difficult to argue that one of these reporting periods was somehow more accurate than the other. If they are both in agreement, though, then the year's worth of evidence that the well performs in this manner is chosen over prior history.

For wells that meet the above masking, I fit $\mathcal{M}$ so that the production forecast matches the last data point. Out of the 5,275 wells without signs of choking, 1,878 wells had their production forecast using this method.

In the Marcellus the fitting procedure identifies 404 wells experiencing boundary influenced or dominated flow, 229 of which are horizontal wells. Production for these wells and the comparison of their initial slope to gas in place are given in Fig. 5.10. The line of best fit is $\mathcal{M} = 6.6482(K/\kappa)^{1.0049}$ in MMcf, with an uncertainty in the slope of 0.0087. This leads to a time to interference slightly under four years. Because the vast majority of wells are far younger than that, they are not expected to switch to boundary dominated flow in the near future, instead beginning to interfere in two to three years. This is in sharp contrast to the early interfering Haynesville field.

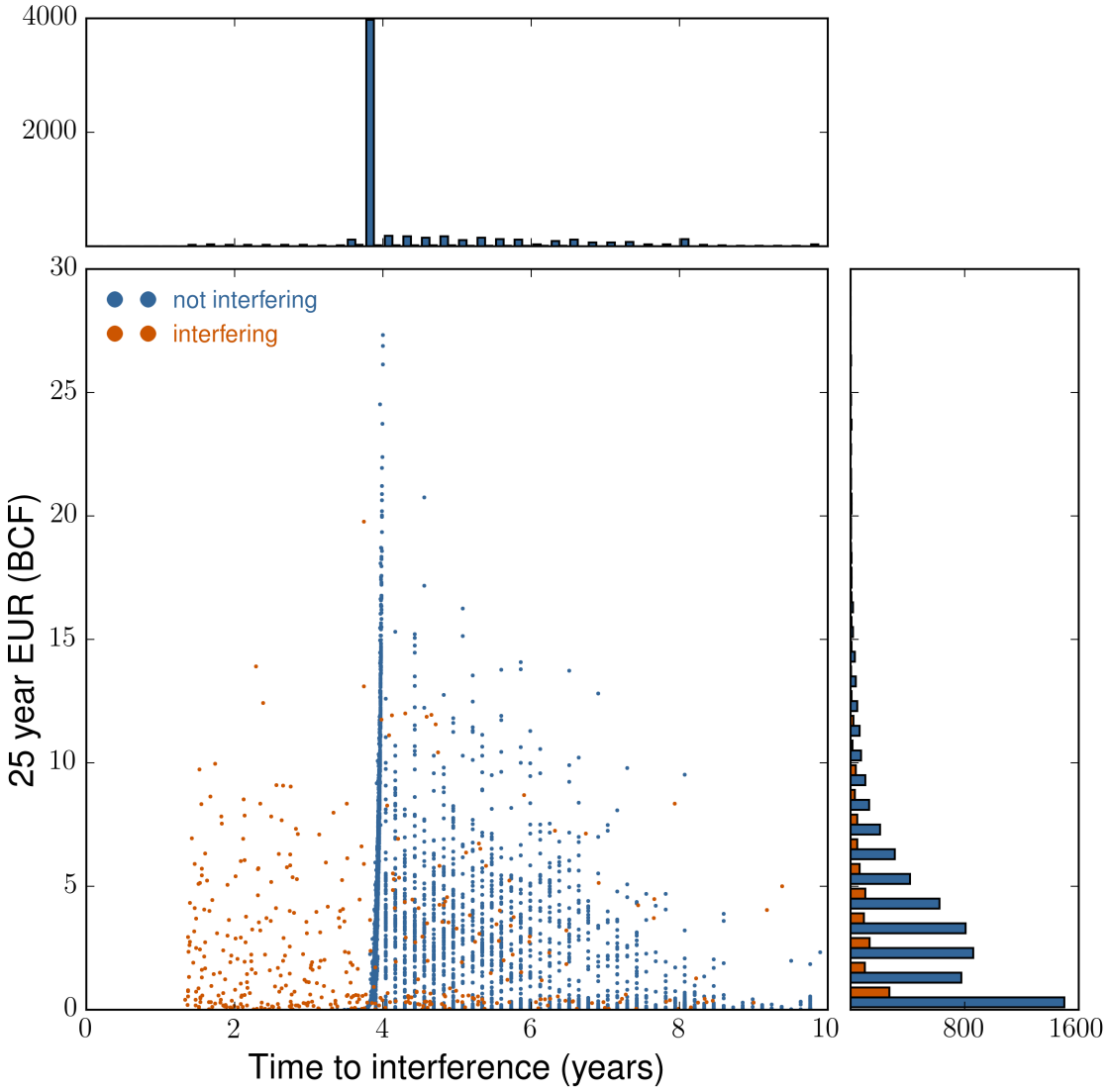

Figure 5.11: Predictions for EUR and time to boundary dominated flow for horizontal Marcellus wells. Blue dots denote wells that have not entered boundary influenced flow and orange dots denote those that have. Nearly four thousand wells are expected to have a τ around 4 years. The upper histogram shows the τ distribution, which is extremely sharply peaked. The right histogram shows the EUR distribution, which appears log-normal.

This procedure yields 25 year forecasts for Marcellus wells with one year of production history. The median horizontal well is expected to produce 3.6 ± 3.6 Bcf of gas in its first 25 years. It is expected to have a $\tau = 3.9 \pm 0.92$ years. The bottom 20% are expected to produce less than 1.8 Bcf and the top 20% are expected to produce more than 6.4 Bcf. Several wells are expected to make more than 20 Bcf, with the best well expected to produce in excess of 35 Bcf. This well is projected to be three times more productive than any shale gas well in any other field. (It is choked.) Production and time to boundary dominated flow predictions for each horizontal well are given in Fig. 5.11.

Marcellus wells show much more scatter in production than wells in other fields. The middle 60% of wells in the Marcellus have a larger variation than the middle 99% in the other fields. This could be due to many factors. First, the geology varies greatly in the Marcellus. There are old vertical wells in West Virginia accessing less than 100 ft of Marcellus shale, and at the same time there are mile-long horizontal wells in Bradford county, Pennsylvania, where the Marcellus is far thicker. Completion practices vary widely for the wells in Pennsylvania, and some wells have production limited by the pipeline's capacity to carry their wells away. These factors and more lead to the differences in production for Marcellus wells.

Chapter Six: Conclusions and Future Work

"God does not play dice with the universe; He plays an ineffable game of His own devising, which might be compared, from the perspective of any of the other players [i.e. everybody], to being involved in an obscure and complex variant of poker in a pitch-dark room, with blank cards, for infinite stakes, with a Dealer who won't tell you the rules, and who *smiles all the time*."

—Terry Pratchett, *Good Omens*

In this dissertation I have explained how physics can inform the problem of analyzing production from shale gas wells. I chose a sensible geometry to consider flow into shale gas wells. Then, I developed the model from first principles and validated it against production from these wells. The problem of determining time to boundary dominated flow in the early production of a well is very difficult, but I developed and applied several solutions. Finally, I used the model to match and predict production from several tens of thousands of producing wells.

Now is the time when I offer what utilities this exercise has provided. There are several conclusions one can draw from this work. First, the goal for this project was to make predictions of how much gas will be produced from as many wells as possible in the four studied shale gas fields. Predicting as many wells as possible and with the best accuracy possible certainly means trade offs must be made. When operators contemplate drilling shale gas wells, they use full scale reservoir simulations with detailed three dimensional geologic information. This is beyond what the Bureau of Economic Geology team can reasonably assemble. The granularity that we can reasonably reach for geologic variables is one square mile. In addition, reservoir simulations can take hours and days per well to dial in and run to yield usable results predicting how a well will perform.

Normally, when given these constraints, aspiring well production forecasters use empirical fitting methods that do not take geology of physics into account and cannot provide insights into why a well is behaving a certain way. Alternatively, forecasters take type curves developed from either empirical equations, simple physical models, or reservoir simulations, and use them to forecast production. This allows them to

Field name	Well count (i)[a]	Production[b]	Median τ	Regression results
Barnett	19,294 (6,153)	1.2±0.9 Bcf	8.0 years	$\mathcal{M} = 8.05(K/\kappa)^{0.98}$
Fayetteville	5,090 (1,253)	1.4±0.8 Bcf	4.8 years	$\mathcal{M} = 5.31(K/\kappa)^{1.03}$
Haynesville	3,036 (2,367)	4.2±2.5 Bcf	2.0 years	$\mathcal{M} = 4.62(K/\kappa)^{0.99}$
Marcellus	6,427 (404)	3.6±3.6 Bcf	3.9 years	$\mathcal{M} = 6.65(K/\kappa)^{1.00}$

[a]number of wells in boundary domianted flow given inside parenthesis
[b]median and standard deviation

Table 6.1: Production and time to boundary dominated flow for each shale gas field. This table summarizes the results of Chapter 5.

include the physics that is most important in determining well production, but still perform forecasts for large sets of wells. They normally have one fitting parameter, the initial production rate. When scaling for initial production rate, all production data is expected to fall on this universal type curve.

In this thesis, I have explained a type curve analysis with two fitting parameters: the total gas in place and the time to boundary dominated flow. I built type curves for four major shale gas fields in the US, individualized for the natural gas PVT properties, effect of adsorption, and reservoir and bottomhole pressures. Each type curve accurately fit production for wells in the field, and the fitting process allowed me to identify whether wells are in the transient or boundary dominated flow regimes. For wells in boundary dominated flow, I forecasted production to 25 years.

Wells in transient flow do not have a known time to boundary dominated flow. To determine τ, I tried several methods, ultimately deciding to use initial production to predict the gas in place, and then use the relationship between initial production, gas in place, and time to boundary dominated flow to determine τ. With this information, the model can forecast production for these wells to 25 years (or any arbitrary time) as well.

The forecasts were given to other members of the BEG team, namely Svetlana Ikonnikova and John Browning. We pored over results, identified weaknesses in the forecasts, and constantly refined the forecasting technique until it was satisfactory. Then, the forecasts were used to build productivity maps for each field. Each square mile block of wells were assigned to a productivity tier, and economic analysis was applied to these tiers. From that economic analysis and a spacing study that identified how many future wells could be drilled in each tier, the economists built a model to

estimate how many wells would be drilled in each tier in each year. This model was used to predict how much each of the four fields will produce in their lifetimes.

Interesting results abound. The Barnett was used as a testing grounds for the physical model. The Fayetteville has the largest contribution from gas desorbing from the rock matrix, and presented an opportunity to extend the physical model to account for desorption. The Haynesville has the shortest time to interference, allowing investigation of how wells perform deep into boundary dominated flow. Its wells have a varying bottomhole pressure because of production choking, which gives reason to expand the model to account for that.

The most difficult and rewarding field I studied is the Marcellus. It has two regions with different fluid properties, the Pennsylvania wells have less frequent production information, and many of the wells are choked for the first several years, never allowed to settle at a constant bottom hole pressure. These were not easy problems to overcome, and the latter two complications make forecasting less reliable than in the earlier fields, but the Marcellus also is where I implemented a new method for forecasting time to boundary dominated flow. This method is more straightforward and transparent than the earlier methods, and provides tighter confidence intervals.

6.1 Future Work

There are several paths this project could follow. The foremost are continuing to develop better methods for determining time to boundary dominated flow earlier, and extending the model to describe oil, water, and even multiphase flow.

The first step in extending the model to oil flow is deriving the analytic solution for a slightly compressible fluid. This is a good baseline for investigating shale oil wells. I plan to use this extension to forecast production from wells in the Bakken tight oil field, the Eagle Ford shale oil field, and the Permian Basin field's Wolfcamp formation.

Oil has a much larger viscosity than gas, so oil shale wells should spend more time in transient flow and have larger τ's. I have examined production from wells in the Eagle Ford with three to four years of production data, and found no oil wells in boundary dominated flow.

There are other considerations in studying oil flow through shale reservoirs. A

rock's permeability to oil can be affected by the presence of water and natural gas This permeability could therefore be constantly varying.

Natural gas flows through the reservoir much faster because it has a lower viscosity than oil. If the natural gas inside the reservoir is depleted quickly, then the pressure gradient that operators rely on to propel oil toward the wellbore disappears. This would lead to oil production dropping faster than the $q \propto 1/\sqrt{t}$ rate expected in linear, transient flow.

There are likely other factors influencing the multiphase flow inside the Eagle Ford and Bakken, which I look forward to investigating. For more discussion of the modeling of oil flow, see Appendix A.

When it comes to determining time to boundary dominated flow for wells in transient flow, there are some ways in which the method can be improved. One improvement would be in adapting the Bayesian method for estimating production and uncertainty that was developed by Gong et al. (2013) to the scaling model developed in this dissertation. Bayesian methods are not utilized for full transient flow models to date, because the models tend to be sufficiently complex to prevent easy adaption to the Bayesian method. Whereas the models discussed in Section 2.3 have significant simplifications and potentially tens of fitting parameters, the model proposed in Chapter 3 has only two scaling parameters τ and $\mathcal{M}$. Wells in transient flow only have one fitting parameter K. This simplification makes the fitting procedure easier than the Duong model, which offers several fitting parameters in the decline equation

$$Q = \frac{q_1}{a} \exp\left[\frac{a}{1-m}\left(t^{1-m} - 1\right)\right],$$

with q_1, a, and m all fitting parameters, and Q the cumulative production. This makes application of the Bayesian, Markov Chain Monte Carlo approach fairly straightforward for the RF curve.

Another goal for the future is determining and reporting uncertainty explicitly. Wells that are still young or where boundary influenced flow has been seen are fairly straightforward. The fitting procedure provides uncertainty on τ and $\mathcal{M}$ for interfering wells. The regression matching $\mathcal{M}$ to initial production provides uncertainty in $\mathcal{M}$ for a specific initial production. The time to boundary dominated flow distribution for already interfering wells has a standard deviation that can be used to give an idea of the uncertainty in τ_0.

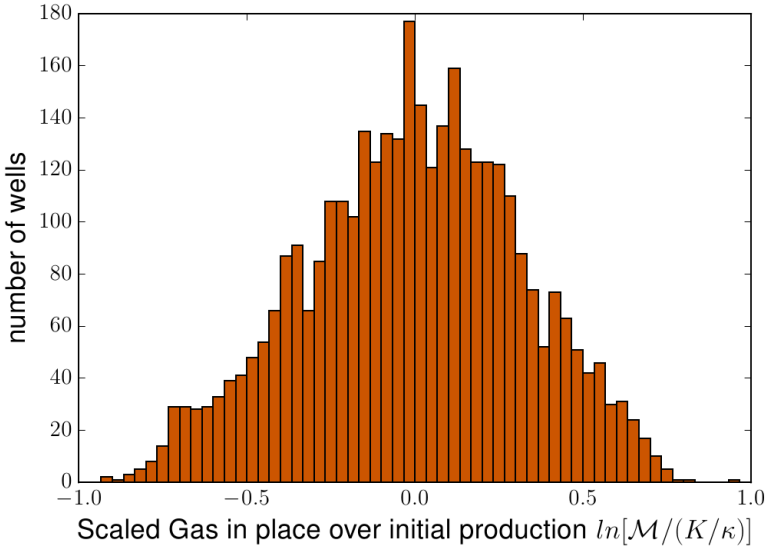

Figure 6.1: Histogram showing relation between initial and total production in the Barnett. Gas in place is divided by the initial slope in production. It is centered at $\mathcal{M}/(K/\kappa) = 1$, then I take the natural logarithm of this quantity. The histogram presents a new way of discussing the relationship betwen initial and ultimate production. It also indicates that a statistical approach can be used to provide estimates of $\mathcal{M}$ and τ from initial production.

There is evidence that this procedure could work. The histogram given in Fig. 6.1 shows that there is a probability distribution for $\mathcal{M}$ given an initial production. This distribution can be used to give confidence intervals for gas in place and time to boundary dominated flow.

Other wells have uncertainties that are not so clear. In some fields, there are wells that have been in transient flow far longer than τ_0. Wells such as this might have a time to boundary dominated flow that lies outside the distribution of τ for already interfering wells, and therefore do not closely follow the relation between $\mathcal{M}$ and initial production.

For these wells, I estimate $.64\tau = t_{max}$ and get $\mathcal{M}$ from (4.2), but there is no clear method for determining confidence in the τ and $\mathcal{M}$ estimates for these wells.

Another set of wells wells are only slightly past the point where $0.64t_{max} = \tau_0$. For these wells, I also estimate $0.64\tau = t_{max}$. The wells are still potentially within the cloud that is created by plotting $\mathcal{M}$ vs initial production, so they are not the same as the earlier group. The uncertainty in τ appears smaller because the lower

half of the τ distribution has been eliminated, but is there actually more certainty in an estimate of τ. What is the certainty here?

Physical intuition and advanced statistics can be used to tackle these problems, given some time and creativity.

Appendix A: Extending the model to oil and condensate flow

In this appendix I will briefly sketch my plans for future work extending the model to oil and condensate flow[1]. The first step in describing oil flow is giving the equations for a slightly compressible fluid flowing through porous media.

There are some well-known differences between natural gas and oil reservoirs, which make extraction of oil from shale more difficult. The neatest packaging of these differences that I have seen was given by Alton Brown in a recent talk, and I will endeavor to offer his ideas in my words. First, oil does not desorb from the rock as pressure decreases. In gas reservoirs, desorbing gas contributes significantly to the final production, and this creates both a larger gas in place $\mathcal{M}$ and a slower and more gentle switch to boundary dominated flow. Oil wells do not get to benefit from this effect.

In addition, there is less energy driving oil from the reservoir to the fracture. Natural gas expands as pressure decreases, allowing for recovery factors to reach above 0.8. Oil is incompressible and does not expand, so theoretical maximum recovery factors are much smaller. In conventional reservoirs, this is alleviated by a pool of gas at the top of the reservoir, which expands as pressure is withdrawn from the reservoir and drives the oil toward the well. In unconventional reservoirs, the permeability is so small that gas does not accumulate, and this effect does not occur.

Pressure diffusion in oil is described by

$$\frac{\partial p}{\partial t} = \alpha(p)\nabla^2 p, \tag{A.1}$$

where the diffusivity is

$$\alpha = \frac{k}{\phi S_o \mu c}. \tag{A.2}$$

When the oil is coexisting with other fluids like natural gas, then permeability k is a function of the gas, oil, and water saturation. Land et al. (1968) found relative

[1]Many derivations of oil flow in one dimension exist in the literature (see *e.g.* Wattenbarger et al. (1998)), but I follow a derivation performed by Tad Patzek from a personal communication, where he considers gas flow. I recast the form of the derivation so that it is consistent with the derivation for real gas in Chapter 3.

permeability functions for multiphase systems. They give relations for gas, oil and water permeabilities depending upon the saturation.

The diffusivity of oil takes values that are often very different from the diffusivity of gas. This is mainly due to two parameters inside (A.2). First, the relative permeability of oil can be very low, sometimes one tenth and lower, when there is considerable water saturation. In the Eagle Ford and Bakken fields, water saturation indeed can be large. Also, the viscosity, μ of oil is one to two orders of magnitude larger than natural gas. These two effects can bring the diffusivity of oil to two to three orders of magnitude lower than the diffusivity of natural gas. This has important ramifications I will discuss below.

With a few assumptions it is possible to derive an analytical expression for oil production rate $q_o(\tilde{t})$ and oil recovery factor $\mathrm{RF}_o(\tilde{t})$. First, consider one-dimensional (rectilinear) flow in the x direction, and use the dimensionless form of the pressure diffusion equation, where

$$\begin{aligned} \tilde{p} &= \frac{p - p_f}{p_i - p_f} \qquad \tilde{t} = t/\tau \\ \tau &= d^2/\alpha_i \qquad \alpha_i = \left.\frac{k}{\phi S_o \mu_o c_o}\right|_{p=p_i} \\ \tilde{x} &= x/d. \end{aligned} \tag{A.3}$$

This creates a pressure diffusion equation very similar to (3.16), but for oil pressure rather than gas pseudopressure. The scaled diffusion equation and boundary conditions are

$$\begin{aligned} \frac{\partial \tilde{p}}{\partial \tilde{t}} &= \frac{\alpha}{\alpha_i}\frac{\partial^2 \tilde{p}}{\partial \tilde{x}^2} \\ \tilde{p}(\tilde{x}, \tilde{t} = 0) &= \tilde{p}_i \qquad = 1 \text{ for most } \tilde{x} \\ \tilde{p}(\tilde{x} = 0, \tilde{t}) &= 0 \\ \left.\frac{\partial \tilde{p}}{\partial \tilde{x}}\right|_{\tilde{x}=1} &= 0. \end{aligned} \tag{A.4}$$

If α is constant for all pressures, then there is an analytic solution to this set of equations. It is messy, but it has been solved before using separation of variables by Carslaw and Jaeger (1959, p 100). For dimensionless space and time, the solution is

$$\tilde{p} = \frac{4}{\pi}\sum_{n=0}^{\infty}\frac{(-1)^n}{2n+1}\exp[-(2n+1)^2\pi^2\tilde{t}/4]\cos\left[\frac{(2n+1)}{2}\pi\tilde{x}\right]. \tag{A.5}$$

From this solution, consider the gradient at the hydrofracture:

$$\begin{aligned}\frac{\partial p}{\partial x} &= 2\sum_{n=0}^{\infty}(-1)^n \exp[-(2n+1)^2\pi^2\tilde{t}/4]\sin\left[\frac{(2n+1)}{2}\pi\tilde{x}\right], \\ &= 2\sum_{n=0}^{\infty}\exp[-(2n+1)^2\pi^2\tilde{t}/4] \\ &\approx \frac{1}{2\sqrt{\pi\tilde{t}}}\operatorname{erfc}\left(\frac{3\pi}{2}\sqrt{\tilde{t}}\right) + \exp(-\pi^2\tilde{t}/4) + \frac{1}{2}\exp(-9\pi^2\tilde{t}/4). \end{aligned} \tag{A.6}$$

This provides the production rate, after being returned to dimensionality. An alternate method for determining the solution is given by Ogunyomi (2015, Appendix A). Production rate is

$$q_o/(\mathcal{M}p^*) = \frac{1}{2\sqrt{\pi\tilde{t}}}\operatorname{erfc}\left(\frac{3\pi}{2}\sqrt{\tilde{t}}\right) + \exp(-\pi^2\tilde{t}/4) + \frac{1}{2}\exp(-9\pi^2\tilde{t}/4), \tag{A.7}$$

where $p^* = (p_i - p_f)/p_i$, which is the fraction of $\mathcal{M}$ that can expand as pressure in the reservoir depletes to the pressure at the fracture. This is not made explicit in other derivations of production because people following Wattenbarger et al. (1998)'s derivation follow the convention of making production dimensionless with the definition

$$q_D = \frac{141.2qB\mu}{kh(p_i - p_f)}, \tag{A.8}$$

which does not explicitly incorporate the oil in place, $\mathcal{M}$. Incorporating oil in place requires accounting for oil compression in the way I have done above. In the gas model given in Chapter 3, gas expansion is handled within the numerical calculation and is not accounted for in this way.

Integrating this over time gives the recovery factor, which is described by the equation

$$\begin{aligned}\mathrm{RF}_o &= \frac{Q_o}{\mathcal{M}p^*} \\ &= \sqrt{\frac{\tilde{t}}{\pi}}\operatorname{erfc}\left(\frac{3\pi}{2}\sqrt{\tilde{t}}\right) + \frac{4}{\pi^2}\left[1 - \exp(-\pi^2\tilde{t}/4)\right] + \frac{8}{9\pi^2}\left[1 - \exp(-9\pi^2\tilde{t}/4)\right]. \end{aligned} \tag{A.9}$$

This recovery factor bears some resemblence to the recovery factor for natural gas wells, but decline is far sharper. Also, the recovery factor assymptotes at approximately 0.52, which means that much more oil is never extracted from the reservoir.

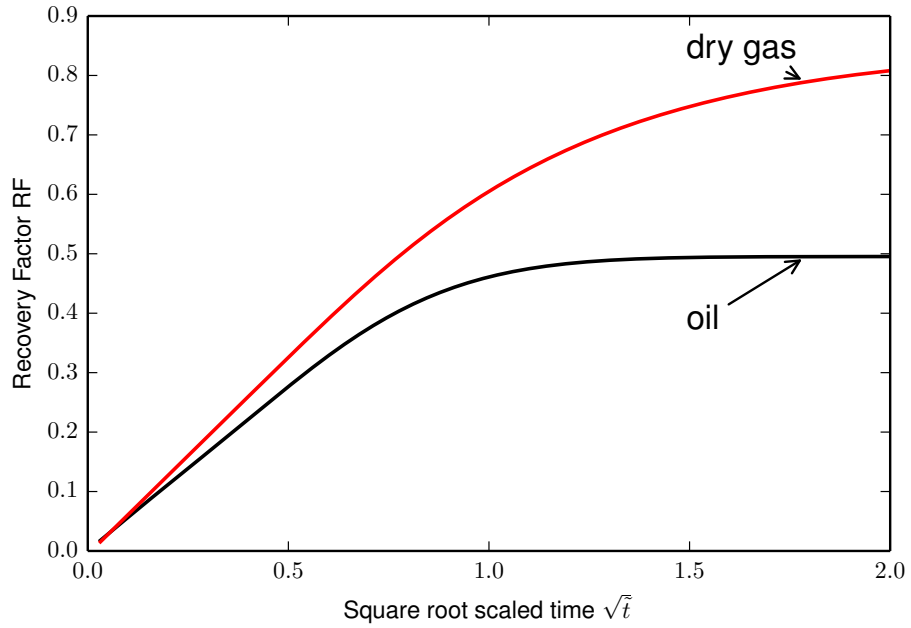

Figure A.1: Recovery factor for a hydrofractured oil well. A direct comparison is given to the recovery factor curve for a hydrofractured natural gas well. The horizontal axis is square root dimensionless time. Natural gas wells yield higher recovery factors than oil wells in this configuration because compressibility varies greatly with pressure for methane. In the oil well curve shown, compressibility does not vary with pressure.

This is because the oil compressibility changes far less with pressure than gas pressure does. As mentioned above, oil is essentially incompressible, and this means that more is left behind when the drained area has reached the same pressure as the fracture (at the end of life).

Oil has a higher viscosity than gas, so the diffusivity of oil through shale is much lower than the diffusivity of gas. This means that time to boundary dominated flow can be delayed until the end of a well's life. An initial look at production from oil wells in the Eagle Ford field, given in Fig. A.2, tends to support that claim. It also appears to show a slight deviation from linear, transient flow which might mean permeability to oil is changing over time.

In the future, numerical solutions to (A.4) will provide more accurate type curves, incorporating a diffusivity that is a function of pressure. The diffusivity can change due to many factors. The largest factors are likely lowered pressure causing phase

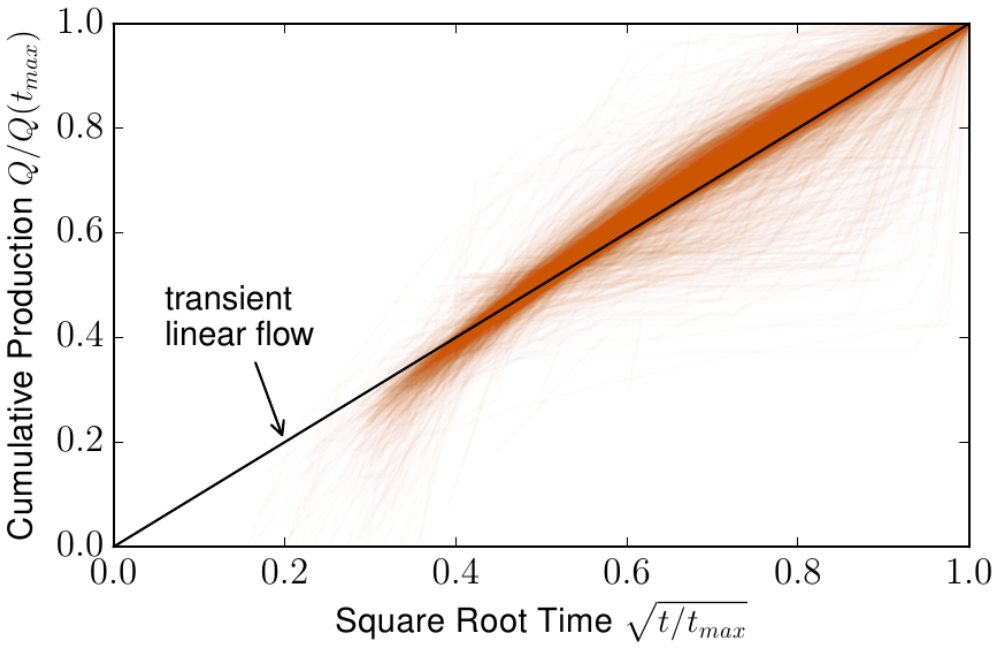

Figure A.2: Eagle Ford oil well cumulative production. There are 3,135 oil wells contributing to this plot. Some wells show erratic production due to the oil pressure in the reservoir being near the bubble point. Other wells show large increases or decreases in production that could be due to refracturing, mechanical problems, or other causes.

separation into oil and gas, and lowered pressure allowing fractures to relax, lowering the permeability.

Bibliography

Elihu Abrahams, PW Anderson, DC Licciardello, and TV Ramakrishnan. Scaling theory of localization: Absence of quantum diffusion in two dimensions. *Physical Review Letters*, 42(10):673–676, 1979. 14

M Ahlskog, M Reghu, T Noguchi, and T Ohnishi. Doping and conductivity studies on poly (p-phenylene vinylene). *Synthetic metals*, 89(1):11–15, 1997. 16

Hasan A Al Ahmadi, Anas M Almarzooq, Robert A Wattenbarger, et al. Application of linear flow analysis to shale gas wells-field cases. In *SPE Unconventional Gas Conference*. Society of Petroleum Engineers, 2010. 26

R Al-Hussainy, HJJ Ramey, and Crawford PB. The flow of real gases through porous media. *AIME Petrol Transactions*, 237:624–636, 1966. 24, 25, 37

Philip W Anderson. Absence of diffusion in certain random lattices. *Physical review*, 109(5):1492, 1958. 14

John D Anderson Jr. Ludwig Prandtls boundary layer. *Physics Today*, 58(12):42–48, 2005. 9

J. J. Arps. Analysis of decline curves. *AIME Petrol. Transactions*, 160:228–247, 1945. 19

J. J. Arps. Estimation of primary oil reserves. *AIME Petrol. Transactions*, 207: 182–191, 1956. 19

Grigory Isaakovich Barenblatt. *Scaling, self-similarity, and intermediate asymptotics: dimensional analysis and intermediate asymptotics*, volume 14. Cambridge University Press, 1996. 16

J. Bertrand. Sur l'homogénéité dans les formules de physique. *Comptes rendus*, 86: 916–920, 1878. 11

Fabrizio Bonani and Giovanni Ghione. On the application of the kirchhoff transformation to the steady-state thermal analysis of semiconductor devices with

temperature-dependent and piecewise inhomogeneous thermal conductivity. *Solid-State Electronics*, 38(7):1409–1412, 1995. 25

Kent A Bowker. Development of the Barnett shale play, Fort Worth basin. *AAPG Bulletin*, 91(4), 2007. 3

John Browning, Svetlana Ikonnikova, Gürcan Gülen, Scott Tinker, et al. Barnett shale production outlook. *SPE Economics and Management*, 5(03):89–104, 2013a. 58

John Browning, Scott W Tinker, Svetlana Ikonnikova, Gürcan Gülen, Eric Potter, Qilong Fu, Susan Hovarth, Tad W Patzek, Frank Male, William Fisher, Forrest Roberts, and Ken Medlock III. BARNETT SHALE MODEL-1: Barnett study determines full-field reserves, production forecast. *Oil and Gas Journal*, 111:62, 2013b. 6

John Browning, Scott W Tinker, Svetlana Ikonnikova, Gürcan Gülen, Eric Potter, Qilong Fu, Susan Hovarth, Tad W Patzek, Frank Male, William Fisher, Forrest Roberts, and Ken Medlock III. BARNETT SHALE MODEL-2 (conclusion): Barnett study determines full-field reserves, production forecast. *Oil and Gas Journal*, 111, 2013c. 6

John Browning, Scott W Tinker, Svetlana Ikonnikova, Gürcan Gülen, Eric Potter, Qilong Fu, Susan Hovarth, Tad W Patzek, Frank Male, William Fisher, and Forrest Roberts. Study develops Fayetteville shale reserves, production forecast. *Oil and Gas Journal*, 112, 2014. 6

Stephen Brunauer, Paul Hugh Emmett, and Edward Teller. Adsorption of gases in multimolecular layers. *Journal of the American Chemical Society*, 60(2):309–319, 1938. 30, 31

Edgar Buckingham. On physically similar systems; illustrations of the use of dimensional equations. *Physical Review*, 4(4):345–376, 1914. 11

AC Bumb, CR McKee, et al. Gas-well testing in the presence of desorption for coalbed methane and Devonian shale. *SPE Formation Evaluation*, 3(01):179–185, 1988. 29

Philip Crosbie Carman. Fluid flow through granular beds. *Transactions-Institution of Chemical Engineeres*, 15:150–166, 1937. 17

Philip Crosbie Carman. *Flow of gases through porous media*. Butterworths Scientific Publications London, 1956. 17

H.S. Carslaw and J.C. Jaeger. *Conduction of heat in solids*. Clarendon Press, Oxford, 1959. second edition. 83

RD Carter. Type curves for finite radial and linear gas-flow systems: constant-terminal-pressure case. *Society of Petroleum Engineers journal*, 25(5):719–728, 1985. 23, 24

Kuldeep Chaudhary, M Bayani Cardenas, Wen Deng, and Philip C Bennett. The role of eddies inside pores in the transition from Darcy to Forchheimer flows. *Geophysical Research Letters*, 38(24), 2011. 17

G Chauveteau and CL Thirriot. Régimes d'écoulement en milieu poreux et limite de la loi de Darcy. *La Houille Blanche*, (2):141–148, 1967. 17

Yueming Cheng, Yuhong Wang, Duane Allen McVay, W John Lee, et al. Practical application of probabilistic approach to estimate reserves using production-decline data. In *SPE Annual Technical Conference and Exhibition*. Society of Petroleum Engineers, 2005. 21

Gregory C Chow. Tests of equality between sets of coefficients in two linear regressions. *Econometrica: Journal of the Econometric Society*, pages 591–605, 1960. 47

Aaron James Clark, Larry Wayne Lake, Tadeusz Wiktor Patzek, et al. Production forecasting with logistic growth models. In *Paper SPE 144790 presented at the SPE Annual Technical Conference and Exhibition, Denver, CO*, volume 30, 2011. 21

Stewart Coleman, HD Wilde Jr, Thomas W Moore, et al. Quantitative effect of gas-oil ratios on decline of average rock pressure. *Transactions of the AIME*, 86(01): 174–184, 1930. 18

John B Curtis. Fractured shale-gas systems. *AAPG bulletin*, 86(11):1921–1938, 2002. 1

L.P. Dake. *Fundamentals of Reservoir Engineering (Developments in Petroleum Science)*. Elsevier Science, 1983. 19

Henri Darcy. *Les fontaines publiques de la ville de Dijon: exposition et application...* Victor Dalmont, 1856. 17

Jelle Zeilinga de Boer, John R Hale, and J Chanton. New evidence for the geological origins of the ancient delphic oracle (greece). *Geology*, 29(8):707–710, 2001. 1

Parke A Dickey et al. The first oil well. *Journal of Petroleum Technology*, 11(01): 14–26, 1959. 1

Jia-Jyun Dong, Jui-Yu Hsu, Wen-Jie Wu, Toshi Shimamoto, Jih-Hao Hung, En-Chao Yeh, Yun-Hao Wu, and Hiroki Sone. Stress-dependence of the permeability and porosity of sandstone and shale from tcdp hole-a. *International Journal of Rock Mechanics and Mining Sciences*, 47(7):1141–1157, 2010. 37

Anh N Duong. An unconventional rate decline approach for tight and fracture-dominated gas wells. In *Canadian Unconventional Resources and International Petroleum Conference*. Society of Petroleum Engineers, 2010. 21, 45

Anh N Duong. Rate-decline analysis for fracture-dominated shale reservoirs. *SPE Reservoir Evaluation & Engineering*, 14(03):377–387, 2011. 21

Jules Dupuit. *Études théoriques et pratiques sur la mouvement des eaux dans les canaux découverts et à travers les terrains perméables: avec des considérations relatives au régime des grandes eaux, au débouché à leur donner, et à la marche des alluvions dans les rivières à fond mobile*. Dunod, 1863. 17

JT Edwards and DJ Thoules. Regularity of the density of states in anderson's localized electron model. *Journal of Physics C: Solid State Physics*, 4(4):453, 1971. 14

Energy Information Administration EIA. U.S. crude oil, natural gas, and natural gas liquids reserves annual report, 2006. http://www.eia.gov/totalenergy/data/annual/archive/038405.pdf. 57

MJ Fetkovich et al. Decline curve analysis using type curves. *Journal of Petroleum Technology*, 32(6):1065–1077, 1980. 20, 23, 24, 39

Michael E Fisher. The renormalization group in the theory of critical behavior. *Reviews of Modern Physics*, 46(4):597, 1974. 13

Philipp Forchheimer. Wasserbewegung durch boden. *Z. Ver. Deutsch. Ing*, 45(1782): 1788, 1901. 17

Qilong Fu, Susan C Horvath, Eric C Potter, Forrest Roberts, Scott W Tinker, Svetlana Ikonnikova, William L Fisher, and Jihua Yan. Log-derived thickness and porosity of the Barnett shale, Fort Worth basin, Texas: Implications for assessment of gas shale resources. *AAPG Bulletin*, 99(1):119–141, 2015. 48, 50

Mohamed Gad-el Hak. Fluid mechanics from the beginning to the third millennium. *International Journal of Engineering Education*, 14(3):177–185, 1998. 8, 9

Xinglai Gong, Yao Tian, Duane A McVay, Walter B Ayers, John Lee, et al. Assessment of Eagle Ford shale oil and gas resources. In *SPE Unconventional Resources Conference Canada*. Society of Petroleum Engineers, 2013. 21, 22, 79

Mario Hugo Gonzalez, Bertram Eugene Eakin, and Anthony L Lee. *Viscosity of natural gases: monograph on API Research Project 65*. American Petroleum Institute, 1970. 50

Alain Gringarten, Henry Ramey, and R. Raghavan. Unsteady-state pressure distributions created by a well with a single infinite-conductivity vertical fracture. *Transactions of the American Institute of Mining, Metallurgical and Petroleum Engineers*, 257, 1974. 24

Ed Hagenbach. Über die bestimmung der zähigkeit einer flüssigkeit durch den ausfluss aus röhren. *Annalen der Physik*, 185(3):385–426, 1860. 8

Rob Heller, John Vermylen, and Mark Zoback. Experimental investigation of matrix permeability of gas shales. *AAPG bulletin*, 98(5):975–995, 2014. 67, 68

Robert Heller and Mark Zoback. Adsorption of methane and carbon dioxide on gas shale and pure mineral samples. *Journal of Unconventional Oil and Gas Resources*, 8:14–24, 2014. 31

Ronald J Hill, Daniel M Jarvie, John Zumberge, Mitchell Henry, and Richard M Pollastro. Oil and gas geochemistry and petroleum systems of the fort worth basin. *AAPG bulletin*, 91(4):445–473, 2007. 50

M King Hubbert. The theory of ground-water motion. *The Journal of Geology*, pages 785–944, 1940. 17

William Hurst. Unsteady flow of fluids in oil reservoirs. *Journal of Applied Physics*, 5(1):20–30, 1934. 23

William Hurst et al. Water influx into a reservoir and its application to the equation of volumetric balance. *Transactions of the AIME*, 151(01):57–72, 1943. 23

Svetlana Ikonnikova, John Browning, Susan Christine Horvath, and Scott Tinker. Well recovery, drainage area, and future drill-well inventory: Empirical study of the Barnett shale gas play. *SPE Reservoir Evaluation & Engineering*, 17(04):484–496, 2014. 48

Dilhan Ilk, Jay Alan Rushing, Albert Duane Perego, Thomas Alwin Blasingame, et al. Exponential vs. hyperbolic decline in tight gas sands: Understanding the origin and implications for reserve estimates using Arps' decline curves. In *SPE Annual Technical Conference and Exhibition*. Society of Petroleum Engineers, 2008. 21

S Irmay. On the theoretical derivation of Darcy and Forchheimer formulas. *Transactions, American Geophysical Union*, 39:702–707, 1958. 17

Ernst Ising. A contribution to the theory of ferromagnetism. *Z. Phys*, 31(1):253–258, 1925. 11

Akand Islam and Tad Patzek. Slip in natural gas flow through nanoporous shale reservoirs. *Journal of Unconventional Oil and Gas Resources*, 7(0):49 – 54, 2014. 18

Kingo Itaya, Shizuo Sugawara, Kunio Arai, and Shozaburo Saito. Properties of porous anodic aluminum oxide films as membranes. *Journal of chemical engineering of Japan*, 17(5):514–520, 1984. 18

Farzam Javadpour. Nanopores and apparent permeability of gas flow in mudrocks (shales and siltstone). *Journal of Canadian Petroleum Technology*, 48(8):16–21, 2009. 18

Zheng Jiexin and Andrew Palmer. Bamboo pipelines in ancient china (and now?). *Journal of Pipeline Engineering*, 8(2):95 – 98, 2009. ISSN 17532116. 1

VA Jochen, JP Spivey, et al. Probabilistic reserves estimation using decline curve analysis with the bootstrap method. In *SPE Annual Technical Conference and Exhibition*. Society of Petroleum Engineers, 1996. 21, 22

DC Johnston. Stretched exponential relaxation arising from a continuous sum of exponential decays. *Physical Review B*, 74(18):184430, 2006. 21

PJ Jones. Estimating oil reserves from production-decline rates. *Oil and Gas Jnl*, 43, 1942. 19, 20

Krunal Joshi and W John Lee. Comparison of various deterministic forecasting techniques in shale gas reservoirs. In *SPE Hydraulic Fracturing Technology Conference*. Society of Petroleum Engineers, 2013. 21

WB Joyce. Thermal resistance of heat sinks with temperature-dependent conductivity. *Solid-State Electronics*, 18(4):321–322, 1975. 25

Leo P Kadanoff. Scaling laws for ising models near tc. *Physics*, 2(6):263–272, 1966. 12

Mohan Kelkar. *Natural gas production engineering*. PennWell Books, 2008. 26, 32

George Everette King et al. Hydraulic fracturing 101: What every representative environmentalist regulator reporter investor university researcher neighbor and engineer should know about estimating frac risk and improving frac performance in unconventional gas and oil wells. In *SPE Hydraulic Fracturing Technology Conference*. Society of Petroleum Engineers, 2012. 2

LJ Klinkenberg et al. The permeability of porous media to liquids and gases. *Drilling and production practice*, 1941. 18

B Kopey. Development of drilling technics from ancient ages to modern times. In *Proceedings of Twelfth World Congress in Mechanism and Machine Science*, 2007. 1

Josef Kozeny. *Über kapillare Leitung des Wassers im Boden:(Aufstieg, Versickerung und Anwendung auf die Bewässerung)*. Hölder-Pichler-Tempsky, 1927. 17

Utpalendu Kuila and Manika Prasad. Specific surface area and pore-size distribution in clays and shales. *Geophysical Prospecting*, 61(2):341–362, 2013. 31

B Lally, L Biegler, and H Henein. Finite difference heat-transfer modeling for continuous casting. *Metallurgical Transactions B*, 21(4):761–770, 1990. 25

Carlon S Land et al. Calculation of imbibition relative permeability for two-and three-phase flow from rock properties. *Society of Petroleum Engineers Journal*, 8 (02):149–156, 1968. 82

Irving Langmuir. The adsorption of gases on plane surfaces of glass, mica and platinum. *Journal of the American Chemical society*, 40(9):1361–1403, 1918. 29

Anthony L Lee, Mario H Gonzalez, and Bertram E Eakin. The viscosity of natural gases. *Journal of Petroleum Technology*, 18(8):997–1000, 1966. 40

W John Lee and Rodney Earl Sidle. Gas reserves estimation in resource plays. *SPE Economics & Management*, 2(2):86–91, 2010. 26, 32

Gregoire Lemoult and Bjorn Hof. The onset of turbulence in a square duct flow. *Bulletin of the American Physical Society*, 59, 2014. 10

Adam Michael Lewis and Richard Gary Hughes. Production data analysis of shale gas reservoirs. In *SPE Annual Technical Conference and Exhibition*. Society of Petroleum Engineers, 2008. 26

Robert G Loucks, Robert M Reed, Stephen C Ruppel, and Daniel M Jarvie. Morphology, genesis, and distribution of nanometer-scale pores in siliceous mudstones of the Mississippian Barnett shale. *Journal of sedimentary research*, 79(12):848–861, 2009. 31

Frank Male, Akand W Islam, Tad W Patzek, Svetlana Ikonnikova, John Browning, and Michael P Marder. SPE 168993MS: Analysis of gas production from hydraulically fractured wells in the haynesville shale using scaling methods. In *SPE Unconventional Resources Conference*. Society of Petroleum Engineers, 2014. 35, 40, 52, 65

Frank Male, Akand W Islam, Tad W Patzek, Svetlana Ikonnikova, John Browning, and Michael P Marder. Analysis of gas production from hydraulically fractured wells in the haynesville shale using scaling methods. *Journal of Unconventional Oil and Gas Resources*, 2015. 65

Frank Male, Michael P. Marder, Tad Patzek, John Browning, and Svetlana Ikonnikova. Marcellus ultimate production accurately predicted from initial production. in preparationa. 69

Frank Male, Tad Patzek, Wei Yu, Svetlana Ikonnikova, John Browning, and Michael P. Marder. Analysis of gas production in the fayetteville formation using scaling arguments. in preparationb. 50, 62

Michael P Marder. *Condensed matter physics*. John Wiley & Sons, 2010. 15

David F Martineau. History of the Newark East field and the Barnett shale as a gas reservoir. *AAPG bulletin*, 91(4):399–403, 2007. 57

L Matter and GS Brar. Compressibility of natural gases. *J Can Petrol Technol.*, pages 77–80, August 1975. 41

Michael J Mayerhofer, Elyezer Lolon, Norman Raymond Warpinski, Craig L Cipolla, Douglas W Walser, Claude Michael Rightmire, et al. What is stimulated rock volume? In *SPE Shale Gas Production Conference*. Society of Petroleum Engineers, 2008. 35

Thane Hubert McCulloh. Mass properties of sedimentary rocks and gravimetric effects of petroleum and natural-gas reservoirs. Technical report, US Govt. Print. Off.,, 1967. 30

TV Moore, RJ Schilthuis, and William Hurst. The determination of permeability from field data. *Proc., API Bull*, 211(4), 1933. 23

Randall P. Munroe. Dimensional analysis, 2010. URL `http://xkcd.com/687/`. accessed 23 Dec. 2014. 11

CLMH Navier. Mémoire sur les lois du mouvement des fluides. *Mémoires de lAcadémie Royale des Sciences de lInstitut de France*, 6:389–440, 1823. 8

Philip H Nelson. Pore-throat sizes in sandstones, tight sandstones, and shales. *AAPG bulletin*, 93(3):329–340, 2009. 17

M. Nobakht, C. Clarkson, and D. Kaviani. SPE 147869 New and Improved Methods for Performing Rate-Transient Analysis of Shale Gas Reservoirs. In *Proceedings of SPE Asia Pacific Oil and Gas Conference and Exhibition*, number 1, pages 1–19. Society of Petroleum Engineers, September 2011. ISBN 9781613991374. doi: 10.2118/147869-MS. 28

Babafemi Anthony Ogunyomi. *Simple Mechanistic Modeling of Recovery from Unconventional Oil Reservoirs*. PhD thesis, University of Texas at Austin, May 2015. 84

Babafemi Anthony Ogunyomi, Song Dong, Nguyen La, Larry Wayne Lake, and C Shah Kabir. A new approach to modeling production decline in unconventional formations. In *SPE Annual Technical Conference and Exhibition*. Society of Petroleum Engineers, 2014. 21

Lars Onsager. Crystal statistics. i. a two-dimensional model with an order-disorder transition. *Physical Review*, 65(3-4):117, 1944. 12

JC Palacio and TA Blasingame. Decline curve analysis using type curves: Analysis of gas well production data. *paper SPE*, 25909:12–14, 1993. 24

Tad Patzek, Frank Male, and Michael Marder. A simple model of gas production from hydrofractured horizontal wells in shales. *AAPG Bulletin*, 98(12):2507–2529, 2014. iv, 27, 35, 57

Tad W. Patzek. SPE 24040: Surveillance of South Belridge diatomite. In *Proceedings of the Western Regional SPE Meeting*, Bakersfield, CA, 1992. 24

Tad W Patzek, Frank Male, and Michael Marder. Gas production in the Barnett Shale obeys a simple scaling theory. *Proceedings of the National Academy of Sciences*, 110(49):19731–19736, 2013. iv, 35, 57

Samuel T. Pees. Oil history, 2004. URL `http://www.petroleumhistory.org/`. Petroleum History Institute. 1

Rudolf Peierls. On ising's model of ferromagnetism. In *Mathematical Proceedings of the Cambridge Philosophical Society*, volume 32, pages 477–481. Cambridge Univ Press, 1936. 12

Fernando Pérez and Brian E. Granger. IPython: a system for interactive scientific computing. *Computing in Science and Engineering*, 9(3):21–29, May 2007. ISSN 1521-9615. doi: 10.1109/MCSE.2007.53. URL `http://ipython.org`. iv

L Prandtl. Über flüssigkeitsbewegung bei sehr kleiner reibung, verhandl. 14. In *Internationaler Math. Kongress Heidelberg*, 1904. 9

M Prats et al. Effect of vertical fractures on reservoir behavior-incompressible fluid case. *Society of Petroleum Engineers Journal*, 1(02):105–118, 1961. 23

W Press. Structure and phase transitions of solid heavy methane (cd4). *The Journal of Chemical Physics*, 56(6):2597–2609, 1972. 30

Lord Rayleigh. On the question of the stability of the flow of fluids. *The London, Edinburgh, and Dublin philosophical magazine and journal of science*, 34(206):59–70, 1892. 11

Otto Redlich and JNS Kwong. On the thermodynamics of solutions. V. An equation of state. Fugacities of gaseous solutions. *Chemical Reviews*, 44(1):233–244, 1949. 40

John J Roche. *The mathematics of measurement: A critical history*. Springer, 1998. 11

Daniel JK Ross and R Marc Bustin. The importance of shale composition and pore structure upon gas storage potential of shale gas reservoirs. *Marine and Petroleum Geology*, 26(6):916–927, 2009. 31

N Rott. Note on the history of the reynolds number. *Annual review of fluid mechanics*, 22(1):1–12, 1990. 10

Subrata Roy, Reni Raju, Helen F Chuang, Brett A Cruden, and M Meyyappan. Modeling gas flow through microchannels and nanopores. *Journal of applied physics*, 93(8):4870–4879, 2003. 18

DG Russell, NE Truitt, et al. Transient pressure behavior in vertically fractured reservoirs. *Journal of Petroleum Technology*, 16(10):1–159, 1964. 23

Ralph J Schilthuis et al. Active oil and reservoir energy. *Transactions of the AIME*, 118(01):33–52, 1936. 19

D. B. Silin. CSUG/SPE 149489: Gas Shale: From Nanometer Observations to Well Modeling. In *Canadian Unconventional Resources Conference*, Alberta, CA, Nov 2011. SPE. 28, 39

D. B. Silin and T. J. Kneafsey. Gas shale: Nanometer-scale observations and well modeling. *J. Canadian Petroleum Technology*, 51(475):475 – 485, 2012. 28

Katie M Smye, Eric Potter, Susan Hovarth, Forrest Roberts, and Scott W Tinker. Geological analysis of the Haynesville Shale for 'bottom up' production forecasting and resource estimation. in preparationa. 68

Katie M Smye, Eric Potter, Guin McDaid, Svetlana Ikonnikova, and Scott W. Tinker. Geological analysis of the marcellus shale for estimating resource-in-place and predicting productivity. in preparationb. 71

Salvatore P Sutera and Richard Skalak. The history of poiseuille's law. *Annual Review of Fluid Mechanics*, 25(1):1–20, 1993. 8

Jonathan Touboul. The hipster effect: When anticonformists all look the same. *arXiv preprint arXiv:1410.8001*, 2014. 14

P. P. Valko and J. W. Lee. SPE-134231: A Better Way to Forecast Production From Unconventional Gas Wells. In *Proceedings of the the SPE Annual Technical Conference and Exhibition, Sept. 19-22, Florence, Italy.* Society of Petroleum Engineers, 2010. 20

AF Van Everdingen and William Hurst. The application of the Laplace transformation to flow problems in reservoirs. *Trans., AIME*, 186(305):97–104, 1949. 23

John P Vermylen. *Geomechanical studies of the Barnett shale, Texas, USA*. PhD thesis, Stanford University, May 2011. 35

Mark P Walsh and Larry W Lake. *A generalized approach to primary hydrocarbon recovery*, volume 4. Elsevier Science Limited, 2003. 20

Robert A Wattenbarger and Henry J Ramey, Jr. Well test interpretation of vertically fractured gas well. *J. Pet. Technol.;(United States)*, 21, 1969. 24

Robert A Wattenbarger, Ahmed H El-Banbi, Mauricio E Villegas, J Bryan Maggard, et al. Production analysis of linear flow into fractured tight gas wells. In *SPE Rocky Mountain Regional/Low-Permeability Reservoirs Symposium*. Society of Petroleum Engineers, 1998. 26, 82, 84

B Widom. Surface tension and molecular correlations near the critical point. *The Journal of Chemical Physics*, 43(11):3892–3897, 1965. 12

B Widom and OK Rice. Critical isotherm and the equation of state of liquid-vapor systems. *The Journal of Chemical Physics*, 23(7):1250–1255, 1955. 12

Kenneth G Wilson. Renormalization group and critical phenomena. i. renormalization group and the kadanoff scaling picture. *Physical review B*, 4(9):3174, 1971. 13

Tai Tsun Wu, Barry M McCoy, Craig A Tracy, and Eytan Barouch. Spin-spin correlation functions for the two-dimensional ising model: Exact theory in the scaling region. *Physical Review B*, 13(1):316, 1976. 14

W Yu, Z Luo, F Javadpour, A Varavei, and K Sepehrnoori. Sensitivity analysis of hydraulic fracture geometry in shale gas reservoirs. *Journal of Petroleum Science and Engineering*, 113:1–7, 2014a. 33, 34

Wei Yu, Kamy Sepehrnoori, Tadeusz Wiktor Patzek, et al. Evaluation of gas adsorption in marcellus shale. In *SPE Annual Technical Conference and Exhibition*. Society of Petroleum Engineers, 2014b. 31